Universidade de Aveiro
2015/2016
Departamento de Electrónica, Telecomunicações e Informática

Bruno André Mansilha Andrade

Análise automática de características não métricas de crânios baseada em modelos 3D.

Towards automatic non-metric traits analysis of skulls based on 3D models.

Universidade de Aveiro
2015/2016
Departamento de Electrónica, Telecomunicações e Informática

Bruno André Mansilha Andrade

Análise automática de características não métricas de crânios baseada em modelos 3D.

Towards automatic non-metric traits analysis of skulls based on 3D models.

Dissertação apresentada à Universidade de Aveiro para cumprimento dos requisitos necessários à obtenção do grau de Mestre em Engenharia de Computadores e Telemática, realizada sob a orientação científica do Professor Doutor Paulo Miguel de Jesus Dias, Professor Auxiliar do Departamento de Electrónica, Telecomunicações e Informática da Universidade de Aveiro, e da Professora Doutora Maria Beatriz Alves de Sousa Santos, Professora Associada com Agregação do Departamento de Electrónica, Telecomunicações e Informática da Universidade de Aveiro.

o júri / the jury

presidente / president

Prof. Doutor José Manuel Matos Moreira
Professor Auxiliar do departamento de Eletrónica, Telecomunicações e Informática da Universidade de Aveiro

vogais / examiners committee

Prof. Doutora Maria Beatriz Duarte Pereira do Carmo
Professora Auxiliar da Faculdade de Ciências da Universidade de Lisboa

Prof. Doutor Paulo Miguel de Jesus Dias
Professor Auxiliar do departamento de Eletrónica, Telecomunicações e Informática da Universidade de Aveiro

Palavras Chave

Craniometria, Modelos 3D, Aquisição 3D, Estruturas 3D, Detecção de estruturas, Morfologia, Segmentação

Resumo

O propósito desta dissertação é a melhoria da aplicação CraMs e a análise craniométrica de modelos 3D através da quantificação e classificação de estruturas e características morfológicas. Uma oportunidade para o desenvolvimento deste projeto apresentou-se no ano de 2012 numa tentativa de colaboração com antropólogos, para criar uma aplicação que os ajudasse e facilitasse a realização de medições craniométricas e no processo de marcação de pontos. A aplicação permite ultrapassar alguns dos problemas existentes com os métodos manuais utilizados pelos antropólogos que podem criar resultados irregulares em medições e danificar os espécimes no seu manuseamento. Esta ideia levou ao desenvolvimento de um programa de computador, CraMs, no âmbito de duas dissertações de mestrado nos anos letivos de 2012-2014. Esta nova abordagem baseia-se na aquisição de modelos craniométricos usando um *scanner* 3D que depois, serão usados para fazer medições e análises normalizadas. O trabalho desenvolvido foca-se na abordagem dos problemas identificados pelos especialistas e na expansão das funcionalidades existentes a fim de criar novos métodos e melhorar a sua usabilidade. Os métodos acima mencionados centram-se na análise da morfologia das amostras e na extração das estruturas de forma uniforme, nomeadamente, a forma da abertura nasal, a depressão pós-bregmática, a espinha nasal anterior e a forma craniana para uma classificação padrão, com o objetivo de identificar a ascendência do indivíduo e o seu género.

keywords

Craniometry, 3D Models, 3D Acquisition, 3D Structures, Feature Detection, Morphology, Segmentation

abstract

The purpose of this dissertation work is to improve the CraMs application and the craniometric analysis of 3D models through the quantification and classification of structures and morphological characteristics. An opportunity for the development of this project presented itself in the year of 2012 in a collaboration with anthropologists, to create an application that would assist those performing craniometric measurements and in the process of marking points. The use of an application can improve some of the problems that exist with the manual methods used by anthropologists, that can create irregular results in measurements and can damage the specimens, while handling them. This idea led to the development of a computer application, CraMs, in the scope of two Master dissertations in the academic years 2012-2014. This new approach relies on the acquisition of craniums using a 3D scanner which will, afterwards, be used to make standardized measurements and analysis. The work developed concentrate in the issues identified by the specialists and in the expansion of the functionalities in order to create new methods and improve the usability. The methods mentioned above focus on the morphology analysis of the specimens and on extraction of the structures uniformly, namely the nasal aperture width, the anterior nasal spine, the postbregmatic depression and the cranial shape, for a standard classification with the purpose of identifying the individual ancestry and gender.

Table of Contents

Index of Figures

Index of Tables

1 Introduction

1.1 Motivation and Objectives

Craniometric analysis is the main tool used in Anthropology to identify gender, ancestry and variations in populations. These are usually determined using craniometric measurements, physically measured in the skulls. These traditional techniques have several drawbacks: poor repeatability (inter- and intra-observer variability), impossibility to perform on fragments and/or in fragmented skulls, inadequacy to describe complex shapes and the need for actual contact with the skulls that may damage the bones.

This dissertation is the continuation of the previous Master dissertations done in the academic years of 2012-2014 (Neves, 2014; Santos, 2013). It presents a new approach to perform craniometric analysis from digital models and how the measurement process could be improved through the usage of an interactive computer application. The goal of the work presented is to further develop the project by improving the software developed (CraMs - Craniometric Measurements) and exploring new methods related to gender and ancestry classification.

After reading through the previous dissertations and receiving feedback from the anthropologists, it was clear that the CraMs user interface needed to be significantly improved if it was to be used in a real scenario. Several features already implemented also needed to be improved and/or expanded in order to obtain more results and to validate the application.

Another topic of interest for anthropologists is the detection and classification of structures of interest, allowing ancestry classification. So, besides the improvements, this creates an objective that lead to exploration of new methodology for ancestry and gender classification, as well as preliminary validation of both approaches.

This project was particularly motivating because this application is already being used and given its potential to help improve the work in the field of craniometry. By integrating more technology into this field and exploring new paths, its boundaries can be pushed and grant access to new information.

1.2 Document Structure

This dissertation is structured in seven chapters, starting with this chapter (chapter 1) that contains a brief introduction to the work developed.

In the second chapter (chapter 2) a brief description about traditional craniometry, geometric morphometrics and the data set are presented. Also, information about 3D scanning equipments and the acquisition process is explained. Finally, the points, measures and structures of interest used when analysing a skull are briefly described.

The third chapter (chapter 3) is dedicated to the CraMs application, the prior status of the application and how it was improved. The issues solved and new features implemented are also explained.

Considering that CraMs is a real-world program, the fourth chapter (chapter 4) is dedicated to the interaction and user interface improvements, which makes the application viable to be used by the anthropologists.

Throughout the fifth chapter (chapter 5) the concepts and methods used for structure detection, the process of ancestry and gender classification are explained.

The sixth chapter (chapter 6) is focused on showing all the results obtained and their discussion.

Finally, the last chapter (chapter 7) presents the conclusion and future work.

2 Craniometry

This chapter explains the concepts and tools used by anthropologists on the field of craniometry and geometric morphometrics. The data set is presented, as well as a description of the acquisition process and the technologies used. Finally, a brief description of the points, measures and structures used in craniometry, is also provided.

2.1 Traditional Craniometry

The use of craniometry in anthropology research as a tool to identify ancestry, sex and human evolution studies in populations is well known (Buck & Vidarsdottir, 2004; Howells, 1973; Stephens, 2000). The roots of anthropometry are traced back to the skull measurement by early scientists. Craniometry, in a simple definition, is the study of human cranial measurements for use in anthropological comparison and classification (Stephens, 2000).

Traditional craniometry analyses consists in the physical manipulation of the skull in order to take measures between predefine landmark points (Stephens, 2000). This evaluation relays on the visual assessment of the exact points location, resulting in slightly different values between anthropologists, or even the same anthropologist on different moments. This happens because the definition of these landmarks is somewhat subjective and to make matters worse each skull has its own characteristics, shapes and suffers different decomposition processes. So, it is important to

evaluate the intra- and inter-observer variability levels to ensure validation of certain measurements.

2.2 Geometric Morphometrics

Geometric morphometric refers to the quantitative analysis of form, a concept that encompasses size and shape. The protocol for ancestry and sex estimation by visual assessment of non-metric traits is based on the extraction of each feature of the skull and then sorting them into categories, depending on geometric morphometric structure evaluation. Geometric studies are based on landmarks, which like traditional craniometric points, might be defined by sutures, lines or other known shapes. By analysing and comparing these landmarks, enough information is provided for categorization and it opens the possibility of gathering more information for further usage in studies (Buck & Vidarsdottir, 2004; Gonzalez, Bernal, & Perez, 2011; Hefner, 2009; Stephens, 2000). However, these methods have been largely criticized for being highly subjective (Gonzalez et al., 2011; Hefner, 2009; Ross, Slice, & Williams, 2010; Sholts, Miller, Wärmländer, & Walker, 2007; Sholts, Walker, Kuzminsky, Miller, & Wärmländer, 2011). Citing Hefner (2009): "The experience based method of ancestry prediction using morphoscopic traits indeed is an art: an art that is intuitive, untestable, unempirical, and consequently unscientific. It is often more appropriate to perform a metric analysis when working with morphological data, since it has proven to be more objective".

Measurement results exhibit lower levels of intra- and inter-observer variability, because they rely on standard landmarks. Linear measurements are commonly evaluated by univariate and multivariate statistical analysis, like discriminant functions. Nevertheless, traditional linear measurements are not able to capture and evaluate different forms of structures, e.g. orbit shape and nasal aperture. Because of that, with a greater emphasis put on shape rather than size, visual assessment methodologies provided the most appreciated way to assess shape differences, at least until recently (Gonzalez et al., 2011; Ross et al., 2010; Sholts et al., 2007; Stephens, 2000).Due to its importance and the available technological capabilities, advanced algorithms and methods to analyse the geometry of morphological structures employing 3D coordinates of anatomical landmarks started to be developed (Buck & Vidarsdottir, 2004);

Anthropologists can visualize results of multivariate analyses, preserve geometric information about the relative positions and assess variation in structures with few or no landmarks (Gonzalez

et al., 2011; Ross et al., 2010; Sholts et al., 2007; Vioarsdóttir, O'Higgins, & Stringer, 2002). Weber (2013) explains how the geometric morphometrics approach can be applied and the numerous advantages it can have when used to extract and analyse information from 3D models. Therefore, geometric morphometrics would be the logical choice when describing differences in structures related with gender, ancestry and human variation.

2.3 Data Set

The data set is composed by two collections. The first one is the same used by Santos (2013) and Neves (2014); later to better validate the results of non-metric traits, another collection was added.

Collection 1:

In 2009, an iDryas[1] team performed a rescue excavation at Vale de Gafaria (Leprosarium Valley); the site is located outside the modern and medieval walls of the city of Lagos in Portugal (Neves, Almeida, & Ferreira, 2010, 2011). Active between the 15th and 17th centuries, this site revealed two occupations. Part of Lagos Leprosarium, only known from historical documents (Neves et al., 2010, 2011), was excavated and eleven individuals were recovered. However, the most significant occupation was an urban discard deposit with an area of more than 1000m2 and a stratigraphic thickness superior to 6 meters, a number of human remains were exhumed, more exactly 155 individuals.

The skulls collection consists of 64 cranial and mandibular remains from 60 slaves and 4 leprosy suffers. All with an age of death above 18 years old, including 20 males, 30 females and 14 undetermined. The preservation of the skulls: 38% have the complete skulls and mandibles, 14% were reconstructed manually (by the anthropologist's team) and 48% were fragmented. The fragmentation result in the missing of some anatomical portions and represents an additional challenge.

Taking into account the worldwide lack of osteoarchaeological series that can illustrate the earliest phase of the European Atlantic expansion (Hefner, 2009), the preliminary search results done with the Lagos collection are a pioneering attempt to characterize African slaves. Giving a little inside history of the modern Atlantic commerce of African slaves, the vast majority of the excavated

[1] http://www.dryas.pt/iDryas/idryas.html

necropolises date from the later periods, between the 17th and 19th centuries and were found in the New World (Blakey, 2001). Furthermore, the anthropological analyses of African slaves' populations was a result of only direct observation of the osteological specimens and only occasionally has it been extensive (Hefner, 2009). The 3D imaging techniques proposed in this project are unprecedented and can provide relevant archaeological and anthropological results.

Collection 2:

Also in 2009, a collaboration between the Life Sciences Department, at the University of Coimbra, and the City Council of Santarém, was established in for the bestowal of non-claimed skeletal remains of the Capuchos cemetery (Ferreira et al., 2014). The reference collection, the CEI/XXI collection, is composed of corpses resulting from the sampling of recent individuals from Portuguese nationality and south European ancestry that were unclaimed or abandoned beyond the legal period.

At the moment, the collection is composed of 240 skeletons, of which 159 individuals have been analysed. All the individuals are Portuguese of both sexes with ages at death between 29 and 99 years, died between 1995 and 2008 and have been exhumed between 1999 and 2013. The male sample is composed by 74 individuals with age between 25 and 95. The female sample has 85 individuals with a lower age at death distribution, the younger with 50 and the oldest with 99 years old. Currently, 89 skulls are still undergoing the cleaning and tagging and the other 70 are already available for study.

Although, this series is an excellent opportunity to test and develop methods in older adults, no testing can be accomplished for sub-adults as a consequence of the absence of sub-adult skeletons. Only a few bones are absent and of the existing ones the majority are fully preserved, concluding that the quantity of bones by skeleton is fairly reasonable. This collection is a fundamental tool for forensic anthropology research, being very relevant when developing and validating studies of sex identification and skeletal aging methods that target elderly adults. In conjunction with the other reference collections it can also be used to investigate secular trends in skeletal development, among others.

As a consequence of the age range of a forensic case which is considerably different from country to country, many of the older collections are considered of little relevance when developing methods that can be reliable, when applied to more recent populations. Furthermore, because reference skeletal collections have low number of human skeletons of recent origin, this second

collection will improve the methods developed in this dissertation regarding sex determination and morphologic traits with more precision.

2.4 3D Scanning and Skulls Acquisition

Until recently, all studies and analyses in the fields of archaeology and biological anthropology were made manually, on the physical specimens. This meant that the specimens could easily be damaged or get lost while transported. Taking into account these factors and the recent evolution of digital technologies, the advantages of an integration of these technologies into these fields became clear, as stated in several articles (Balzeau et al., 2010; Wachowiak & Karas, 2009; Weber, 2013).

Nowadays, three-dimensional scanning is an well-established technology capable of producing high precision 3D digital models, for documentation of the reality, through Reversed Engineering, thus being particularly adapted to the documentation of cultural heritage remains (Balzeau et al., 2010; Wachowiak & Karas, 2009). Reversed Engineering provides powerful, non-destructive tools to create a point cloud of geometric samples on the surface of the subject. These points can then be used for a microscopic analysis, allowing a rigorous measurement of their features, surface geometry, texture and volume, using virtual examination, i.e. not requiring repetitive contact with their surface.

However, many of 3D scanning techniques, capable of producing high precision three-dimensional digital models, don´t exclude physical manipulation of the object being scanned. So, since the preservation of the objects original physical integrity is especially important, when dealing with fragile human osteoarchaeological remains, the most adequate scanning techniques are those that do not involve any kind of physical contact.

Initially, in Santos (2013) and Neves (2014) the specimens from the first collection (collection 1), recovered in the rescue excavation at Vale de Gafaria (Neves et al., 2010, 2011), were scanned using a Breuckmann SmartSCAN [2] structured light scanner shown in Figure 1. However, the Faculty of Science and Technology of the University of Coimbra also acquired recently a new scanner, the

[2] http://aicon3d.com/products/breuckmann-scanner/smartscan

NextEngine 3D Laser Scanner[3]. This scanner is “low cost” and implies models with less resolution when compared with the Breuckmann scanner (Table 1).

	Breuckmann SmartSCAN 3D	*NextEngine*
Price	c. €60 000 - €90 000	c. €1 990 - €2 650
Automatic turntable	yes	yes
Camera resolution	1384 x 1036 3 Megapixel	1384 x 1036 3 Megapixel
Accuracy	9µm	125µm
Operating system	32 bit (64bit optional) 64bit	32 bit (64bit optional) 64bit
Software included	OPTOCAT	Scan studio HD Pro
Texture	yes	yes
Data interface	ASCII, BRE, STL, PLY, VRML	VRML, STL, U3D, PLY, XYZ, OBJ

Table 1 - Scanners Specifications

To ensure that CraMs worked with models obtained with the NextEngine (Figure 2), as well as the ones obtained with the Breuckmann SmartSCAN, the first collection (collection 1) was scanned again and later the results were compared to evaluate the possibility of using both scanners on craniometric analyses. The CEI/XXI collection (collection 2) also was scanned with the NextEngine.

Figure 1 - Breuckmann 3D Scanner. Image taken from Santos (2013).

[3] http://www.nextengine.com/

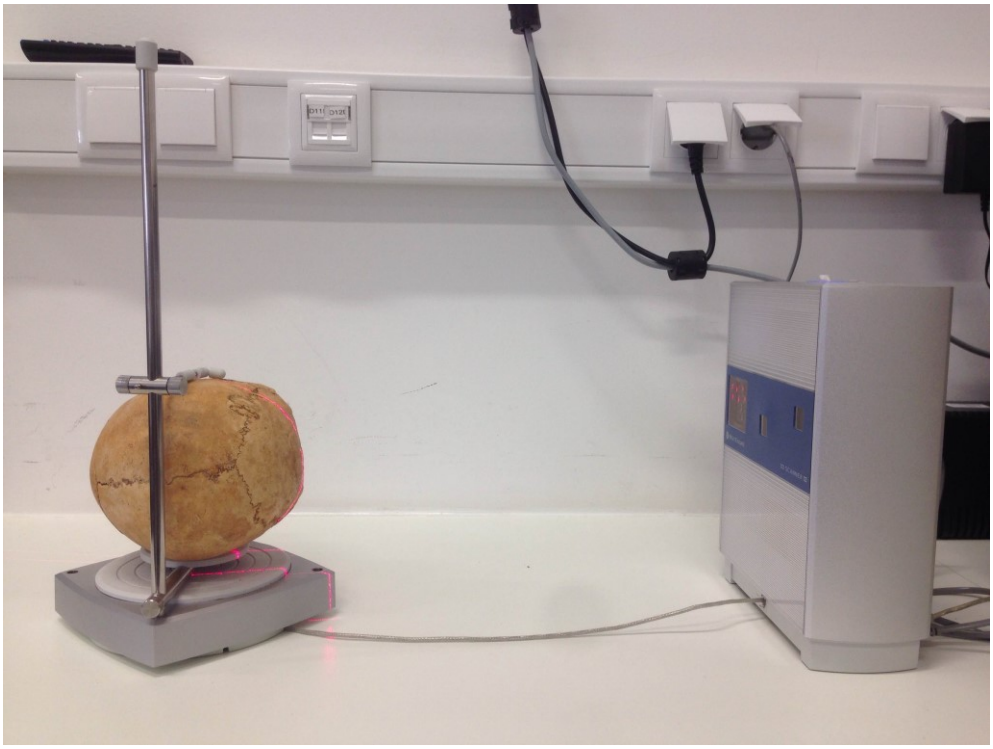

Figure 2 - NextEngine 3D Scanner.

Breuckmann SmartSCAN projects a set of stripe patterns onto the object and then proceeds, extracting its geometry by comparing the known projected patterns with the projected image of the pattern. NextEngine 3D Laser Scanner is based on multi-stripe laser triangulation (MLT), the device projects a multiple laser-stripes and registers the point's position with a CCD camera. The laser strikes a surface and depending of the distance to the surface, the laser dot appears at different places in the camera's field of view. Kannan (2008): "This technique is called triangulation because the laser dot, the camera and the laser emitter form a triangle. The length of one side of the triangle, the distance between the camera and the laser emitter is known. The angle of the laser emitter corner is also known. The angle of the camera corner can be determined by looking at the location of the laser dot in the camera's field of view. These three pieces of information fully determine the shape and size of the triangle and give the location of the laser dot corner of the triangle" (Figure 3). NextEngine uses a laser stripe, instead of a single laser dot, to sweep across the object in order to speed up the acquisition process. It also uses a rotating table, almost removing the need for manual handling.

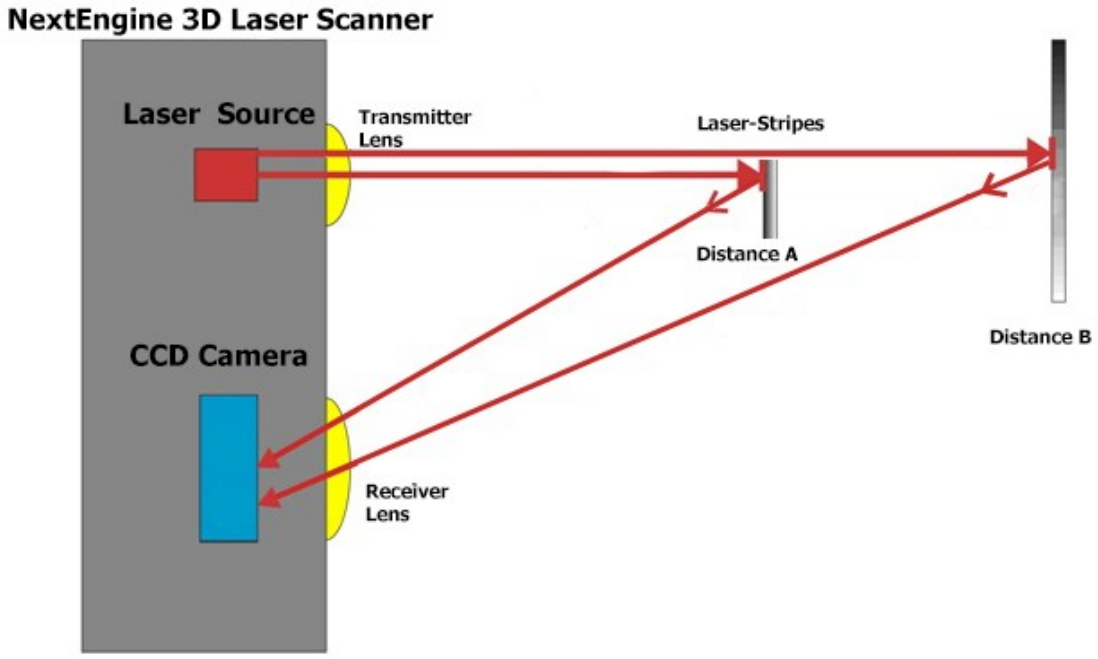

Figure 3 - NextEngine 3D laser scanning system.

Both processes are repeated several times while rotating the object and adjusting the pattern and light setup, then the overlapping captures are combined and blended together into a single fully healed model in order to obtain a complete and precise 3D model.

The acquisition with the Breuckmann SmartSCAN was done by a team from iDryas, including a 3D acquisition technician and several anthropologists to ensure the process would capture all the important sections of the skulls. Further details about the scanning and acquisition process can be found in Santos (2013). With the NextEngine 3D Laser Scanner the acquisition was performed by the previously trained anthropologists.

2.5 Points, Measures and Structures of Interest

As explained earlier, in craniometry it is essential to define a set of landmarks in the model. Several of these points are essential to perform the 24 measures that the anthropologists at a forensic lab (iDryas) use (see Annex 2 – Points of Interest for more details). Initially 21 points were defined as being of interest (see Annex 1 – Measures for more details); however, some additional points were used in order to accomplish specific measures, adding a total of 26 craniometric points.

Traditional methodologies, introduce a significant error. Measurement or observational error is the difference between a measured value of quantity and its true value (Dodge, Cox, & Commenges,

2003). During the manual analysis the variability between measurements must be considered, namely:

- Inter-observer error: the difference between the interpretations of two or more individuals observing the same phenomenon;
- Intra-observer error: the difference between the interpretations of an individual observing the same phenomenon at different times.

Technology keeps evolving, becoming more precise and complex. Through its integration in this field, the acquisition and further digital analysis of the skulls is expected to assure repeatability of the results, reduce variability between observers and, at same time, reducing the measurement error.

Skulls have a large amount of morphologic characteristics that can be used to perform studies, considering them as structures of interest, means they can be used for shape or volume comparisons. These structures are defined by the shape of the bone in the specific area of the skull. So, taking this into account, information about distances, volume and shape differences can be retrieved to further analyses. Its use is commonly seen in studies of facial proportions and changes in the overall skull appearance (angle and size differences) or when comparing structures or sutures.

3 The CraMs Application - Craniometric Measurements

This chapter presents the CraMs application. It is divided in two main sections, in the first one the prior state of the application is presented and in the second the modifications and improvements accomplished in this work are explained.

3.1 Previous version of the application

This section concisely presents the status of the application developed by Santos (2013) and continued by Neves (2014). It describes the architecture and specifications, how the alignment process works, the point selection methods, the algorithms created to detect structures and the limitations found by the domain experts when they used the application.

3.1.1 Architecture and Specifications

The application developed in Santos (2013) and continued by Neves (2014) follows the work flow shown in Figure 4. This process requires a previous acquisition of the models, which follows the procedure explained in section 2.4. After the 3D model is loaded, it is necessary to align it. This procedure can be done manually or through ICP (Iterative Closest Points)(Besl & McKay, 1992) using a template model (an already aligned model). After the alignment is done, two paths can be chosen.

It is possible to manually mark or detect points and structures. Of the twenty-six points supported by the application, some can be detected automatically, others can be determined using a semi-automatic method based on the curvature and the alignment information, and the additional points are fully manual. Table 2 shows that half the points can be detected by automatic (six points) or semi-automatic (seven points) methods.

There are two types of structures, sutures and orbits. Both imply the selection of some manual points between which a search will be performed in order to determinate the morphology. Based on the points and structures marked, it is possible to calculate the measures showed in Table 3.

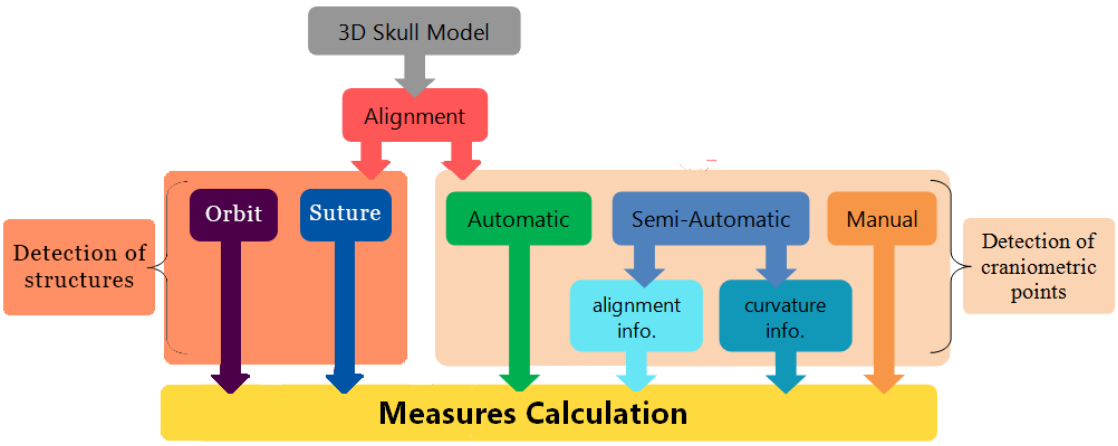

Figure 4 - Work flow of the application. Adapted from Neves (2014).

Table 2 - List of points and the information used to define each one (see Appendix A for more details). "N.L." stands for Neighbourhood Level which quantifies the topological space being considered. Adapted from Santos (2013).

	Point	***Information used (details)***
Automatic	Zygion (bilateral)	*Coordinates (max & min X with negative Y)*
	Basion	*Coordinates (min Y on Z axis)*
	Vertex	*Coordinates (max Y)*
	Bregma	*Coordinates (min Y in coronal suture)*
	Opisthokranion	*Coordinates (min Z on Frankfurt plane)*
	Lateral Sagittal Plane (bilateral)	*Coordinates (max & min X with Z<= 0)*
Semi-Automatic	Glabella	*Curvature* (convex *with 5 N.L.)*
	Nasion	*Curvature* (concave *with 10 N.L.)*
	Prosthion	*Curvature* (concave *with 5 N.L.)*
	Ektomalare (bilateral)	*Curvature* (convex *with 3 N.L.)*
	Biauricular (bilateral)	*Curvature* (concave *with 3 N.L.)*
	Nasospinale	*Curvature* (concave *with 10 N.L.)*
	Frontomolare-Temporale (bilateral)	*Curvature* (convex *with 3 N.L.)*

Table 3 - Measures calculated (see Annex 1 for more details). Adapted from Neves (2014).

ZYB	bizygomatic width	**BBH**	Basion-Bregma height
XCB	maximum skull width	**BNL**	Nasion-Basion length
GOL	maximum skull length	**FRC**	frontal line
PAC	parietal line	**FOL**	length of the Foramen Magnum
OBB	orbital width	**OBH**	orbital height
EKB	bi-orbital width	**DKB**	inter-orbital width
BPL	*Basion-Prosthion* length	**AUB**	Biauricular width
UFHT	superior facial height	**NLH**	nasal height
MAB	*Maxillo-Alveolar* width	**UFBR**	superior facial width
MAL	*Maxillo-Alveolar* length	**MDH**	height of the Mastoid process
WFB	minimum facial width	**NLB**	nasal width
OCC	occipital line	**FOB**	width of the Foramen Magnum

CraMs was developed using the C++ Programming Language, mainly because of the innumerable libraries available, such as VTK and QT. VTK is a visualization Toolkit for 3D computer graphics, image processing, visualization and interaction parts (Schroeder, Martin, & Lorensen, 2006). QT is a cross-platform application framework that provides the tools for building the user interface (Blanchette, Summerfield, Gorman, & Mcfarlane, 2004). Presently, the application runs on both GNU/ Linux Operating System and Microsoft Windows and can be easily built in other platforms.

A simple and succinct view of how CraMs is structured is shown in Figure 5. VTK and Qt run on top of the operating system, exchanging messages in order to make possible the API's integration (visualization, interaction, windowing system, etc.). Santos (2013) and Neves (2014) developed the application with four distinct modules:

- Tools: methods developed to analyse models, take care of alignment, find points of interest, etc.
- GUI: graphical user interface containing all the Qt code that handles window creation, menus, etc.
- Interaction: contains all code necessary to handle the interaction with the 3D models.
- Utils: contains some utility functions and structures.

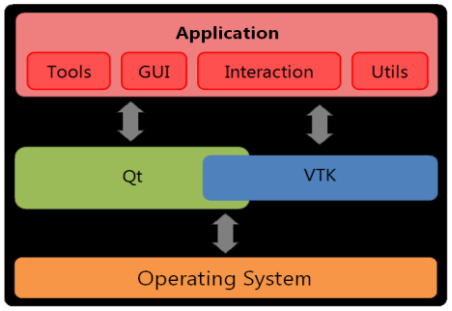

Figure 5 - Application architecture. Adapted from Santos (2013).

3.1.2 Alignment

When taking measurements using traditional methods or during the acquisition process of the models, the skulls are positioned and manipulated by the anthropologist to obtain the best results. The Sagittal, Coronal, and Frankfurt (Figure 6) planes are extensively used by the experts when analysing the skull (Pereira & Mello e Alvim, 1979). So, when working with a virtual environment it is essential to have the 3D model placed in the same 3D referential before any analyses can be done.

The alignment, using these three planes, allows the model to be divided into several sections, left/right, top/bottom and front/right providing additional information when detecting landmark points.

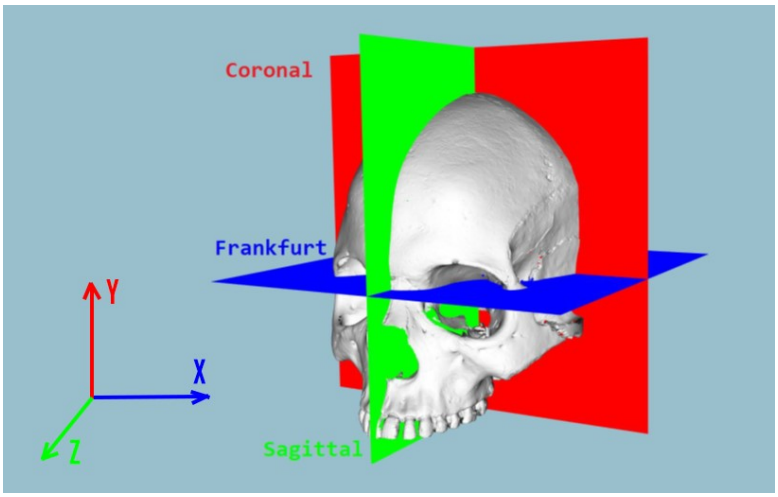

Figure 6 - Craniometric planes. Adapted from Santos (2013).

Santos (2013) implemented two methods of alignment:

- Manually – As the name indicates, the alignment is totally manual. The user must specify seven landmark points on the 3D model, in order to define the three anatomic planes. Based on their position it is possible the computation of the 3D transformation and consequently the alignment of the skull.
- Semi-Automatically: The user can visually compare the model with a template (an already aligned model), rotating and adjusting its orientation in order to provide a better estimate, then the ICP algorithm (Besl & McKay, 1992) will overlap the model and the template in order to find the best match. Neves (2014) added an option to align the models centroids, to aid the user in case the template and the model under study were displayed too far apart, which could increase the difficulty of the pre-aligning (Figure 7).

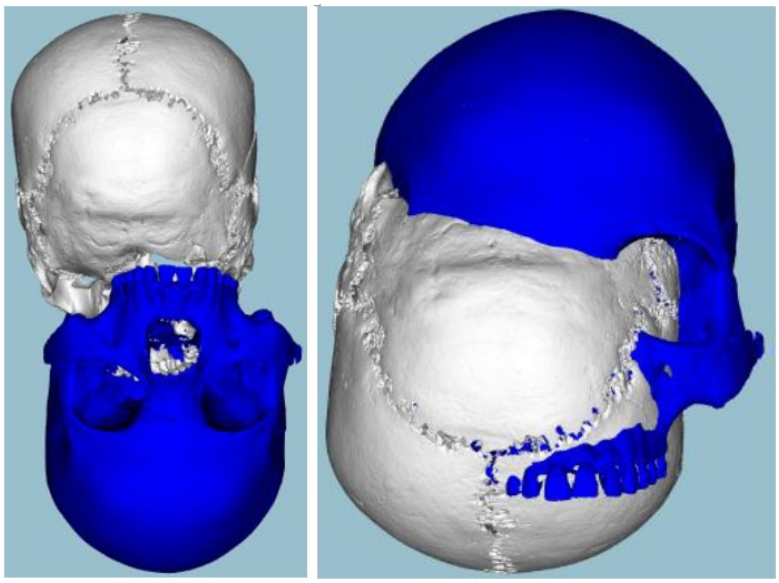

Figure 7 - The results without (left) and with (right) the aligned centroids in the pre-alignment process. Adapted from Neves (2014).

3.1.3 Point selection methods

To perform craniometric measures landmark points have to be marked. In this version of the application these points could be marked using three methods:

- Manually: The user picks the location of the landmark point without any additional information.
- Semi-Automatically: The user specifies an initial guess of the location of the point and based on the neighbourhood/curvature/coordinates the application computes the point with the most similar characteristics to the target point.
- Automatically: The application analyses the aligned 3D model in search of several points, relying on the locations of specific regions, on the reference planes and combining this information with the neighbourhood, curvature and coordinates.

The knowledge (neighbourhood, curvature and coordinates) used by the application to find each point can be adjusted to achieve better results. The neighbourhood level can be adjusted to any positive natural number higher than two, however the larger the neighbourhood the higher the complexity, resulting in worse performance of the application. The curvature can be set to convex or concave in order to better locate the point being searched. The axis can be used to find a landmark point. For example, the point in the model with the highest/lowest coordinate(s) in relation to one or more of the reference axes.

3.1.4 Structure detection methods

Neves (2014) developed two semi-automatic methods to detect sutures and the orbits. Both methods use an interactive approach and are both use values obtained by extracting information about the type and degree of curvature on a surface and perform an additional filtering of the points with high curvature with an adaptation of a method called region growing. This method was described by Vieira & Shimada (2005) and uses a concept which the authors call Sharp Edges (Figure 8). Further details about this method can be found in Neves (2014).

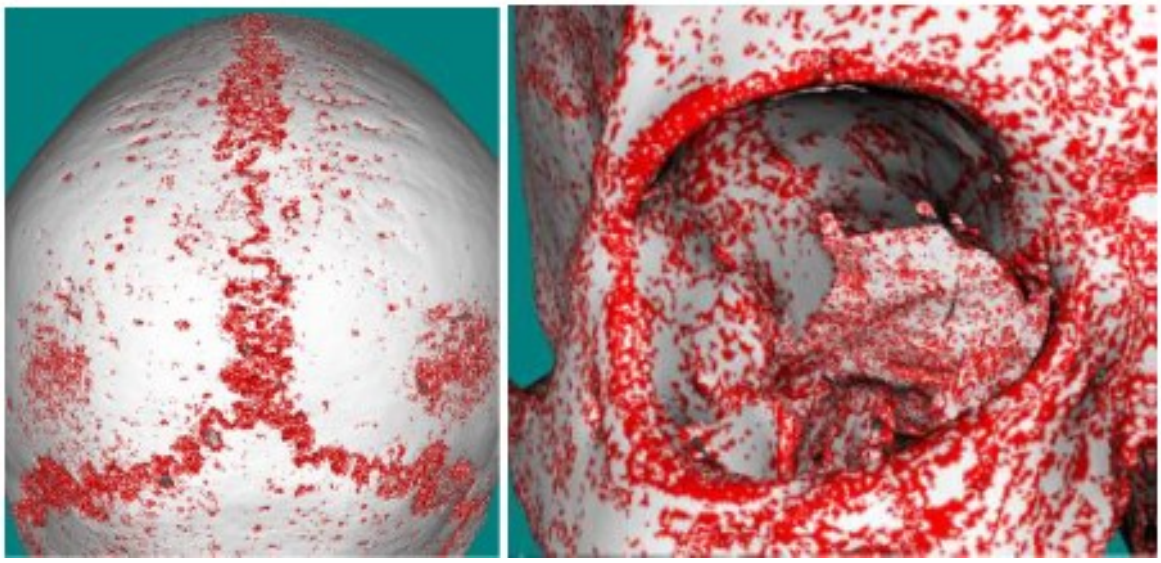

Figure 8 – The method Sharp Edges applied to a model. The result obtained on the suture (left) and on an orbit (right). Adapted from Neves (2014).

Orbit detection

Initially, the user picks some seed points and then their neighbourhood is analysed, based on maximum/minimum curvature and using Sharp Edges, it creates a list of points between each pair of seeds.

The algorithm tries to connect two points picked by the user, A and B, by analysing the curvature. The method starts in A and runs a cycle that searches in the neighbourhood for a sharp edge (point C), within certain parameters, closer to point B. If point C isn´t found, the search area is increased. When point C is found the method will be run again but with C as the starting point. The method finishes when point C is the same as B.

Suture detection

The suture detection method requires the user to mark two reference points at the extremities of the suture being analysed.

The algorithm starts by searching a structure composed of sharp edges which defines a direct path connecting the two reference points. Using this structure as a starting point the first neighbourhood level (points directly connected) of each point is analysed in search of more sharp edges. This cycle is then repeated for each of the new sharp edges found. When no more sharp edges are found or when a neighbourhood threshold is reached the process stops and the results are computed (Neves, 2014).

3.1.5 Limitations

In the earlier stages of this work, a survey was made with the anthropologists, in order to gather the limitations encountered after some extensive use of the application, when obtaining all craniometric measures. The main issues found were:

Software issues:

- The application stops responding in some unexpected situations;
- It was not possible to reload a new model;
- The algorithm used in the orbital structure, for the connection points, resulted several times in a “Not Responding” problem;
- Some automatic points were recurrently in the wrong place.

Usability issues:

- The list of points that have to be marked in the Manual Alignment process only appear in the console and had to be marked in a certain order;
- The alignment could not be saved;
- The manual could not be open from the application;
- Some automatic points could not be corrected if they were in the wrong place;
- Some terminology was incorrect;
- Difficult interaction (when marking points, a key need to be pressed before each mouse click, but the key was only recognized sometimes).

3.2 Modifications and improvements to CraMs

After reading the previous dissertations (Neves, 2014; Santos, 2013) and meeting up with the domain experts, who have specified a list with some problems in the application, the first objective of this work was fixing these problems and then developing some features to improve and facilitate the use of the application by the experts. This section describes these improvements and new features.

3.2.1 Software issues

When a new 3D model was loaded, the memory wasn´t released and some variables were not reset, leading to application failure. Several verifications were added in order to prevent these situations from happening.

In most cases the skulls have deformations both in terms of the position of bones and fragmentation, causing some automatic points to be misplaced. So, thresholds were added in order to guarantee that the search was done only in certain restrict defined areas, increasing reliability.

The algorithm used in the orbital structure for the connection points, result several times in a "Not Responding" problem. As explained in section 3.1.4, the algorithm tries to connect two points, A and B, by analysing the curvature. Two corrections had to be made to guarantee that this error wouldn't happen again. The first was to ensure that when a point matching the criteria wasn't found and the neighbourhood increased, only the new neighbours were checked, passing for a cycle (n!)! to n!. The second correction was implemented, in order to prevent the algorithm "infinity" loops, by defining a neighbourhood limit area, meaning that if the point was not found inside this limit, the best point was returned.

3.2.2 Usability issues

Manual alignment

One of the issues mentioned by the specialists, when using the application, was the manual alignment. The points required were shown in a pop-up window (in a table with their names and order) that could not be opened again and the user had to close it to proceed. The specialists would have to memorize it or write it down. Neves (2014) changed this by printing the list of points in the

console window at the beginning of the manual alignment process. Although this improvement was essential, it wasn´t enough to avoid being mentioned again by the specialists as an issue. So, at the beginning of the manual alignment process, a pop-up window was added, remaining visible until the process is concluded (Figure 9). Furthermore, the user can choose the order he/she wants to use.

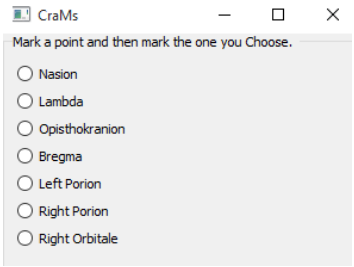

Figure 9 – Pop up window which allows the user to choose the order in which he/she wants to mark the points.

Terminologies correction in Labels

The specialists also mentioned that some of the terminology used in the application was not correct. Table 4 shows the terms that were changed.

Table 4 – Labels that had the wrong terminology and had to be correct.

BEFORE	AFTER
Biauricular	Auriculare
Nasal Limits	Alare (instrumentally determined as the most lateral points on the nasal aperture in a transverse plane)
Eurion	Euryon
Ektokonchion	Ectoconchion

The measures EKB (bi-orbital width) and DKB (inter-orbital width) had to be changed because they were switched.

Threshold added in Orbit Detection

The orbit reference points that needed to be marked when running the orbit detection method, had no control, frequently resulting in the selection of a point inside the skull and not on the orbit. Once a point was marked inside the skull, the algorithm attempts to connect the two points that are on opposite sides (the one on the orbit with the one inside the skull), causing an avalanche of events that would cause the application to crash. To avoid this from happening, the first point marked is used as reference, with a threshold, ensuring that any of the next selected points with a depth greater than the threshold of the reference point are not allowed. The user can mark the first point as many times as he/she wants without any consequences.

Open manual

The menu option in the application just opened a pop-up saying to “consult the manual.pdf”. This option was modified so that when clicked, the manual.pdf is automatically opened.

Euryon Only Automatic

An option to correct the Euryons manually was added. Considering that they were only possible to be discovered automatically, if in the wrong position it was impossible to correct them.

Nasospinale from Semi-Automatic to Manual

Nasospinale is a point found on the bottom of the nasal region. Santos (2013) determined that it is a shape of an extreme concave surface and that the curvature analyses was able to find it, given a large area of neighbouring search. Santos (2013) attributed 10 N.L., the acronym "N.L." stands for Neighbourhood Level and quantifies the topological space that is taken into consideration. Despite the initial results, the experts mentioned that the nasospinale was rarely in the right position, so it was decided to make the nasospinale a fully manual point.

3.2.3 Additional features implemented

More automatic points and Improved Measures

The algorithm developed to detect the nasal opening structure, explained in Section 5.3, allows four more automatic points and two improved measures (Table 5).

Table 5 – Points and measures that were automated

POINTS	MEASURES
right nasal limit	NLB (nasal width): maximum width of the nasal aperture;
left nasal limit	
rhinion	NLH (nasal height): distance between the nasion and nasospinale;
nasospinale	

3D Model Information

An option was added allowing the user to get more information about the model 3D, specifically the number of points and polygons (Figure 10).

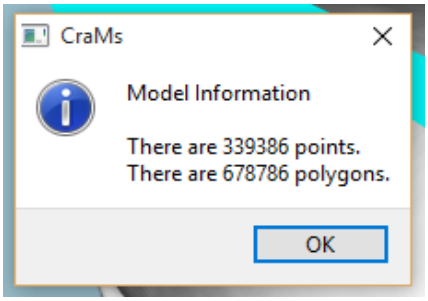

Figure 10 - Pop-up window with the Model information.

Decimation

The high resolution of the 3D models requires a large amount of computational resources, causing an impact on the user interaction. The complain of the experts, due to the application slowness and the time that each interaction took, prompted Neves (2014) to make a preliminary study to determine if the usage of models with lower resolution would have a significant impact in the application speed. In this study, it was concluded that the decrease of quality shouldn't have a significant influence on the measures obtained, consequently the acquisition process has changed to acquire models with slightly less resolution.

To allow the users to use all models, without being necessary a new acquisition, an option to decimate the model was included in the application (Figure 11).

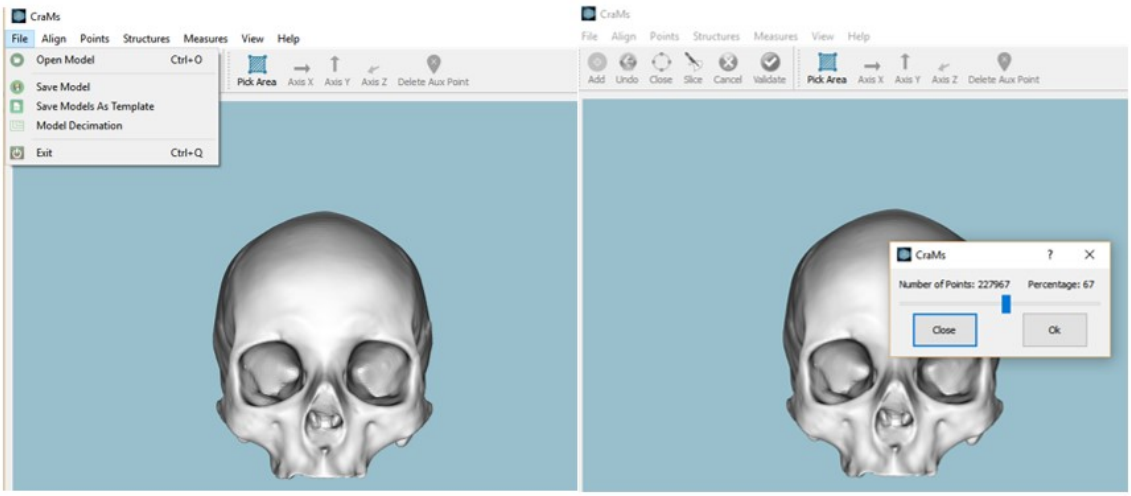

Figure 11 - The option to decimate the model was added. On the left the option is shown in the menu, on the right, the bar slider where the user can choose the percentage of the decimation is shown.

3.2.4 Measures using Planes

Some points are very difficult to mark precisely by anthropologists with traditional methods, even when taken by the same person many times. Since some of these points depend on the intersection between the model and a specific plane in order to obtain their position, a new method was developed.

The first application of this method was on the process of marking the lambda position, which is the point resulting from the intersection between the sagittal plane and lambdoid sutures. So, when marking the lambda (as shown in Figure 12), a window appears with the projection of the intersection, allowing the user to mark it more precisely.

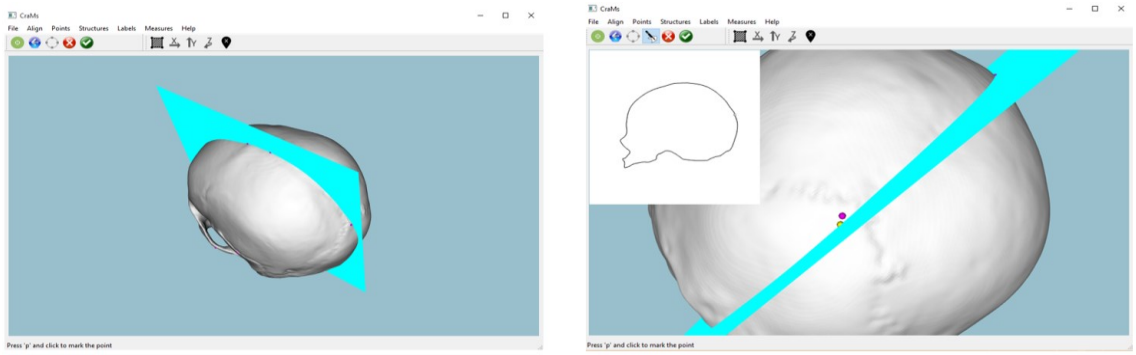

Figure 12 – On the right projection of plane, on the left the cross-section resultant of the intersection between the plane and the model intersection allowing the user to mark the point without any variability.

Later a Cut tool was developed to allow the user to interact with the plane, changing its size and orientation, giving a live projection of the result (Figure 13). This tool was not transferred to CraMs due to the fact that the experts concluded that there were no more points depending on the planes position, in addition to lambda.

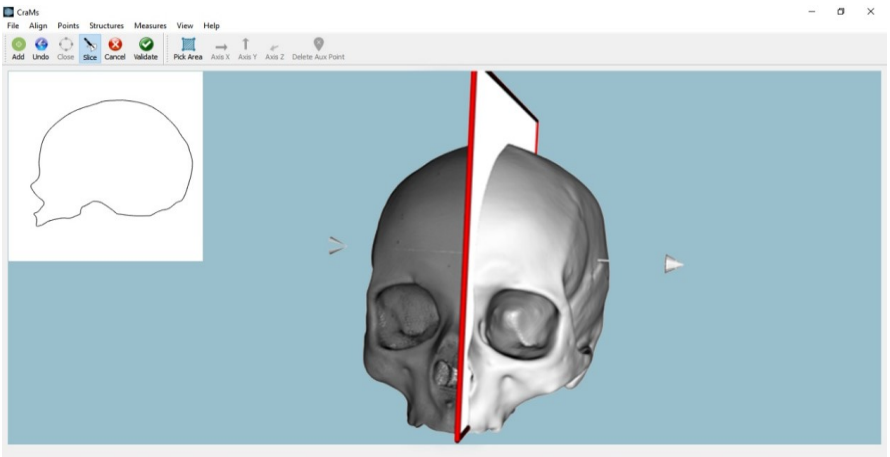

Figure 13 - Cut tool that allows the user to interact with the plane, changing its size and orientation. In the corner it is displayed the intersection giving the user a live projection of the result.

3.2.5 Farthest point Tool

Having a 3D model of the skull gives a huge advantage in comparison with visual analyses and traditional methods. The importance of a tool that could provide the farthest point of each axis in a certain area was highlighted by the experts. For example, the Zygion, an automatic point, is the most lateral point on the zygomatic arch. When it is not correctly detected automatically (e.g. due to 3D acquisition errors) it becomes very difficult to correct it manually.

Therefore, an auxiliary tool was developed, allowing the user to select an area of search and the axis to be analysed (Figure 14 and Figure 15). The user can use this tool to mark one landmark or to mark one auxiliary point.

Figure 14 - Options of the farthest point tool.

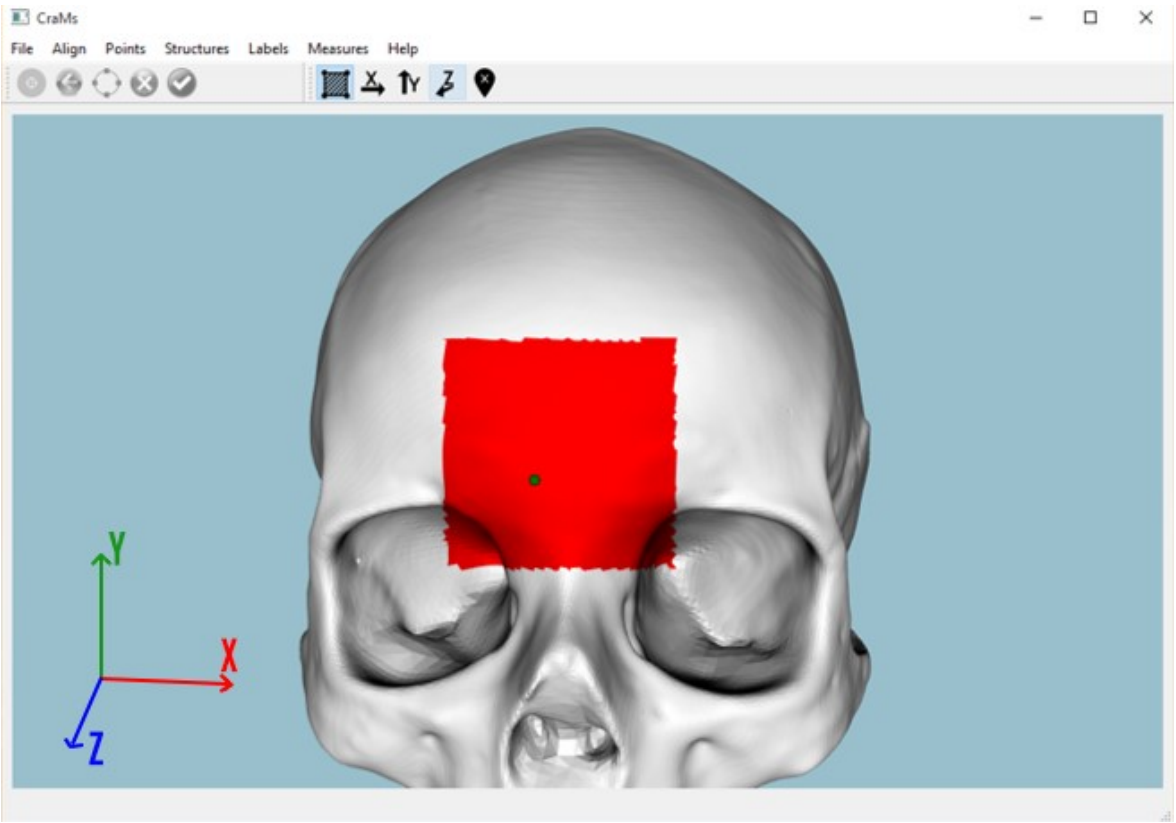

Figure 15 – Farthest point Tool being used to find a point.

3.2.6 Save Transformation

CraMs allows the users to mark points, calculate measures and save this landmarks and measures into files, but not the alignment. This means that every time a model is loaded the alignment had to be performed, even in the models that were already analysed and marked. So, a problem emerges, since the file with the landmarks depends on model alignment, when a 3D model is loaded again the landmarks will be in slightly different positions, meaning that every landmark will have to be marked again. To overcame this, the possibility to save the alignment when the model is aligned was introduced (Figure 16).

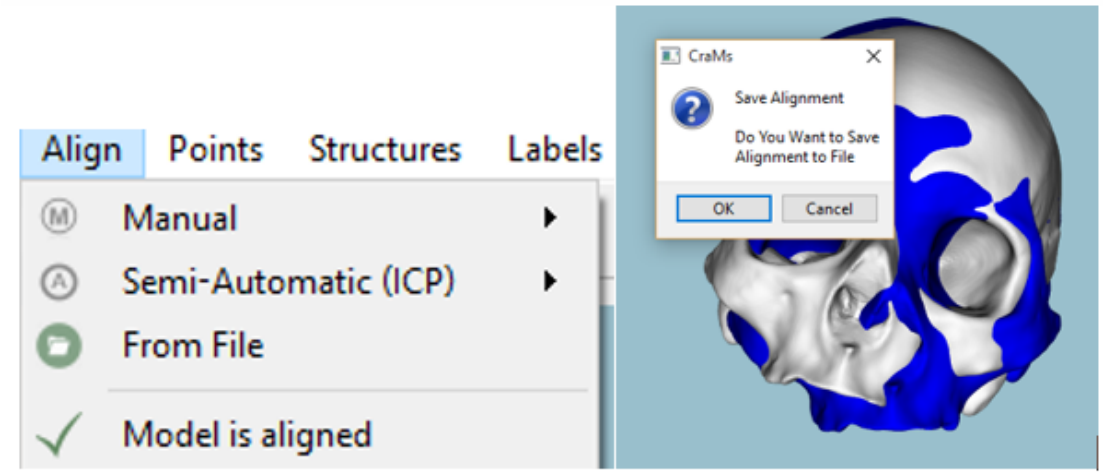

Figure 16 – On the left, option to align the model from a file. On the right, the pop-up windows that appear when a model is aligned.

4 CraMs Interaction and User Interface

A good user interface must have a correct balance between design and interactivity, being easy to use and with simple navigation. It is important to make a functional application, considering that CraMs is already being used by anthropologists. So, an effort had to be made to ensure an intuitive User Experience with clean presentation, good design and responsiveness. In this chapter, we analyse the interface taking into account the user feedback regarding the user experience and interaction. A usability test was developed, with the anthropologists, to better evaluate the software application, to find out if some of the modifications were well accepted and also what could be improved.

4.1 Overview

Human-computer interfaces can be evaluated in many different ways. Speed and accuracy are two related performance measures, in many of the tasks, which affect a person attitude towards the system. “In addition to performance measures, the time it takes to learn a system and the retention of acquired knowledge over time are associated with how effectively a system can be used. User acceptance of a system (i.e., subjective satisfaction) is also a critical measure of a system's success” (Chin, Diehl, & Norman, 1988). A program evaluated with a good rating in every performance

measure, can be left out or not be used often, because of the user dissatisfaction with the program interface.

Shneiderman (1998) developed a questionnaire that focuses only in the user's subjective rating of the human-computer interface. His book led to the development of a measurement tool, called the Generic User Interface Questionnaire (QUIS).

A usability test was developed (Appendix B – Usability Test), based on an adaptation of this measurement tool. The primary purpose was to assess the usability of the new program version, from the participants' perspectives as revealed by their observed performance and self-reported satisfaction. As complementary to the test and since the participants are the actual users of the application, they were also asked to identify usability issues.

4.2 Modifications and Improvements to CraMs

After solving the application problems (Section 3.2), CraMs still have some issues that didn't derivate from errors or bugs. In this section, we address usability problems and improvements that should be attended in order to make the application easier to use.

4.2.1 Executable and load screen

The first step was to create a more appealing experience, so an icon was added in the executable file and in the application load screen (Figure 17). To improve the user experience, icons were adapted or created and added in the menus (Figure 18).

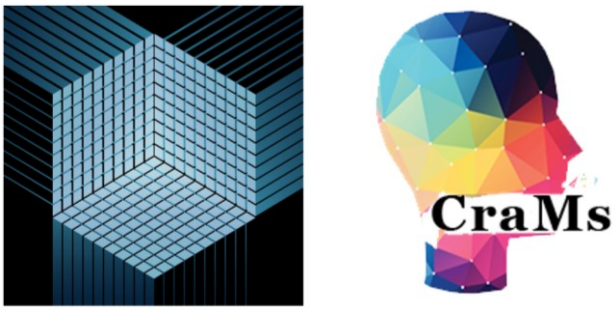

Figure 17 - Executable Icon (left), Load screen (right).

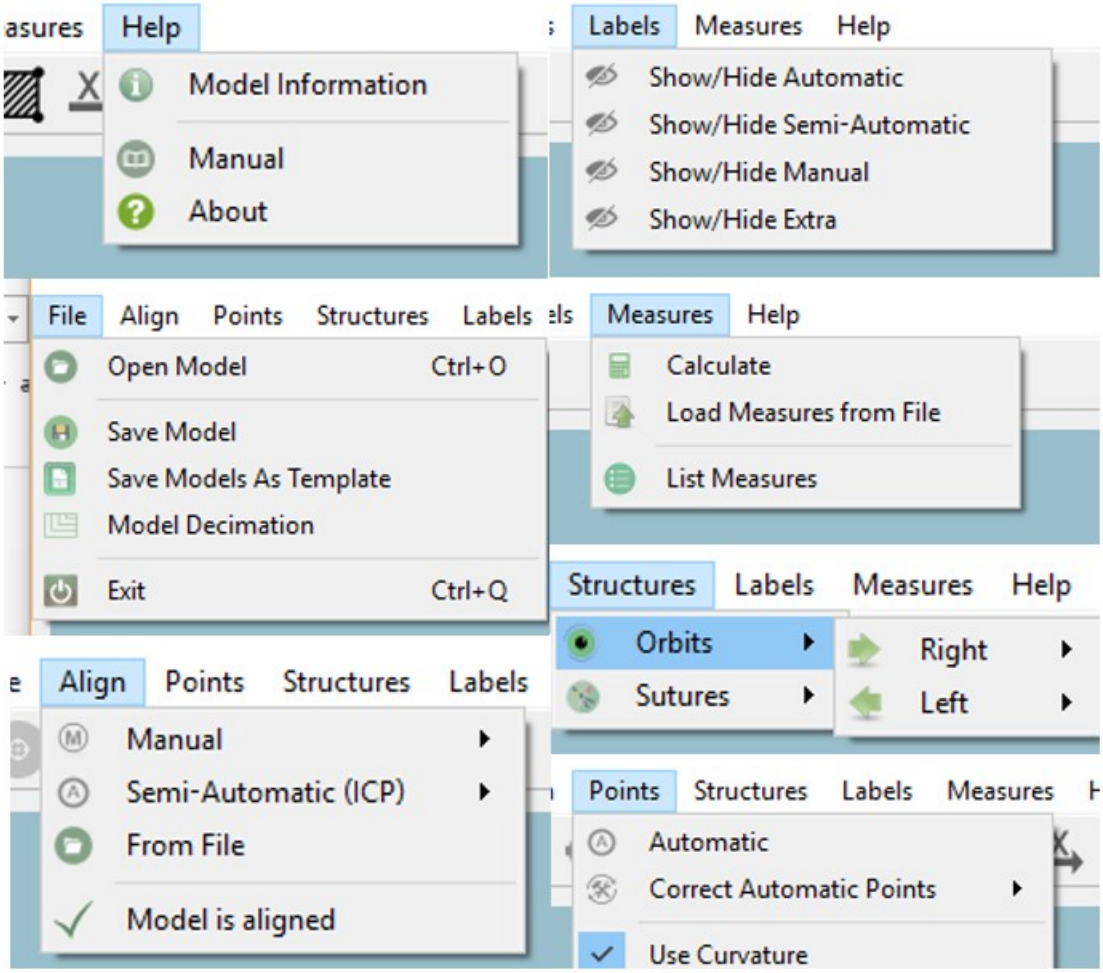

Figure 18 - To improve the user experience, icons on labels were added in the menus.

4.2.2 Undo last command

One of the biggest issues identified by the experts, was the impossibility to undo the last action. This mean that, once the user marked a point, the only way to reverse the action was to delete the point and select it again, requiring the user to access the menu twice. To solve this problem an icon was added, as well as, a keyboard shortcut (Ctrl+z) that delete the last point and allows the user to mark it again.

4.2.3 Mark points process Toolbar.

The experts also mentioned several issues on the basics operations, mainly some interaction difficulties when marking points. For example, many of the operations require the use of the keyboard and many times the keys were not recognized or were causing a decrease on

performance. So a toolbar was developed specifically to deal with all the interaction between the user and the model (e.g. marking points or structures) (Figure 19).

Figure 19 - Mark landmarks toolbar.

This toolbar gives the user quick access to important features:

- Pick Points- Activate to pick points or deactivate to move the model
- Undo – Undo the last action or actions
- Close structure – Close structure when marking orbit
- Slice – Activate a cut to help mark some points (Lambda)
- Cancel – Cancel action
- Validate – Validate last action made (point or structure marked).

4.2.4 Styles

Before performing the usability test, an alternative version was developed, a black version, allowing the user to select between both versions (the black and base version).

In the usability test, 4 out of the 5 users (eighty percent) preferred the black version, saying that it gave a more professional experience. So the black version became the base version and a menu was added, giving the option to change between styles (Figure 20).

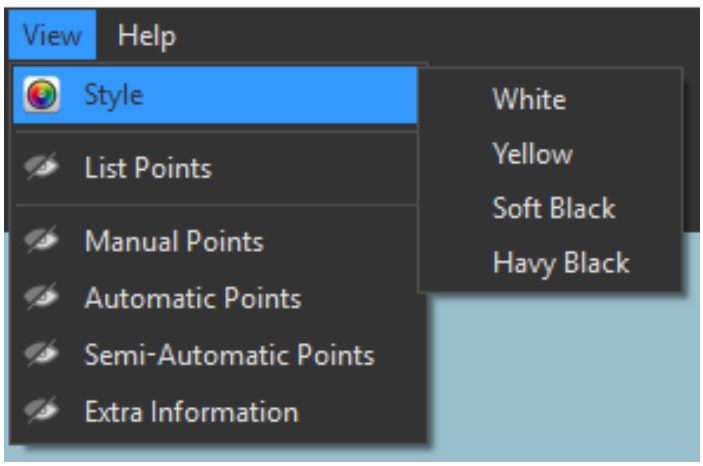

Figure 20 - Menu option to change Styles.

Later on, more styles were added to the application (Figure 21).

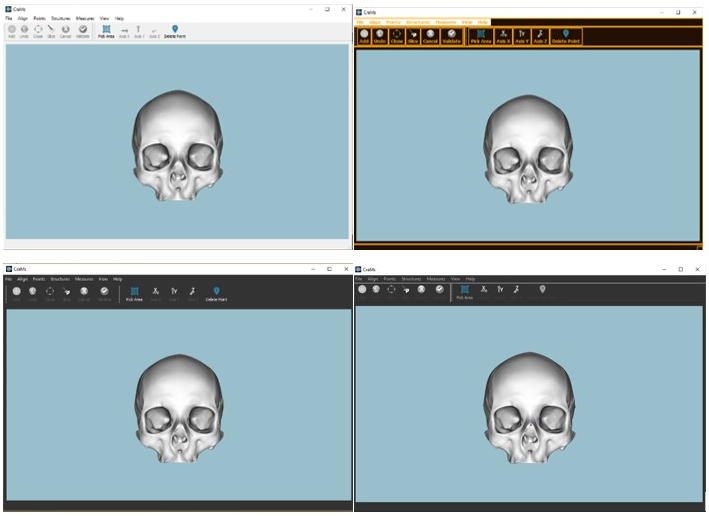

Figure 21 - CraMs with different styles being used.

4.2.5 Console Utility

When meeting with experts, they were questioned about the utility of the console as a complementary information and if it was really needed. Since much of the information was already displayed in a bar in the bottom area of the application, they said the only use they gave to the console was when marking the orbit, to know if the program crashed or if it was still computing information. Since this problem was fixed, as explain in section 3.2, there was no longer need for its existence (Figure 22).

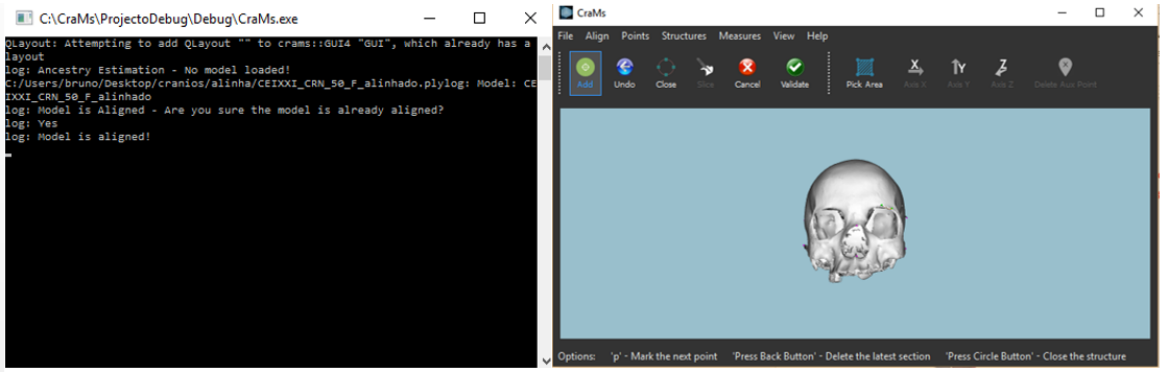

Figure 22 - Console used to show complementary information (left), information being displayed in a bar at the bottom area of the application (right).

4.2.6 List of Points side panel

Tests were performed in order to evaluate how much time a user needed to mark all landmarks and the number of error during the process. It was estimated that a user needs about 20 seconds to correct a point, just taking into account the time needed to go to the menu, delete a point and go again to select the point that he/she wants to mark. So having 36 landmarks, the time expended could go up to 12 minutes, considering that no point is marked more than twice and that every point is marked in the wrong position one time.

This problem was improved with the undo button, which gives the user the option to delete the last point marked. However, if the user does not realise that the point is in the wrong place and wants to correct the point later, the problem emerges again. Another problem is the inexistence of a real time information about which points are already marked and which need to be marked.

To solve all these issues a toolbar with a landmark list was added (Figure 23). This bar allows the user to delete and mark each point without having to access the menu. It gives the user the information of which landmark points are marked and those which aren´t, as well as the types of landmarks (automatic as green, semi-automatic as blue, and manual as orange).

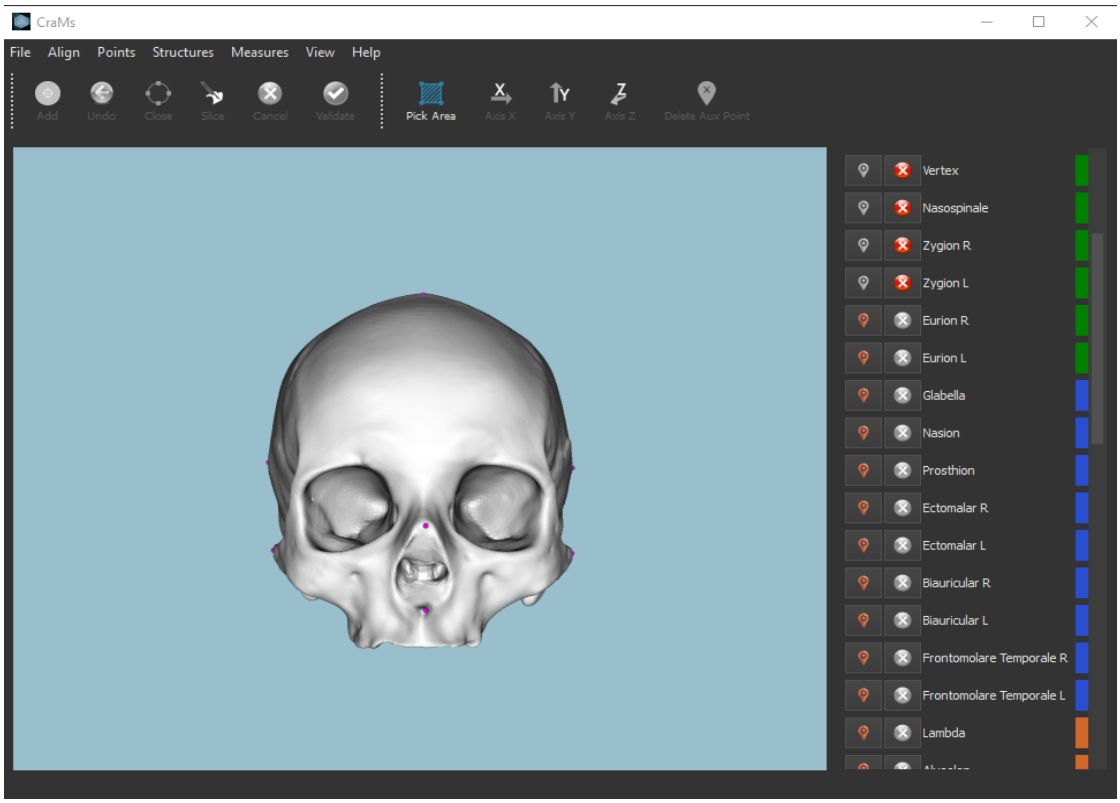

Figure 23 - Application with the introduction of the Landmarks List.

4.2.7 Installer

The installation process is the first user experience with CraMs and previously the user received a folder with all the content (images, libraries and the executable). With the help of NSIS[4], an open source script-driven Installer for Microsoft Windows, the new distributed installer became only an executable. It allows an intuitive and easy installation process, putting all the content in the program folder, hidden from the user (Figure 24).

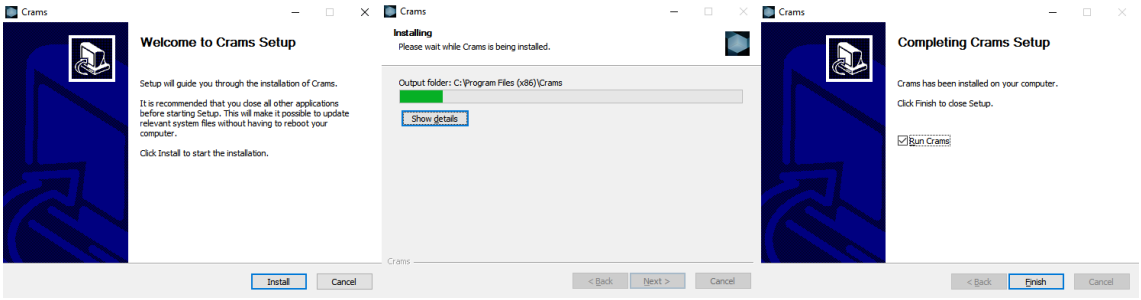

Figure 24 - CraMs new installation process.

4.3 Phantom – Using force feedback

We decide to modify the user interaction in order to evaluate a different approach that could improve the user interaction of the anthropologists with CraMs through the integration of the phantom Omni[5] 2010, a force feedback device.

While using the application, the manipulation of the skull to mark points and structures is completely different to what users are familiar within craniometry. Furthermore, there are points, positioned in depressions, they require the sensibility of touch to be located. The goal of integration of the haptic device was to create a more intuitive and realistic interaction with the digital world.

This device provides true three-dimensional entry with force feedback, integrating a sense of touch. The device use engines to create the forces that turn the hand of the user to simulate the touch and interaction with virtual objects.

[4] http://nsis.sourceforge.net/Main_Page

[5] http://www.geomagic.com/pt/products/phantom-omni/overview

The first step was to test the device with the demos provided and create a simple application that allows the user to mark points that were susceptibility to the mesh surface (e.g. points positioned in depressions). When this was accomplished, a full integration with CraMs was the next step. Although the drivers and the configuration application ran without any problems, the same could not be said about the demos. Only some of the available programs worked and none requiring force feedback manipulation. Tests were made with difference versions of software (Windows 7 to 10, phantom drivers, visual studio 10 to 15) and in different machines without any success. However, an application that allows the user to manipulate the 3D model (rotate, resize, mark points) was developed (Figure 26), however without any force feedback and thus this study was left aside.

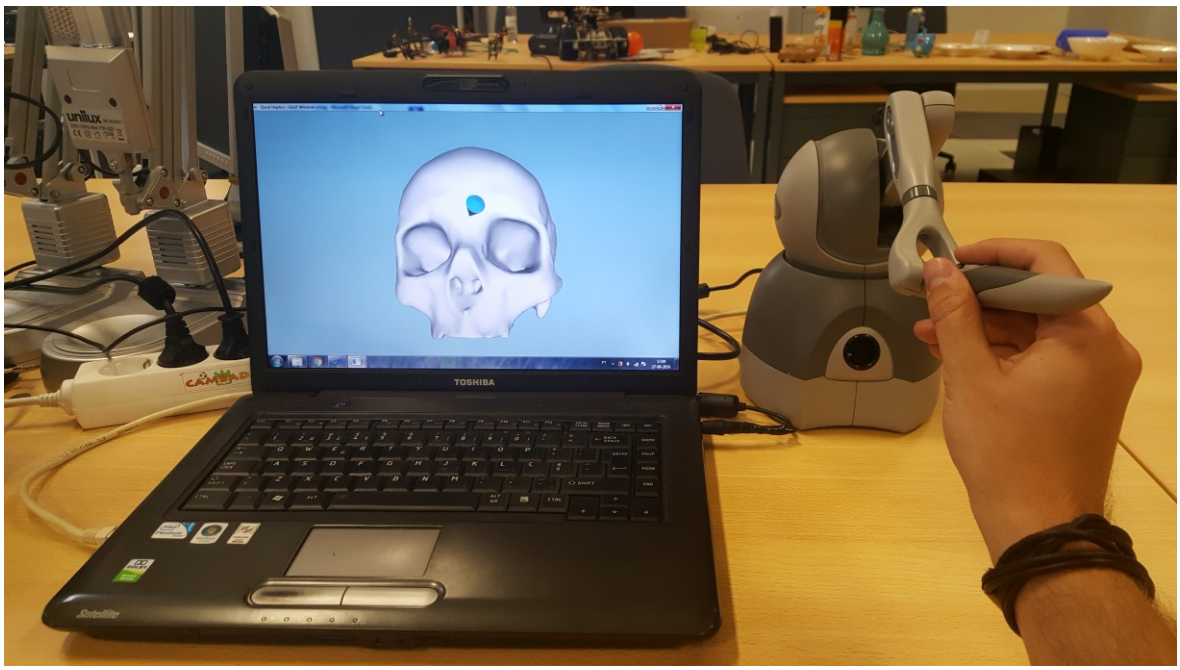

Figure 25 – Using phantom Omni, force feedback device, to manipulate a skull 3D model.

4.4 Usability tests

In order to evaluate the usability of the application, a list of tasks and questions was established. The list of tasks was created, taking into account the most important steps that every user must accomplish with in the program and the new features he/she must be able to use. The tasks were realistic, in a context, incremental and no clues were given, with the purpose of giving a normal scenario, so the users engage with the interface and pretend to perform real activities (the tasks are listed in table 5).

This list of tasks and questions was given to five anthropologists, two that had already used the application and three that had not, to evaluate the interface and usability of the application. The users could use the application manual (Appendix A – CraMs User Manual) to clarify any doubts when performing the tasks. The evaluation with the anthropologists that had the first contact with CraMs was not presential.

Additionally, the percentage of tasks that the users completed correctly was measured in order to evaluate the overall usability of the application. Table 6 -shows the overall usability of CraMs and also the success rate of each of the tasks, performed by the five experts. The success rate is the average of users that complete each task.

Table 6 - Success rate of each of the tasks performed by the users in the usability test.

Task	**1**	**2**	**3**	**4**	**5**	**6**	**7**	**8**
	Load a Model	Align the model using the semi-automatic method and save the alignment	Click the option that search the automatic points	Correct the position of the bregma, an automatic point	Mark the point Lambda, using the auxiliary tool "Slice"	Calculate the measures and save to a File	Search for the highest point in the parietal bone	Identify the probability of being African ancestry, knowing that the PBD is "Absent"
% of success	100	100	100	100	100	100	20	80

Most of the users could not perform task 7, because they did not understand which tool should be used or how it should be used. This happened because some of the participants were regular users of the application and to complete this task they had to use a new tool that they didn´t know existed, even though it was explained in the manual. After this test, the section in the manual explaining this tool was improved.

When questioned about what could be changed or added to improve the user´s experience the participants gave the following suggestions:

- In order to facilitate the ancestry evaluation process, when identifying the morphologic traits manually, Hefner representation images could be showed for an easy comparison.

- The possibility of the application automatically decimates the mesh, in case of large models, or through a pop-up window warning the user and giving him/her that

possibility. This was suggested, as sometimes when loading the two models (model to evaluate and template), the application doesn't have enough memory and crashes or slows the interaction.

- Providing ordering capabilities. The possibility to change the order of the List of Points by name, points already marked or anatomically (e g. higher to lower, anterior to posterior), not only by the type of points.

- Change the icons in the List of Points into more intuitive ones.

The participants used the application with and without the sidebar (List of Points). All five users appreciated the addition of functionality that the List of Points brought, when comparing the application with and without it. They said that the side panel is preferable, it is easy to use and the input and possibilities that it gives the user is an asset to the software. Tooltips were also added to buttons.

Figure 26 shows the classification, given by the experts, to the different aspects of the application. These results, all with satisfaction above 75%, show that the application is already mature and fairly usable.

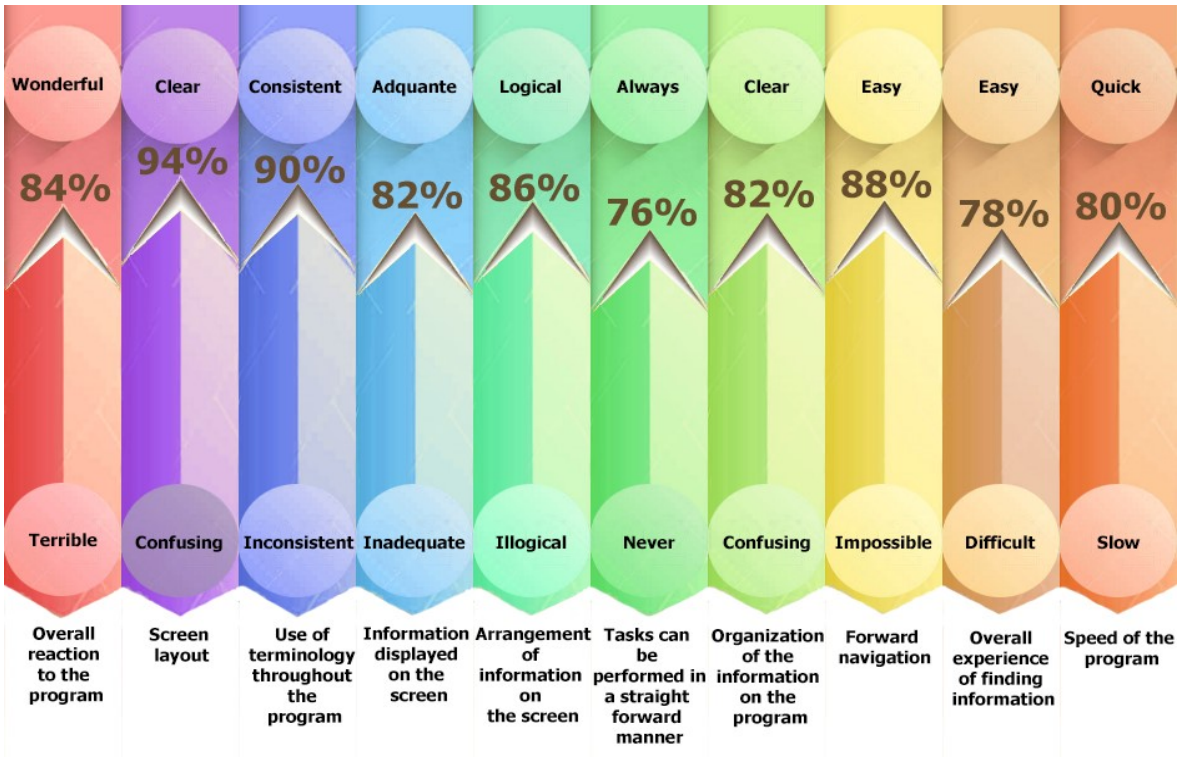

Figure 26 - Classification, given by the experts in the usability test, to the different aspects of the application

5 Non-metric traits

Despite the wide applicability of traditional craniometry in biological profile estimation (i.e. sex and ancestry estimation), it still does not allow the quantification and the classification of structures and their contours in a homogeneous way. Morphologic studies are being conducted in order to achieve a standardization of the morphological methods, so that subjectivity is no longer a problem (Ferguson, Kerr, & Rynn, 2011). The use of applications, such as CraMs, that allow the extraction of the structures automatically, has been contributing to the decreasing of the subjectivity in morphologic methods.

To estimate ancestry of an unknown individual, we may resort to metric and morphological methods developed for the cranial and post-cranial skeleton. The skull is the skeleton region where we can find the largest number of features, allowing the analysis of population affinities (Brues, 1990; Byers, 2011; Gill, 1998; Klepinger, 2006). Furthermore, when carrying out a forensic anthropological analysis, one of the first and most important steps is sex estimation (Spradley & Jantz, 2011). In this chapter, the studies, regarding the estimation of an individual ancestry and their gender, are explained. Some of the related work and the concepts used for detecting the structures are also explained.

5.1 Concepts used for detecting structures

Morphological shape extraction is closely related to Feature Detection or Feature Extraction. There are some interesting papers and dissertations on these topics, some focus on 3D polygonal meshes (Agathos, 2009; Benhabiles, 2013; Colombo, Cusano, & Schettini, 2006; Pavlidis & Liow, 1990; Shamir, 2006), others focus on 3D point clouds instead of polygonal meshes (An, Li, & Shao, 2013; Gumhold, Wang, & MacLeod, 2001; Pauly, Keiser, & Gross, 2003).

Mesh segmentation is defined as the process of decomposing a polygonal surface into different regions of uniform properties, either from a semantic or a geometric point of view. It is a critical step toward content analysis and mesh understanding. There are several algorithms regarding mesh segmentation (Agathos, 2009; Benhabiles, 2013). The Watershed, normally applied to 2D images and the hierarchical clustering, that strives to cluster the faces of the mesh so that clusters can be effectively approximated by one of the fitting primitives employed. The spectral analysis method uses the eigenvalues of properly defined matrices based on the connectivity of the graph in order to partition a mesh ("the nodes representing the graph used are the triangular faces and each node is connected with another if their representative triangles share a common edge"). Skeleton based methods make use of the shape skeleton to deduce the different segments. There are also interactive methods (that need user input), learning segmentation methods (using databases), spectral segmentation, interactive clustering, region growing and others (Agathos, 2009; Benhabiles, 2013).

Most of the algorithms extract well defined shapes or structures, e.g. body parts, based on geometric proxies (spheres, cylinders, developable surfaces), difference in normal of vertices or angles between faces, curvature (already used by Neves, 2014), medial axis and geodesic distances (Shamir, 2006).

5.2 Ancestry

Hefner (2009) conducted a study in European, Asian and African populations that showed eleven morphological characteristics which were correlated with population groups, as follows: the anterior nasal spine (ANS), the inferior nasal aperture (INA), the interorbital breadth (IOB), the malar tubercule (MT), the nasal aperture width (NAW), the nasal bone contour (NBC), the nasal overgrowth (NO), the postbregmatic depression (PBD), the supranasal suture (SPS), the transverse

palatine suture (TPS), the zygomaticomaxillary suture (ZS). Based on the data collected by Hefner and a simple Bayesian Classifier (Conditional Independence), David Navega and João Coelho developed a website[6], that allows the user, when analysing a skull, to input their visual classifications of the different traits and obtain an ancestry classification (Fig. 28).

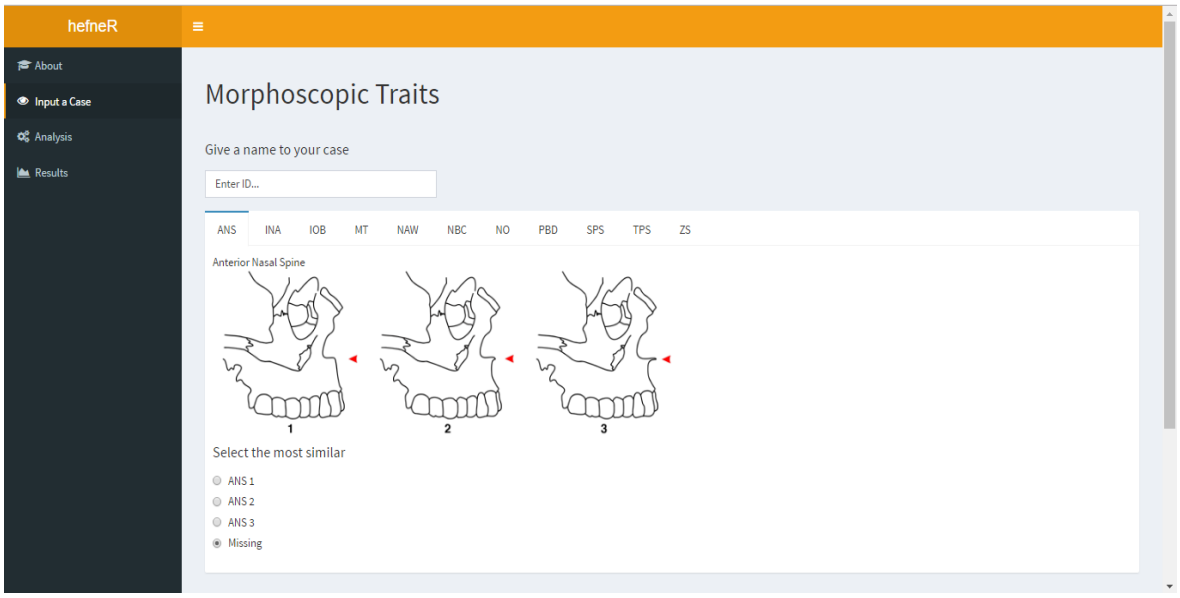

Figure 27 – Screen capture of the website that allows cranial non-metric traits ancestry estimation

The objective was to perform the classification of ancestry through the development of automatic methods for the detection and classification of the morphological characteristics identified by Hefner. After meeting with the experts, priority was given to the postbregmatic Depression and the anatomical structures of the nasal region, more specifically the nasal aperture width, the anterior nasal spine, the inferior nasal aperture and the nasal bone contour.

Wherefore, after analysis and discussion with the experts we concluded that the zygomaticomaxillary, the transverse palatine and the supranasal sutures were excluded at first because the process implied user interaction as a study by Neves (2014) already had proven (based on two user-marked reference points, the application finds a path that connects them based on the curvature). Moreover, many of these sutures are missing due to time erosion or the fact that the new models have less detail. The nasal overgrowth is most of the times damaged, missing or fractured (anti-, peri-, or post-mortem). The interorbital breadth depends of sutures location, as well as the malar tubercle.

[6] http://apps.osteomics.com/hefneR/

Using the Data study conducted by Hefner (2009) that calculated the frequency distributions of each characteristic and based on the mentioned website, a data entry window designed for the collection of non-metric traits of the skull was integrated in this work (manually or automatic using the methods developed) (Figure 28) and calculate the probability classification of each population group.

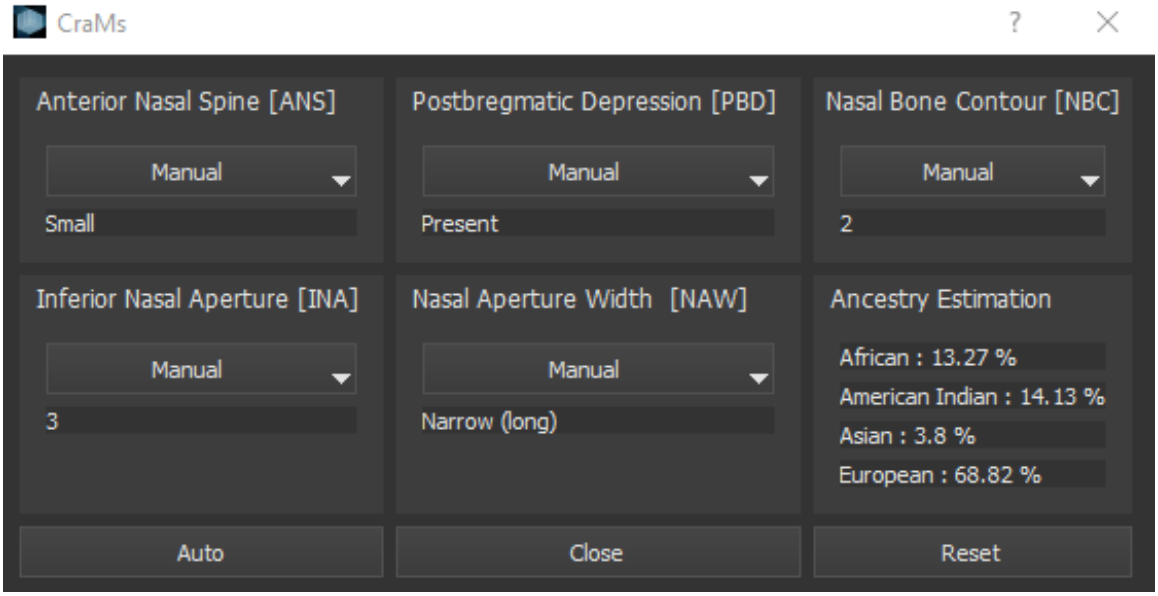

Figure 28 - Data entry window, designed for the collection of skull non-metric traits studded in this work (manually or using the methods developed), that gives the ancestry probability classification.

5.3 Nasal Aperture Width (NAW)

Byers (2011) asserted that the nasal region plays an important role in the evaluation of population affinities and for each population group, there is a unique form of nasal aperture. Analysing the nasal aperture characteristic, we can define three different models for each of the population groups (European, African and Asian), the close, very large and central enlargement nasal opening (Figure 29; Coelho, 2012).

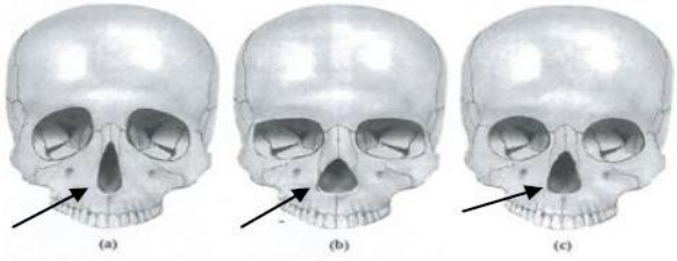

Figure 29 - Different forms of the nasal opening illustration 3D. (A) Triangular or close characteristic of Europeans, (B) very large feature of Africans, (c) extended in the center characteristic of Asians. Adapted from Hefner (2009: 139).

An objective of this work was the development of an automatic method to extract the nasal aperture width and compare it with the different nasal apertures, proposed by Hefner, for predicting ancestry. To have an automatic method, without an interactive approach, we need to create a system that detects relevant points (seed points), in the nasal opening, that could be used to create a closed 2D structure and compare it with one of the three types (Figure 30).

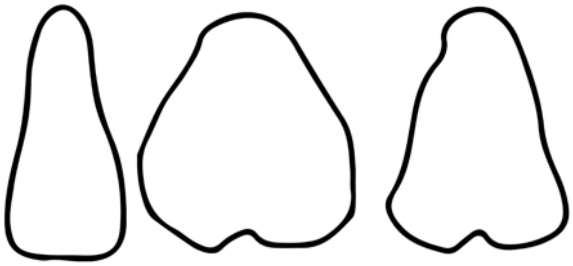

Figure 30 - Different forms of nasal opening, Illustration 2D. Adapted from Byers (2011: 139).

After reading through the articles mentioned above and since the work under development is new and considering that the curvature values had already been used in CraMs by Neves (2014) when detecting structures and sutures (explained in 3.1.4), we decided to use the curvature in conjunction with a region growing algorithm when detecting the nasal aperture width. To identify the positions of some relevant landmark needed in the process, we used the vertices normals. Later the process will be explained.

Region growing is the most intuitive method to segment a mesh (Eck et al., 1995; Kaufhold & Hoogs, 2004; Lavoué, Dupont, & Baskurt, 2005; Razdan & Bae, 2003; Zuckerberge, Ayellet, & Shlafman, 2002). Initially, it starts by selecting a seed element (a vertex), and then a growing process is done by incrementing successively compatible elements (vertices within a certain criteria). This leads to the creation of a region. This process is repeated with a new seed element each time the previous growth is interrupted. The algorithm stops when all the seed elements are visited. The main difference between the region growing algorithms lies in the choice of the criterion which decides whether an element can be added to a given region (Benhabiles, 2013).

The first step of the NAW detection process was to define craniometric points, that could be used to delimit the nasal opening. After a meeting with the anthropologists, the rhinion (rhi) and the nasospinale (ns) positions were defined as points of interest allowing us to establish the limits of the structure (Figure 31). The rhinion is the lower end of the suture between the nasal bones and the nasospinale is lowest point in the inferior edge of the piriform aperture at the base of the nasal

spine. In an aligned skull, they are located on the Sagittal plane (an anatomical plane which divides the body into right and left half) (Figure 6).

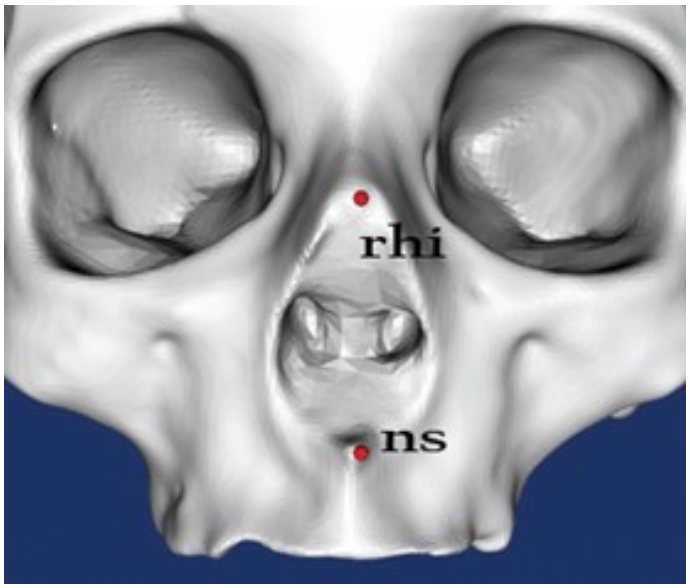

Figure 31 - On the right, the rhinion and the nasospinale points.

5.3.1 Find Reference Points for Nasal Detection

Based on the previous conclusions, we developed a method that could find the rhinion and the nasospinale points. The logical approach was to analyse the intersection between the sagittal plane and the skull (Figure 32). This became possible, knowing that the sagittal plane is the plane x=0, in a correctly aligned skull, otherwise it is the YZ-plane that intersects the bregma, an automatic point already detected by CraMs (Figure 33). This was done using the cut tool mentioned in section 3.2.4.

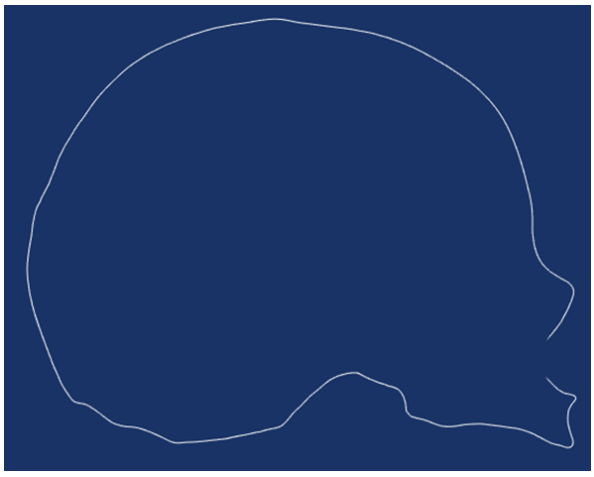

Figure 32 - Cross section resulting from intersection between the plane (x=0) and the skull.

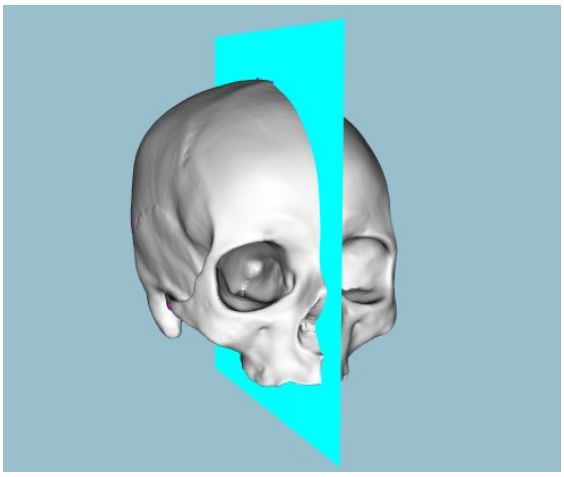

Figure 33 - YZ-plane that intersects the bregma.

The idea is to analyse this section, based on the curvature and applying different thresholds and filters in order to reduce the number of occurrences of curvature changes until we get the points of interest. To analyse the curvature, we need to calculate the normal slope (Figure 34), that is the slope of the perpendicular line to the tangent (Equation 1).

$$m_n = -\frac{1}{m_t} \tag{1}$$

Where m_n is the normal slope and the m_t the tangent slope

Understanding that the 2D image is defined by a set of points and consequently the curves are represented by a set of points too, the tangent is the line equation for each pair of points (Equation 2).

$$m_t = \frac{(y_1 - y_2)}{(x_1 - x_2)} \tag{2}$$

Where m_t is the tangent slope and (x_1, y_1) and (x_2, y_2) are the coordinates of each pair of points

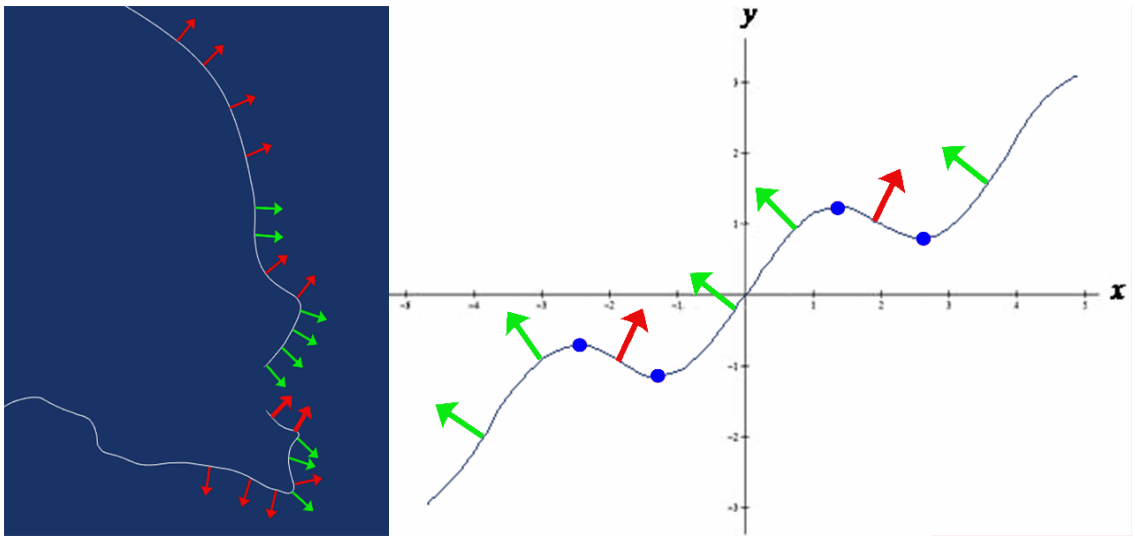

Figure 34 - Representation of normals with positive slope (red) and negative slope (green) (left), representation of critical points (right).

The first idea, to study the curvature, was to find all points where the derivative is null or undefined, this means that the slope tangent is zero (critical points, Figure 34). Adapting this to our case, our goal is to find all points where the slope changes its sign.

With this information, we created an algorithm that goes through the line resultant from the cross-section, finding and marking all critical points taking into account the following factors:

- Neighbourhood – analyses the neighbourhood and checks if the critical point results from a progressive change or if it is a local/punctual defect. We need to define the neighbourhood (ex: analyse the 10 to 50 previous points).
- Minimum distance – if any critical points are detected in the vicinity, chose the one with greater slope variation.

After some experiences, with different skulls, we noticed that the rhinion and nasospinale points were detected (Figure 35). However, we soon realized that in some cases the two points were not detected due to the degradation state of the skulls (causing segment discontinuity) or because the ANS was no projection (Figure 56) jeopardizing this first approach (Figure 36).

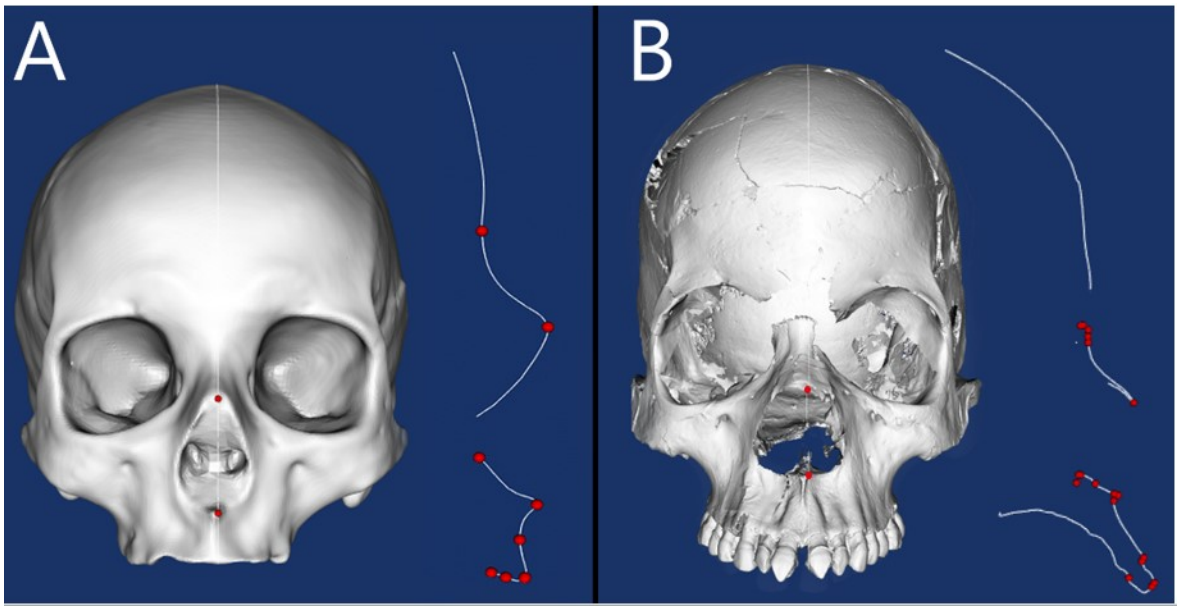

Figure 35 - Analyse of 2D image based in curvature (different thresholds). In situations A and B, the rhinion and the nasospinale were correctly detected.

Although the initial results were promising, we had to redefine the initial solution by adding more factors, in order to overcome these problems. So, two more factors were added to the algorithm to solve those issues.

- Search of slope variance – marks slope changes larger than a threshold.
- Discontinuity – situations are highlighted where the cross section being examined is not continued, meaning where the connectivity breaks.

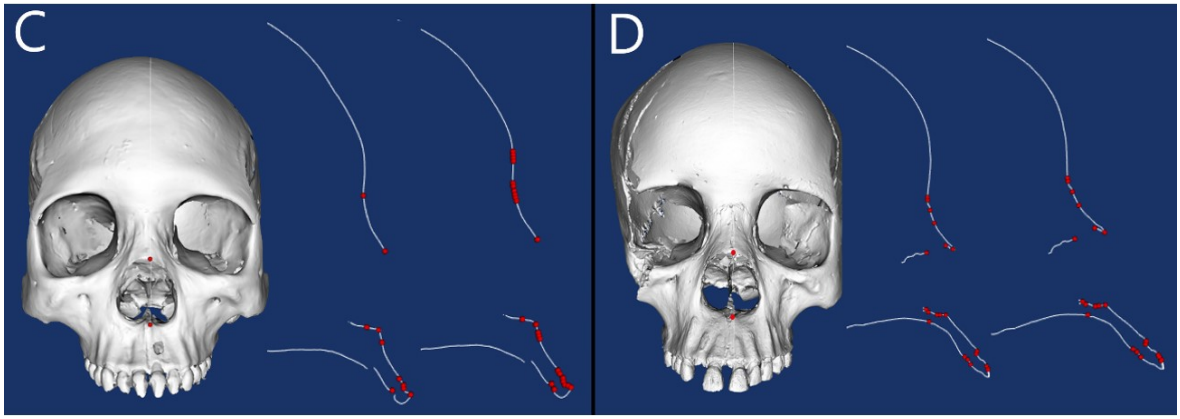

Figure 36 - Before and after implementation of the new factors. In C we search slope variance, in D we have to consider situations in which the segment was discontinued (the green points are the points that should be detected).

Now the objective is to filter the resulting list (Figure 35 and Figure 36), with the relevant points, in order to discover the two nasal points (rhi and ns) coordinates.

It is essential that the rhinion is found first because the nasospinale depends on its location. With some *a priori* craniometric information, finding the rhinion was straightforward, we just have to pick the point with the highest z-coordinate above a threshold. The threshold is defined by the zygion (the most lateral point on the zygomatic arch, automatic point) and is needed because some points between the stephanion (ss) and the prosthion (pr) can have bigger Z-coordinate than rhinion (Figure 37).

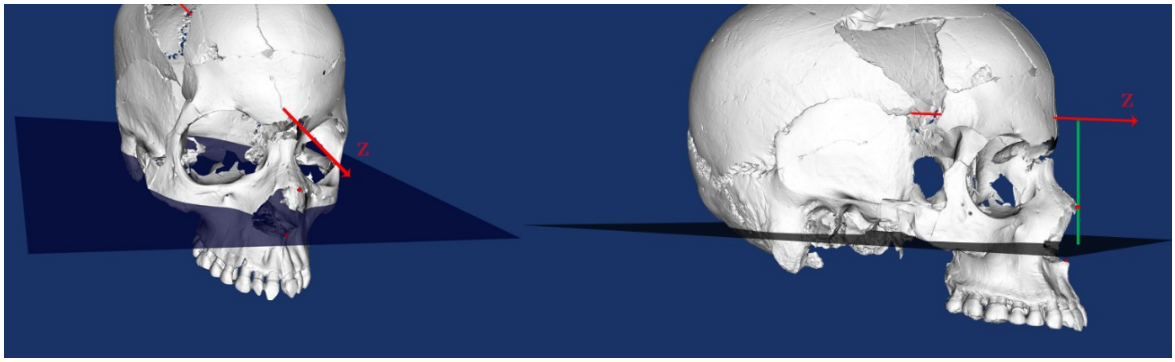

Figure 37 - Zygion Plane – used to delimit the search areas of rhinion (located above the plane) and the nasospinale (located below the plane).

The nasospinale location is define as the point whose Y-coordinate must be inferior than the one of the zygion point and at the same time has the highest value given by equation (3). This equation tries to minimize the distance (d) between the rhinion and nasospinale, and using the nasospinale ordinate (ns_y) to ensure the point is not detected inside the structure.

$$factor = \frac{ns_y}{d} \quad (3)$$

Where d represents the distance between the rhi and the ns being considered. The ns_y represents the y-coordinate value of the ns being considered.

The outcomes were very close or identical to the actual position (Figure 38), except in some cases where skulls were damaged.

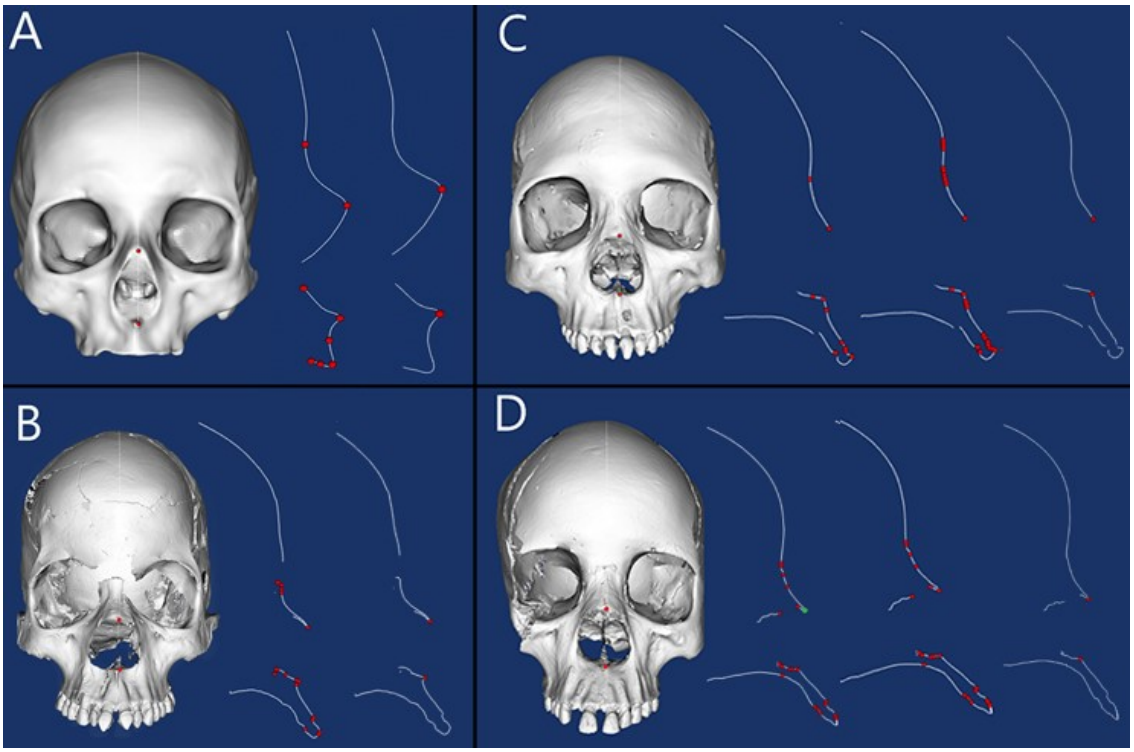

Figure 38 - Results of the search for the ns and rhi points.

5.3.2 Detection of other Seed Points

The nasal opening is the most salient region between the rhinion and the nasospinale. With that in mind, we can compute the midpoint (blue dot, Figure 39). This center point is used as a seed to the method that extracts the nasal region. The rhinion (rhi) and the nasospinale (ns) will be used as a boundary reference.

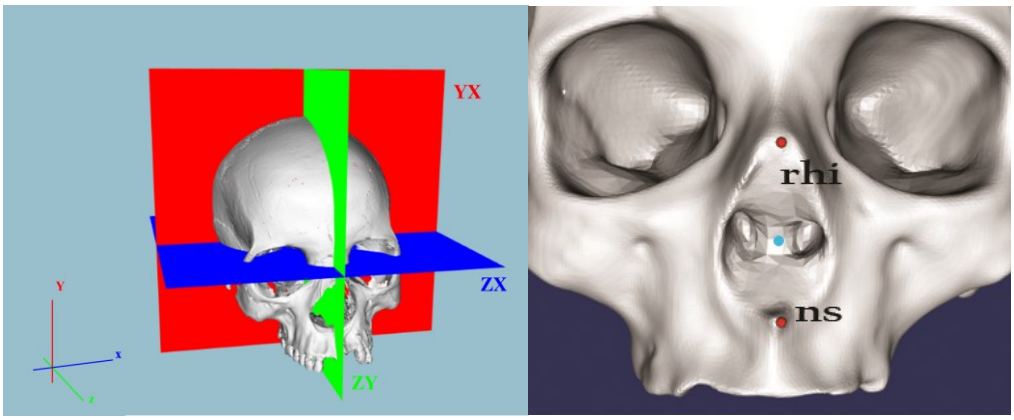

Figure 39 - Cartesian coordinate system, where plane x=0 (ZY-plane) is the Sagittal plane (colour green on the left), rhinion and the nasospinale points (right).

The next step is to create a method that analyses the 3D model in order to find the points that will define the structure.

We want to create a radial search algorithm with spatial partitioning, the idea is to find points defining the structure approximately equidistants. So, we determinate bounds by creating perpendicular planes to the plane z=0 (YX-plane), with the origin in the midpoint point and congruent angles between them (Figure 40) and doing so, we guarantee a radial search. The number of planes is defined by the resolution, chosen by the user in number of points, of the structure that we want to obtain. Bounds of the search are established based on the resolution selected by the user.

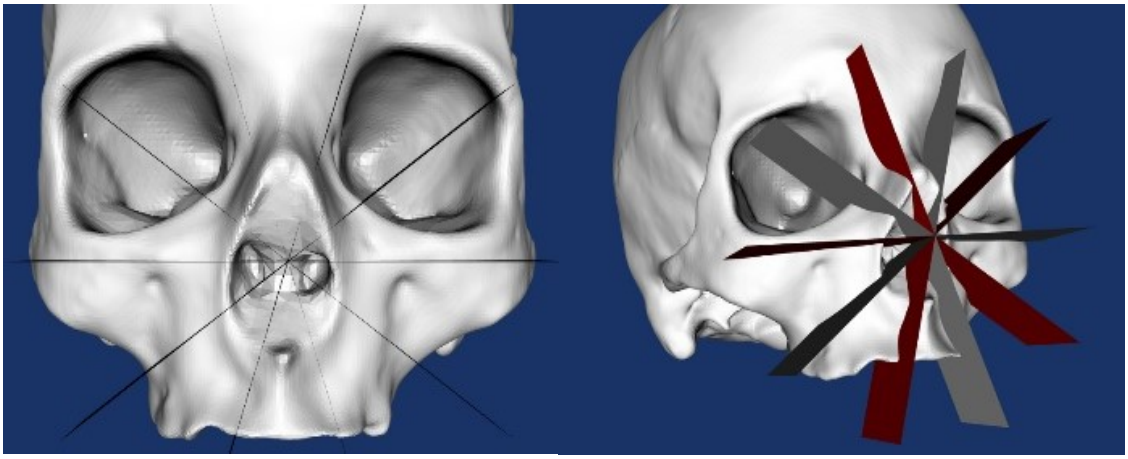

Figure 40 - Illustration of section bounds.

Analysing each point of the surface model, with Y-coordinate lower than the rhinion, looking for the point with the highest Z-coordinate, in each region (Figure 41).

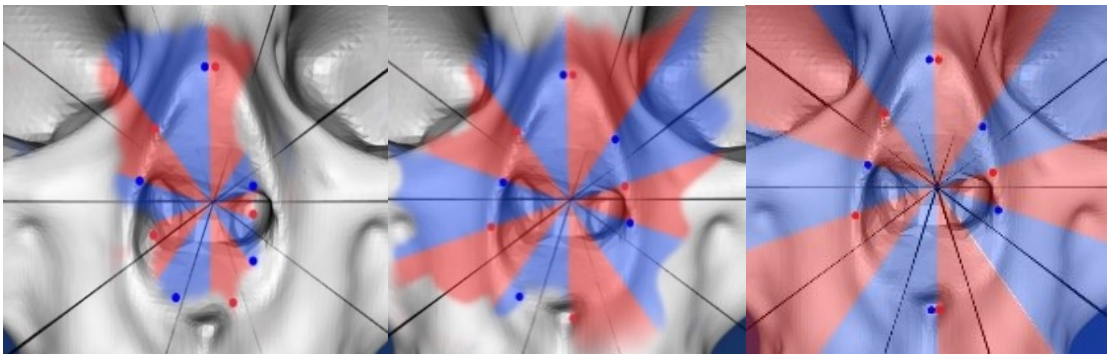

Figure 41 - Algorithm searching for the point with the largest z-coordinate in different sections.

Although, preliminary tests show the algorithm detected all points in the nasal structure, there were several skulls with pronounced prognathism (i.e. maxilla projection, very common trait in individuals of African ancestry), which has a larger projection than the nasal structure (Figure 42).

This creates a situation where the chosen points with the highest z detected by the region growing algorithm will not belong to the nasal structure.

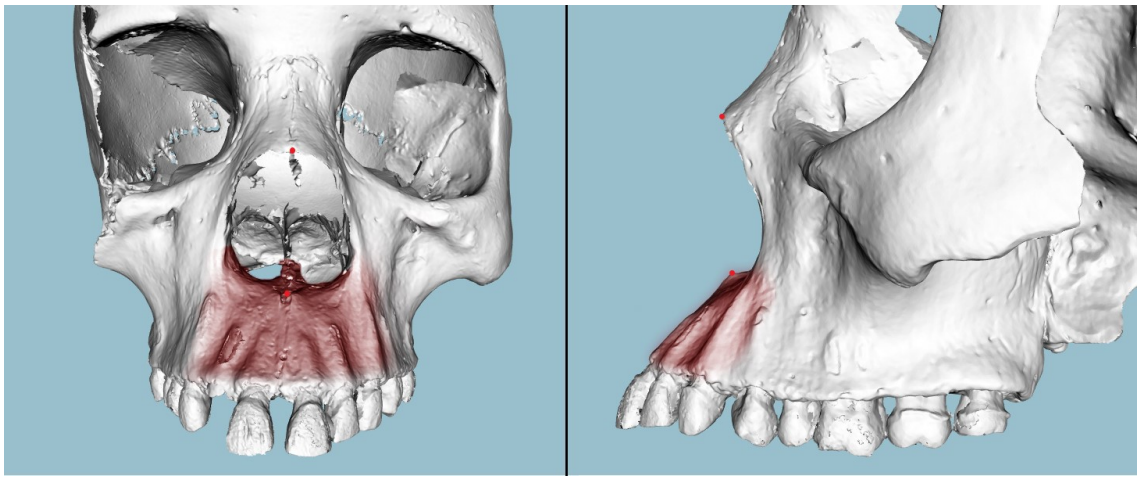

Figure 42 - Bottom area of the maxilla that has a larger projection than the nasal structure creating a situation where the method will not work.

To overcome this problem we tested two solutions. The first one is that no point could be chosen with a Z-coordinate higher than the most salient point of the rhi and ns. The second is to ensure that the points were limited by a XZ-plane defined by a distance of 5 below units of the ns (Figure 43).

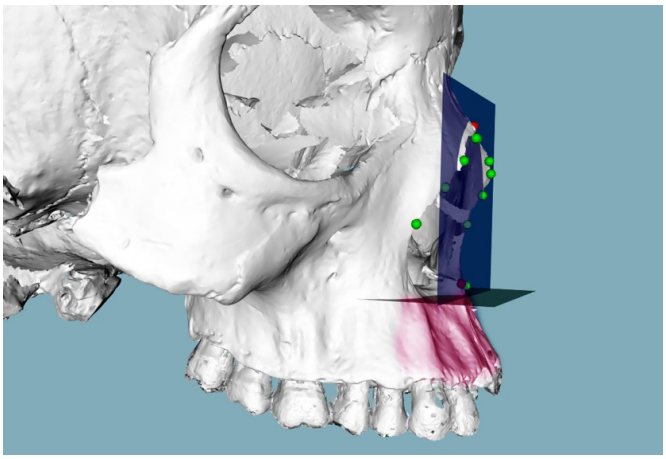

Figure 43 - Plane at the most salient point of the rhinion and nasospinale and a XZ-plane defined by a distance of 5 mm of the nasospinale.

Because this not resolve the problem (top, Figure 46) and knowing that this problem was only verified on the lower points of the nasal opening, we decided to create an area delimited by two planes parallel to XZ-plane (y=0), using a threshold characterized by the distance to nasospinale (passing in the point with Z-coordinated ns ± 5mm respectively)), where the points inside would only be considered by the algorithm if they intersect a sphere with center at the midpoint point, of the nasal opening, and passing at the nasospinale (Figure 44).

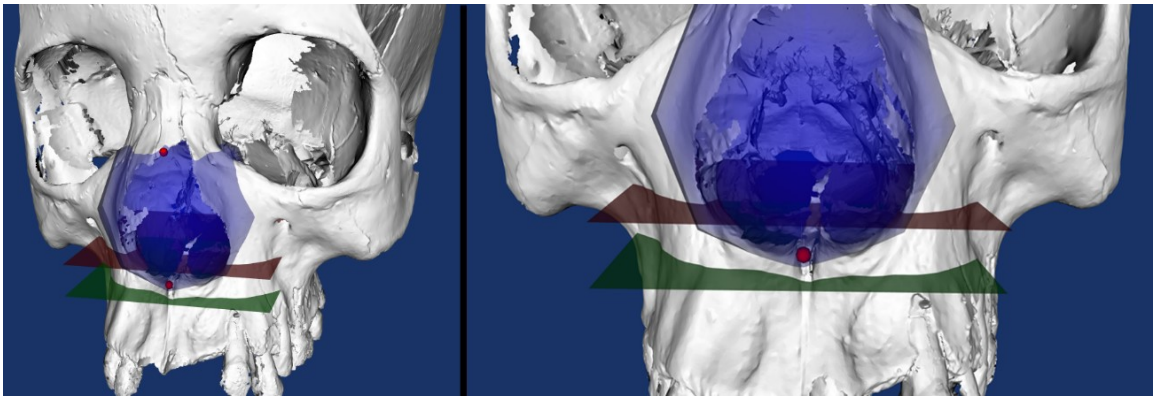

Figure 44 – Area between the two planes where the points are only considered by the method if they belong to the blue sphere.

This improvement allowed us to overcome the previously mentioned issue and made the algorithm more robust and effective for the situations where the bottom area of the maxilla has a larger projection than the nasal (Figure 45, bottom).

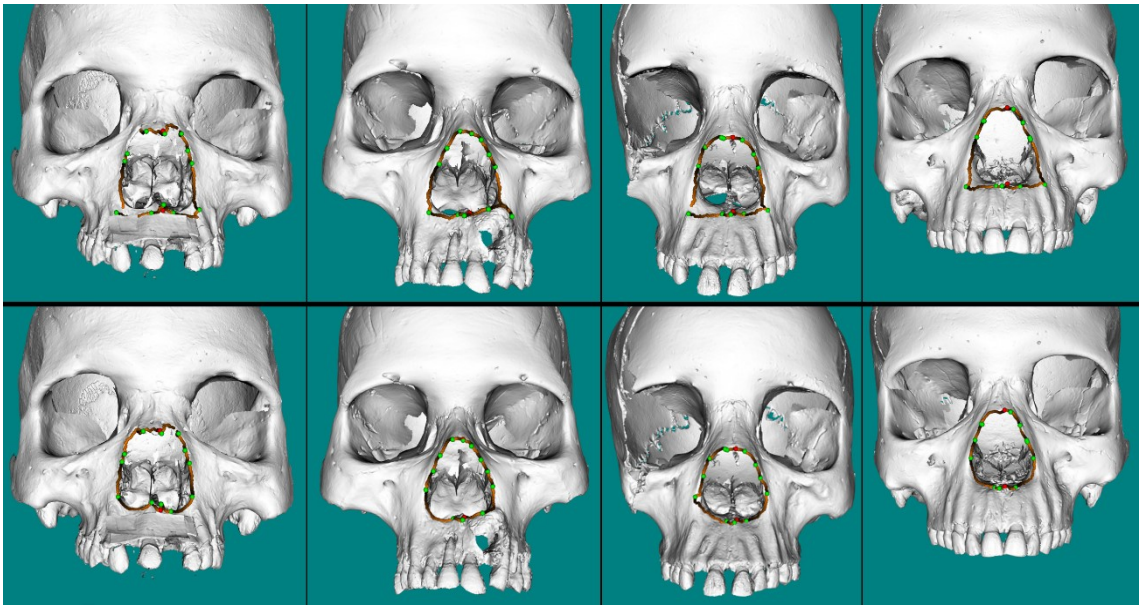

Figure 45 - Examples where the bottom nasal seeds (green points) found were not the correct ones (top image), and the results with the new modifications (bottom image) using 12 sections.

Connecting the obtained points and analysing the results with different resolution we could assess that the results with low resolution (10, 20 and 30 sections) produce in a 2D image without enough information to make an evaluation. When tested with a higher resolution (100 and 200 sections) too much noise was added (Figure 46). The initial results obtained using this algorithm were a good starting point. However, we could see that increasing the number of seed point the results were less satisfactory. So, the next step to improve the results was to use less seed points and connect them with another method.

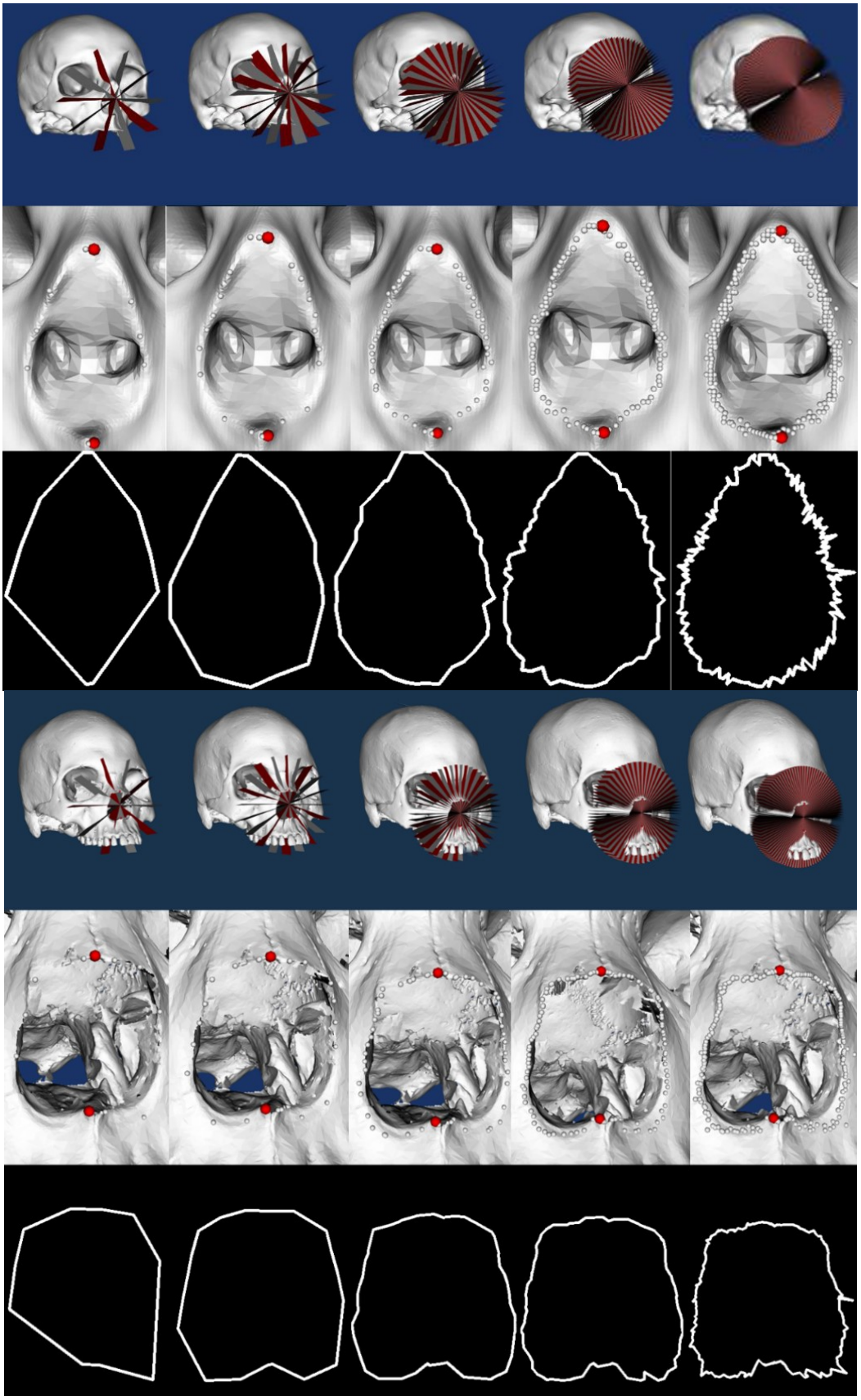

Figure 46 - Result of algorithm with two skulls and different resolutions, 10 - 20 - 50 - 100 - 200 points (Visualization on the skull on top and 2D at the bottom)

5.3.3 Closing the Nasal Structure

Curvature analysis of the models surface could reveal regions of interest since they have an accentuated variation on the surface. A method could be implemented to retrieve landmark points on these regions for further analysis (Santos, 2013).

Neves (2014) developed a semi-automatic method to detect the orbit structure. Initially, the user picks seed points and then their neighbourhood is analysed, based on maximum/minimum curvature, creating a list of points between the seeds. So, we adapted this method to connect seed points already discovered automatically (Figure 47).

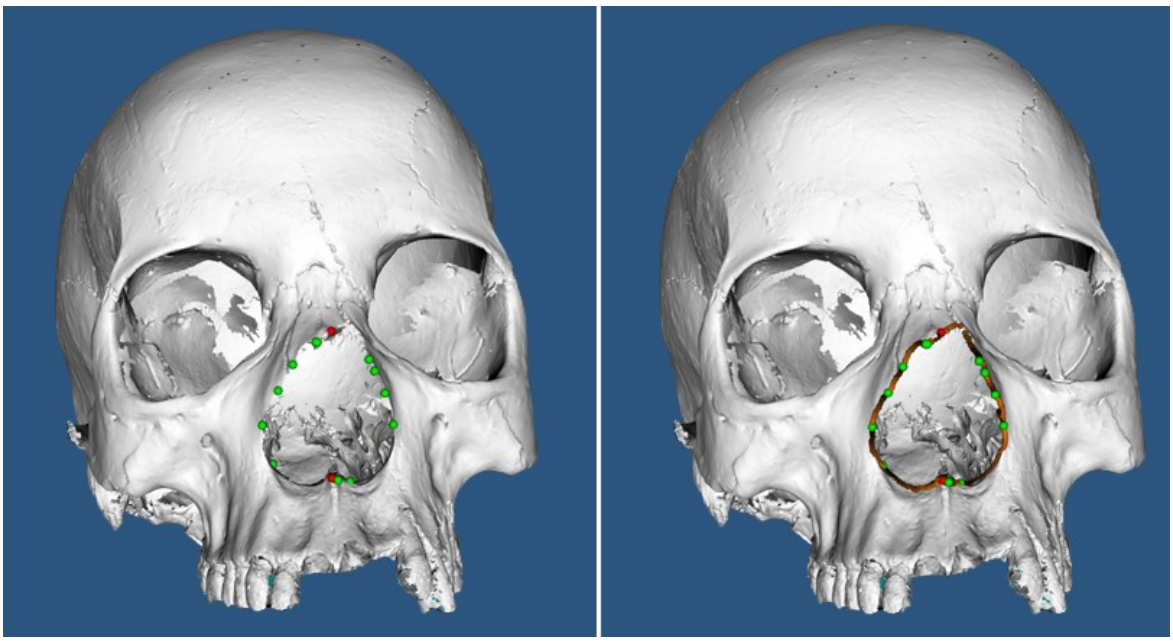

Figure 47 - New method developed to find the seed points (left), connected seed points with the existing method (right).

With the nasal structure identified, it is possible to determine the farthest coordinate for each side of the nasal opening, in order to calculate automatically the maximum width of the nasal aperture, i.e. the nasal breath measure (NLB).

5.3.4 Classification of the Nasal Opening

3D to 2D

The main focus should be the 2D shape of the nose, because we are comparing the structure with 2D reference images. After the extraction, the points are projected on the coronal plane in order

to get a 2D representation of the structure. This is accomplished by doing an orthographic projection in the coronal plane (plane z=0) (Figure 48).

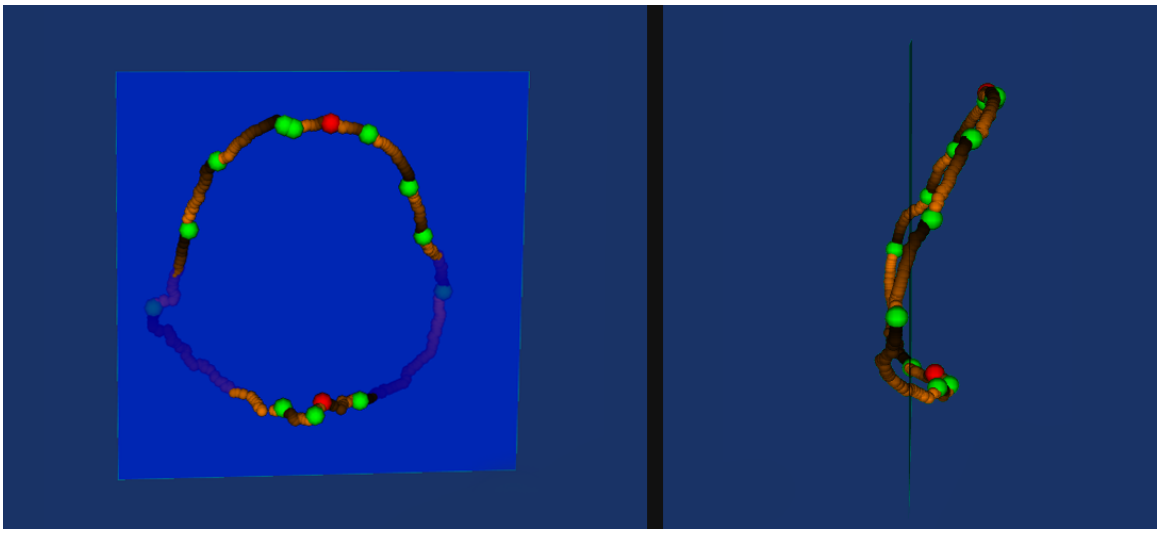

Figure 48 - Points 3D.

Even though all the projected points are situated on the plane, everything is still using a 3D coordinate system. In order to compare two images, it is required to discard the z, obtaining 2D points. The transformation is direct and done using the equation (4).

$$P(x, y, z) = P(x, y) \tag{4}$$

P(x,y,z) represents the coordinates of the 3D points, P(x,y) represents the coordinates of the 2D points

Using the 2D points as vertices of a polygon, it is possible to create a binary image, defined by a matrix of zeros and ones (0 Black, 1 white) (Figure 49).

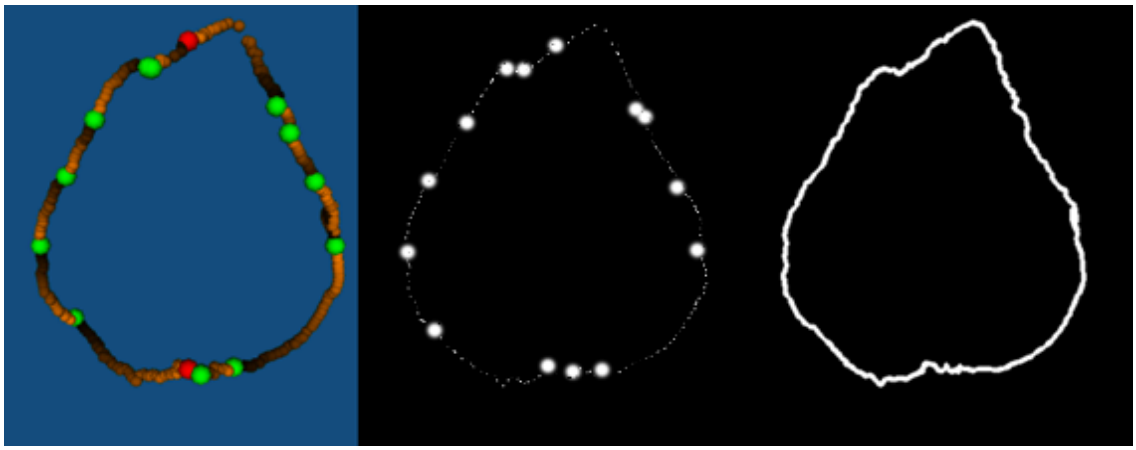

Figure 49 - Creating a 2D image from 3D Points.

Identification

To compare the structure with the standard images, adapted by Hefner (2009), it was necessary to ensure that they have the same proportions. So, we have to align all images and resize the three template images, ensuring that all have the same height as the structure representation.

At this time the comparison is possible, we just have to analyse each white pixel of the 2D representation of the nasal structure and find the closest white pixel of the template image (Figure 50). The euclidean distance is used to calculate the distance between each of these two points and represented by the following equation (5).

$$d(p,q) = d(q,p) = \sqrt{(p_1 - q_1)^2 + (p_2 - q_2)^2 + \cdots + (p_n - q_n)^2} = \sqrt{\sum_{k=1}^{k} (q_k - p_k)^2} \quad (5)$$

Where d represents the distance between two points in euclidean n-space, p and q. (p1, p2,..., pn) and (q1, q2,..., qn) represent the cartesian coordinates of the point p and q, respectively.

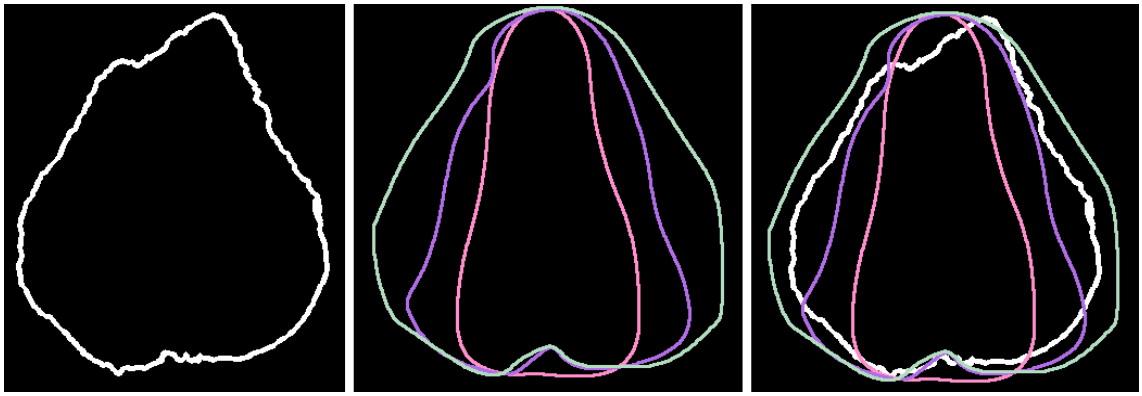

Figure 50 - 2D representation of the nasal structure (left), overlapping the nasal representation of three types of ancestry (middle), overlap of all images to identify the closest match (right).

Three new images are created where each pixel has the value of the distances, i.e. the distance of the respective template image to the closest point of the 2D representation of the nasal structure. If the pixel is black the distance value is zero. So at this stage, we get a measure, showing the similarity to each type of nasal structure by adding the distance value of each position. The one that produces the smaller value is the one that better identifies the structure (Figure 51).

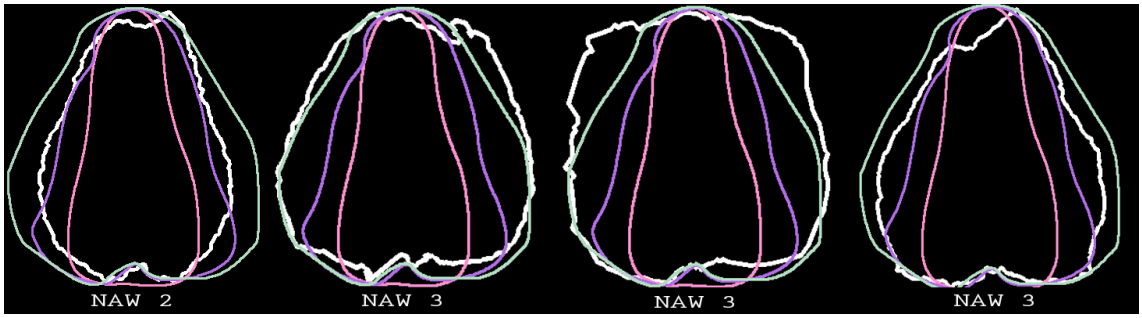

Figure 51 - Compare the result image (white) with the three-possible nasal aperture width.

The probability of the assessment, for each classification of the nasal aperture width, is given by the equation (6). This equation is obtained through the probability calculation applied to the sample space that results from the use of the inverse probability (because the shorter the distance the better the result).

$$p_x = \frac{d_1+d_2+d_3}{d_x^3 \times \sum_{i=1}^{3} \frac{d_1+d_2+d_3}{d_i^3}} \times 100\% \quad (6)$$

p_x is the probability of each classification and d_x is the mean euclidean distance.

d_1,d_2,d_3 is the mean euclidean distance to the respective Hefner image

5.4 Postbregmatic Depression (PD)

The postbregmatic depression is a morphologic characteristic observed in the lateral profile. It can be classified as present or absent (Figure 52).

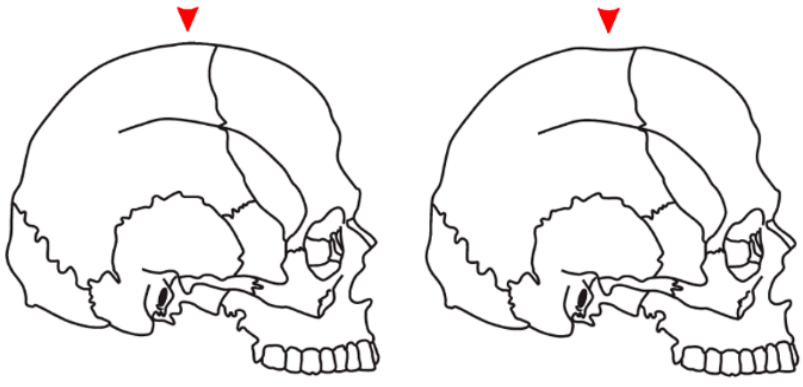

Figure 52 - Postbregmatic Depression absent (left) and present (right). Adapted from Hefner (2009).

The lateral profile is not the same that the cross section resulting from intersection between the plane (x=0) and the skull (Figure 32), so to automatize this non-metric trait, the first step was to

extract a 2D projection of the skull lateral profile. So, first we need to know how a 3D computer graphics library works, in this case VTK.

The users view the 3D objects through the viewport, a two-dimensional rectangle. The 3D scene, within the view frustum, is projected to the viewport window and can be seen on screen. The view frustum is the 3D volume defined by the near and far clipping. It is the field of view of the fictional camera. The amount of information that gets included in a rendering is limited by a minimum and maximum depth from the viewport. The front and back clipping planes intersect the projection vector and are used to eliminate date either too close or too far away from the camera (Ferraro, 1995; Schroeder et al., 2006) (Figure 53).

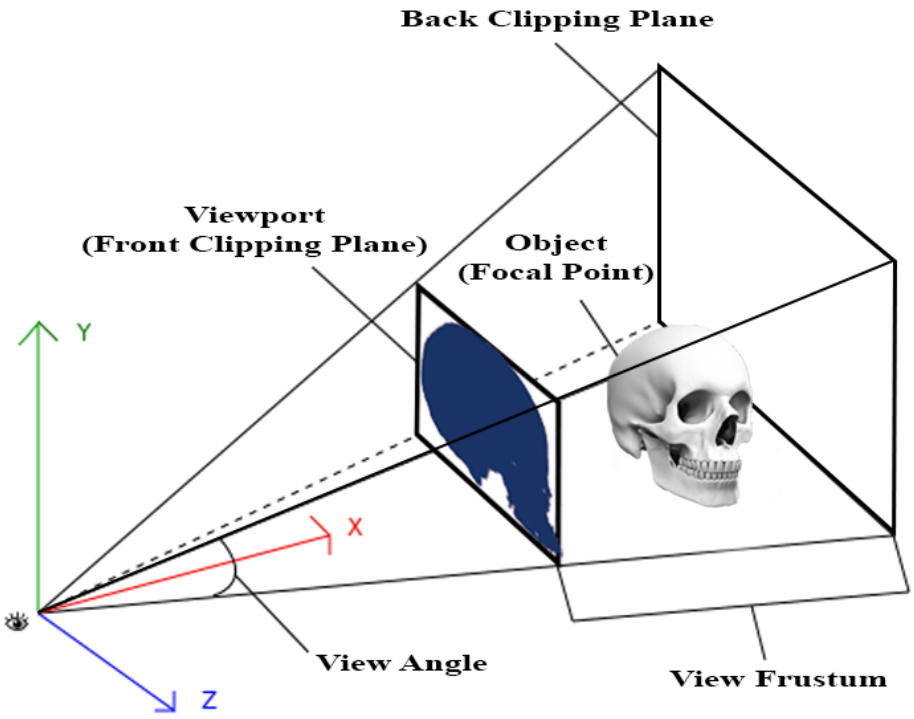

Figure 53 - The diagram illustrates the idea behind perspective projection. Adapted from Schroeder et al. (2006).

Based on this information, we obtained the 2D lateral profile of the skull by extracting the image being projected in the viewport when the camera is positioned at a ninety-degree angle. We compute the external contour of the 2D image (Figure 54) in order to analyse it. The contour is constituted by a list of 2D points.

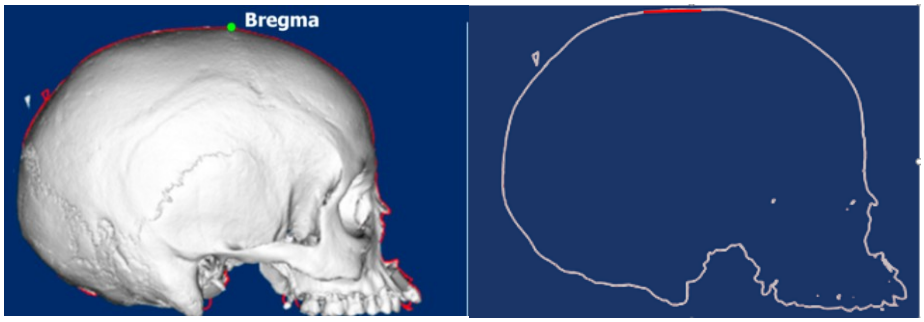

Figure 54 - External contour of the 2D lateral profile of the skull.

With *a priori* knowledge we know the postbregmatic depression is a slight depression along the sagittal suture and posterior to bregma. So this trait is verified in the section between the bregma (point A) and the point with highest y coordinate and also posterior to bregma (point B). With this information, the idea is to analyse the points in this section and calculate if the majority of them is higher or lower than an imaginary line between point A and B. If lower, we classified the postbregmatic depression as present, otherwise it is classified as absent (Figure 55).

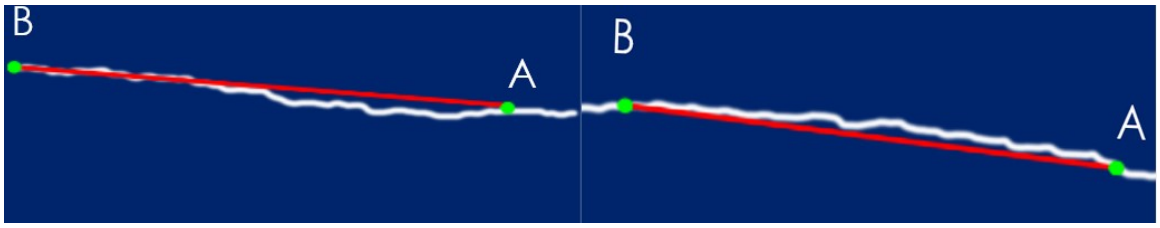

Figure 55 - The idea is to calculate if the majority of the points is higher or lower than an imaginary line between point A and B. If lower, the postbregmatic depression is classified as absent (right) otherwise, it is classified as present (left).

5.5 Anterior Nasal Spine (ANS)

Hefner (2009) states that the anterior nasal spine is assessed as slight, intermediate, and marked (Figure 56).

- Slight: minimal-to-no projection of the ANS beyond
- Intermediate: a moderate projection of the ANS
- Marked: a pronounced projection of the ANS beyond the INA (inferior nasal aperture).

One of the common problems when classifying the ANS is the severe fragility of the area, which often presents defects peri- or post-mortem.

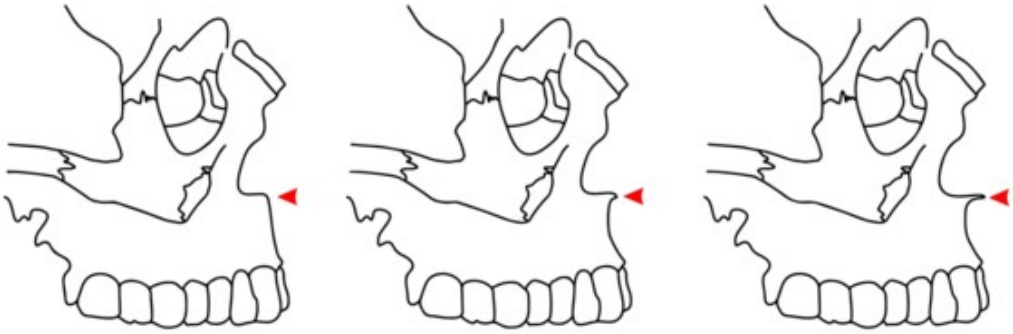

Figure 56 - Different state representation of the anterior nasal spine morphology. Classification as slight (left), intermediate (middle) and marked (right). Adapted from Hefner (2009).

The method developed to evaluate the anterior nasal spine is based on the position of the nasospinale landmark, which has become an automatic point (process explained in section 5.3.1). The next step is to analyse all points in the vicinity (within a five millimetres distance) of the nasospinale and in the cross-section, resulting from a cut made in the plane parallel to YZ-plane and that passes in the nasospinale, using the cut tool previous developed, explained in section 3.2.4 (Figure 57).

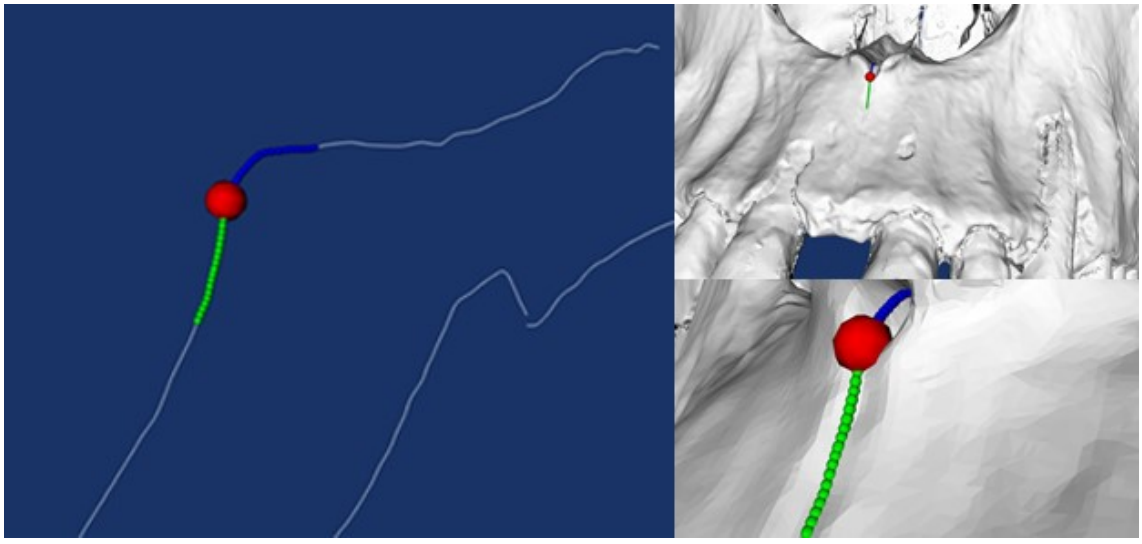

Figure 57 - Skull(right) and the cross-section resulting from a cut made in the plane parallel to YZ-plane containing in the nasospinale (left). Red dot is the nasospinale, the blue and green dots are the points at five millimetres before and after the nasospinale respectively.

The classification processed is based in two phases. The first one is to ascertain if the projection of the ANS is wider than the nasal structure, analysing the points beyond the nasospinale. If all points have a Z-coordinate higher that the nasospinale is classified as slight, this is possible analysing the points above and below the nasospinale (blue and green respectively in Fig. 59). Otherwise the process passes to phase two that analyses the projection of the ANS. To differentiate a moderate

from a pronounced projection of the ANA, using equation (7). If the projection is outside the area defined by the equation it is designated as intermediate, else it is marked (Figure 58). The values that define the area were calculated empirically (in fifty models), in order to obtain the best results.

$$P_y > N_y - t_y \quad \cap \quad P_z < N_z - t_z \tag{7}$$

Pz and Py are the coordinates of the point being analysed.
Nz and Ny are the coordinates of the nasospinale.
tz and ty are values that define the area.

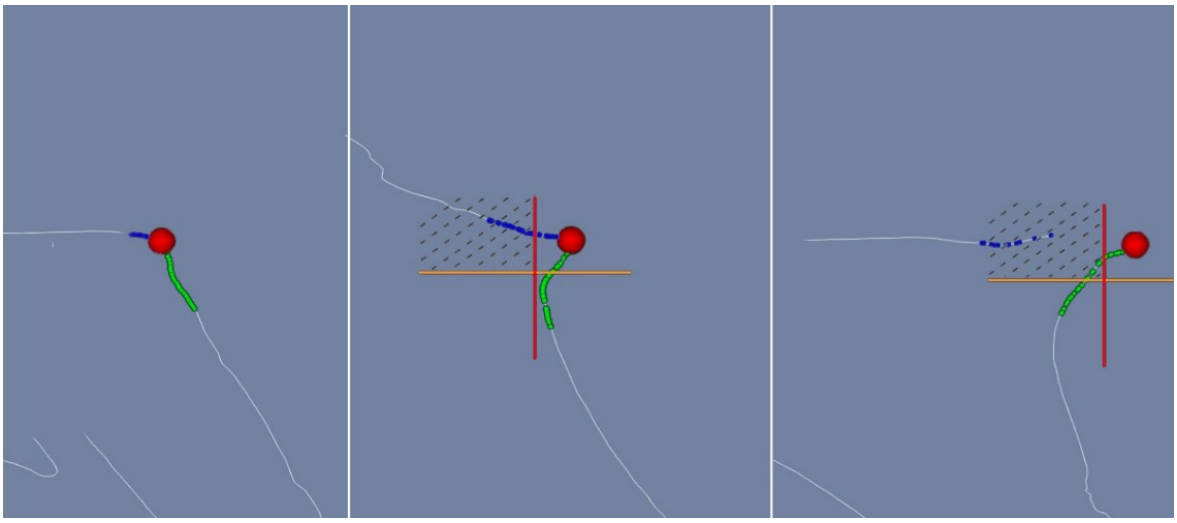

Figure 58 - Classification as slight (right), intermediate (middle) and marked (left). The axes and the dashed lines represent the area that allows to differentiate the classification intermediate and marked.

There was another way of detecting this trait, the difference was in the process of obtaining the anterior nasal spine and not in classifying it. The idea was to use the same method as in the postbregmatic depression, the profile of the skull, instead of the points in the nasospinale plane (Figure 59). The rest of the process remained the same. However, this approach was not explored, due to the good results already obtained.

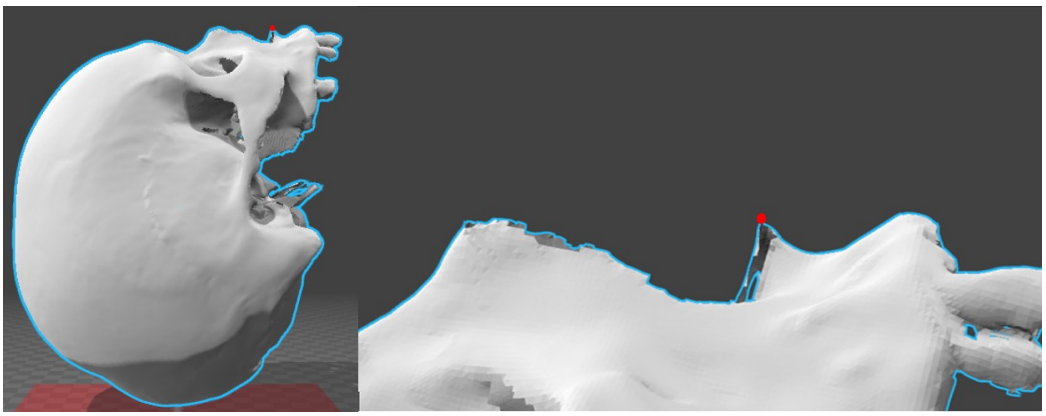

Figure 59 – Another possible approach to detect the anterior nasal spine.

5.6 Other Morphologic Traits

In this section, two characteristics that initially showed good probability of being determined are presented, but the developed methods were not conclusive and further work would be necessary to get viable results. The anthropologists said that the definition of the inferior nasal aperture and the nasal bone contour given by Hefner (2009), when applied in the real world, it was very difficult to make a classification and in most of the cases the specialist couldn't reach a consensus.

5.6.1 Inferior Nasal Aperture (INA)

The inferior nasal aperture is a combination of the most inferior portion of the nasal aperture and the lateral alae, constituting the "transition from nasal floor to the vertical portion of the maxillae, superior to the anterior dentition" (Hefner, 2009). The INA is classified according to shape of the nasal aperture inferior boarder. When the bilateral asymmetry is present, the left side must be used.

The possible classifications are (Figure 60):

1. A smooth transition resulting from an inferior sloping of the nasal floor beginning within the nasal cavity and terminating on the vertical surface of the maxilla;
2. Sloping of the nasal aperture beginning in a position more anteriorly than in INA 1, and with more angulation at the nasal opening exit;
3. The transition between the nasal floor and the vertical maxilla is not slopping, nor is there an intervening projection. Most of the times, this morphology is a right angle;
4. A discrete vertical ridge of bone that traverses the inferior nasal border created by a superior inclination of the anterior nasal floor;
5. An evident and conspicuous ridge obstructing the nasal floor-to-maxilla transition.

The morphology INA1 is distinct from INA2 regarding the more posterior origin and the greater slope.

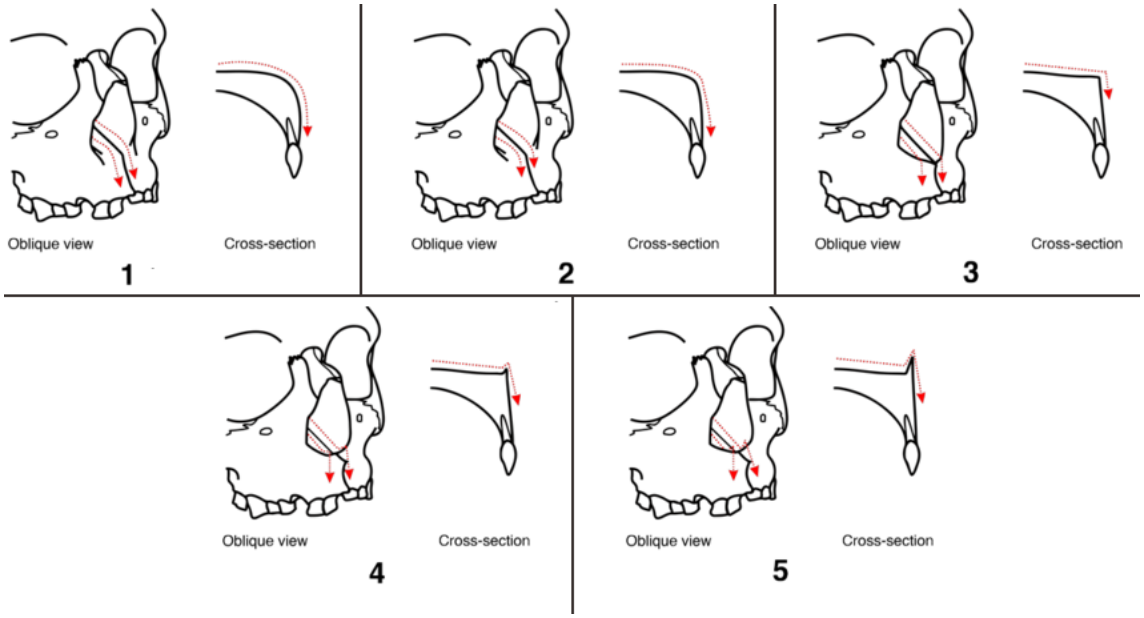

Figure 60 - Different state representation of the inferior nasal aperture morphology. Adapted from Hefner (2009).

We create a similar method to the one used to obtain the anterior nasal spine, explained in section 5.5. Cut the skull in a parallel plane to YZ-plane, with a distance of five millimetres to each side of the nasospinale landmark (Figure 61). Then find the point with more transition slope, where occurs the transition between the nasal floor and the vertical maxilla (point x), and analysed the points before and after. Three methods were developed to evaluate INA.

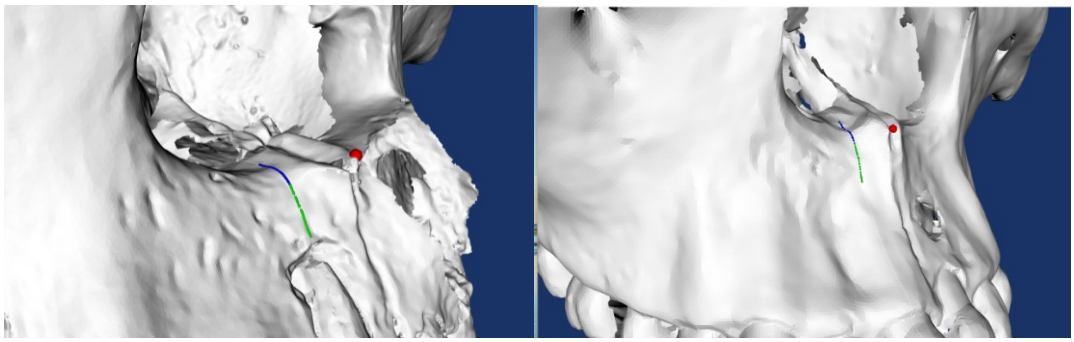

Figure 61 - Two representations of the relevant point in the skull resulting of a cut in a plane parallel to the YZ-plane, with a distance of five to ten millimetres to one side of the nasospinale landmark.

The first step of evaluation was to see if the points before point x had a Y-coordinate higher or lower, allowing to differentiate the classification one, two, and three from four, and five respectively. Relatively to one, two and three we try to calculate the slope. To distinguish four to five, we analysed the height of the ridge. Although the first step showed good results, no conclusions could be taken from the second step. Initially, we tried to analyse the slope of the curve, then we tried to find the max slope presented in one millimetre distance to point x, however, none of these alternatives provided good results.

The second method was an adaptation of the algorithm used in section 5.3.4 to identify the nasal aperture width, by comparing the structure detected with the standard images, adapted by Hefner (2009), ensuring the proportions and centralizing the images at the location of point x. As before, each black pixel of the 2D representation of the morphology is analysed (Figure 62). With the five images, the results obtained were very close to each other, so a third method was developed.

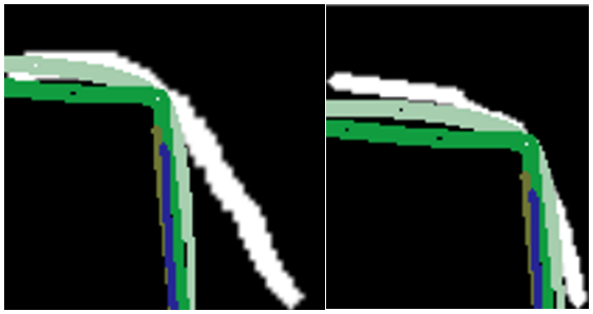

Figure 62 - Two different 2D representation of the inferior nasal aperture overlapping with the five possible classifications, in order to identify the closest match.

The third method merged the first two methods, by creating two groups with the classifications one, two, and three and other with the four, and five. Then, comparing the 2D projection of the inferior nasal aperture with the images of the respective group. Not presenting better results than before the method was dropped.

5.6.2 Nasal Bone Contour (NBC)

Nasal bone contour is the contour of the midfacial region, ten millimetres below the nasion. According to Hefner (2009), the visual evaluation of the morphology is not very effective, because of the high inter- and intra-observer variability, advising the use of auxiliary tools, like the contour gage. When performing the evaluation using the contour gage, the anthropologists are instructed to place it directly on the nasal bones (10 mm) inferior to nasion landmark and maintaining the tool perpendicular to the palate (Annex 3, Fig.7) and parallel to the orbits.

The NBC possible classifications are (Figure 63):

1. NBC rounded and low;
2. NBC elongated, high, with rounded lateral walls and oval shape;
3. Steep sidewalls and a broad flat upper surface “plateau”
4. Steep sidewalls and a narrow superior surface ‘‘plateau’’;
5. Cross-section is triangular, lacking a superior surface ‘‘plateau’’;

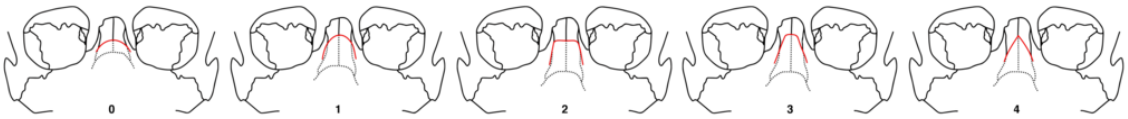

Figure 63 - Different state representation of the nasal bone contour morphology. Adapted from Hefner (2009).

As defined above, to determinate the position of the nasal bone contour, we first need to find the location of the nasion, a manual point in the application. Then, after meeting with the experts it was agreed that we should use the cut tool, explained in section 3.2.4, in order to obtain the cross-section between the skull and the YX-plane that passes in a point ten millimetres below the nasion (the starting point). The anthropologists defined that the points at less than twenty millimetres to each side and below the starting point, are analysed.

As in section 5.6.1, the idea was to adapt the algorithm used in section 5.3.4 to identify the nasal aperture width. So, overlapping the nasal bone contour with the ones in the standard images (adapted by Hefner, 2009) and using the euclidean distance, we could calculate the most similar. The proportions are ensured by the measures, applied above, used to define the area of analysis (Figure 64).

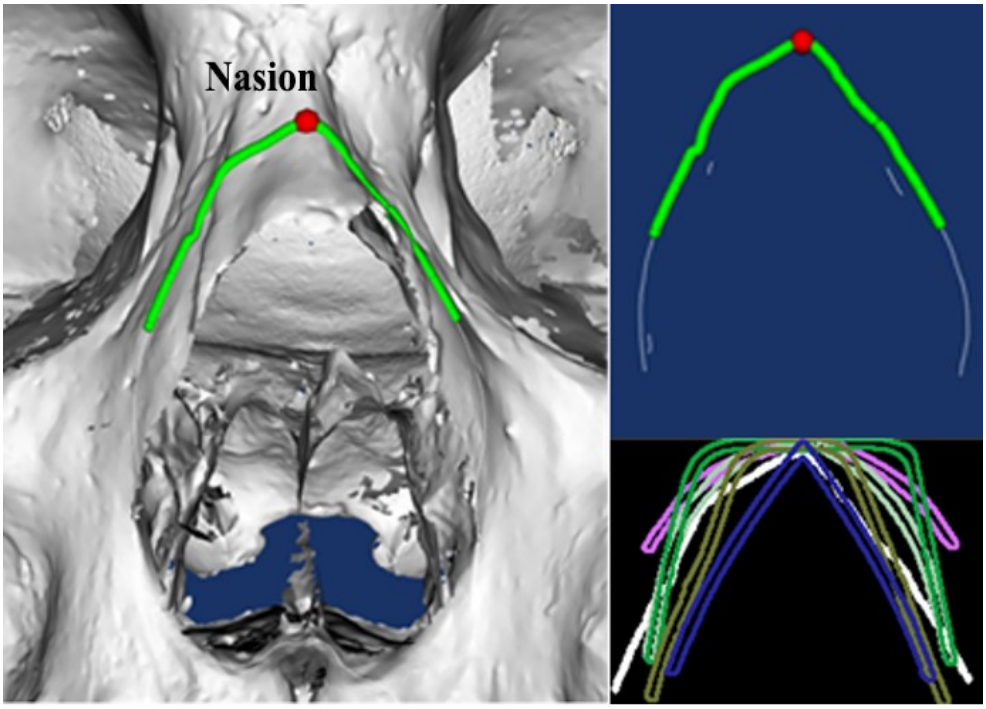

Figure 64 - 3D (left) and 2D (top right) representation of the nasal bone contour overlapping with the five possible classifications, in order to identify the closest match (bottom right).

The results obtained were not promising. The large number of possible classifications and the similarity among them created almost identical results, making impossible a clear classification.

After discussing the issue with the anthropologist, it was considered that a lower number of possible classifications using also their frequency values, might improve the results producing a more precise classification in the four ancestral groups; however, no more work regarding this method was conducted.

5.7 Gender - Cranial shape analysis from landmarks

In Bass (2005) and Byers (2011) the pelvis is defined as the most reliable indicator of sex assessment and the skull the second best. The taphonomic processes (processes responsible for the decaying organisms over time and how they become fossilized), resulting from the individual being left in an outdoor context, causes, many times, the skull to be the only part remaining of the skeleton (Spradley & Jantz, 2011).

In a meeting with the anthropologist, it was decided to develop a 3D geometric morphometric technique in order to perform individual gender classification. Morita, Ogihara, Kanai, & Suzuki (2013) developed a technique of neurocranial quantification of shape variation using the shortest paths connecting pairs of anatomical landmarks. In this study, a method that could define landmarks on neurocranium surfaces (Figure 66) is presented allowing a comparison through the analyses of the skull shape. The idea is to create a data set of landmarks that could be later transformed into an understandable structure allowing to make predictions (Figure 65).

A plugin called CraMs MA (Craniometric Measures Mesh Analyser) was developed that reads a file containing the skulls database and for each one, reads the respective CraMs output file (with the points positions and measures) and creates a data set of landmarks. The user must specify the number of neurocranium divisions and how many landmarks each division should have.

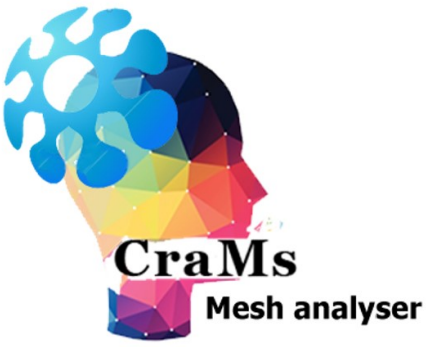

Figure 65 -Craniometric Measures Mesh Analyser Application Icon.

To ensure that only the neurocranium is analysed, the skull is divided using a plane defined by the opisthion and the nasion landmarks (Figure 66).

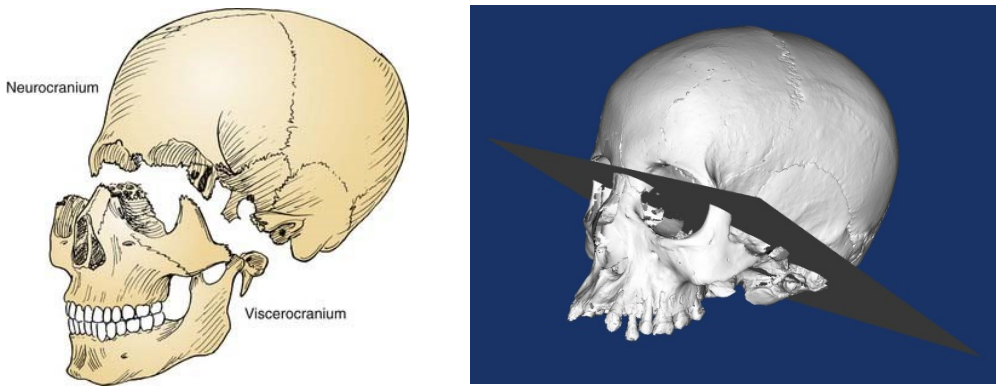

Figure 66 - Skull divided showing the junction of the neurocranium with the viscerocranium in the manual (left) (Flint et al., 2015) and the application (right).

Once divided, the neurocranium is sliced in equiangular parts, according to the user input, between the nasion and the opisthokranion (Figure 67). The opisthokranion is chosen, in preference to the opisthion, because, in addition to being an automatic point the opisthion is often missing.

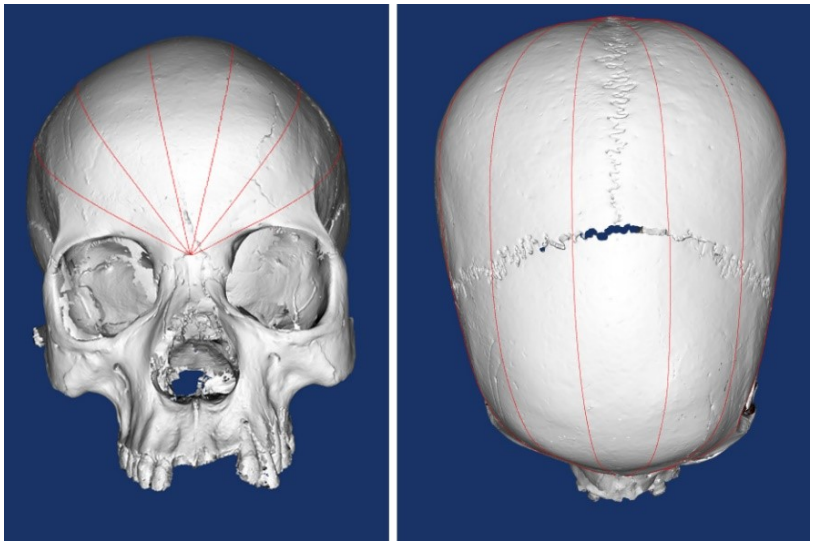

Figure 67 - Neurocranium diveded in equiangular parts between the nasion and the opisthokranion.

Each surface line is measured and divided (Figure 68), according to the user input, and each point originates a landmark. A file is created, containing the landmark list of each skull. This file is then used in a machine learning algorithm that, knowing the gender of each skull, can recognise patterns and make a method for gender classification. This was possible with the collaboration of the anthropologists, that based on a similar work done but with the talus, they use the files created by CraMs MA to evaluate the performance of several machine learning algorithms. the conjunction of this files form a landmarks database, that contains the skull shapes.

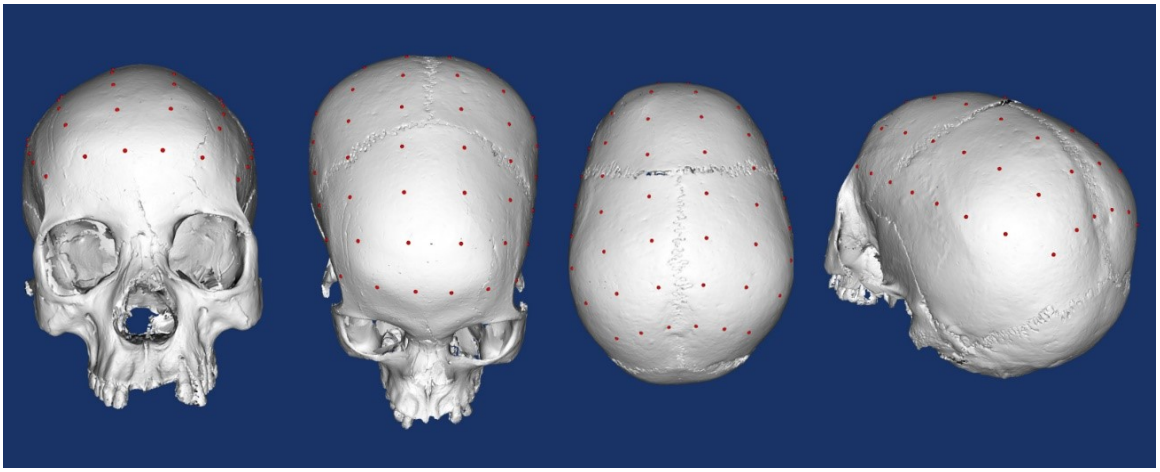

Figure 68 - Each surface line is measured and divided. Each coordinate originate a landmark.

As long as the landmarks are obtained from labelled skulls (with known sex), the machine learning algorithms can be trained to learn the geometrical features of both factors (i.e. 'male' and 'female') and then predict and identify the unlabelled ones. The statistical shape analysis was performed using R (Team, 2015) with the aid of *geomorph* and *caret* packages (Adams, Collyer, Sherratt, & Adams, 2016; Kuhn, 2008).

The processed data was trained using ten different well-established machine learning algorithms (Table 7) with 5-fold cross-validation as a default sampling parameter. Useful statistical metrics such as predictive value, sensitivity, and overall accuracy are also calculated. Results can be consulted in section 6.8.

"Statistically, the most efficient use of the data is to train the model using all of the samples and use resampling (e.g., cross-validation) to evaluate the efficacy of the model." (Kuhn, 2008). Cross-validation techniques were used to avoid overfitting and obtain reasonable accuracy metrics

Table 7 - List of classification algorithms used in our test-study.

MODEL	ARGUMENT VALUE	PACKAGE	TUNING PARAMETERS
SINGLE C5.0 RULESET	`C5.0Rules`	C50	None
SINGLE C5.0 TREE	`C5.0Tree`	C50	None
K-NEAREST NEIGHBOURS	`knn`	base	k
SUPPORT VECTOR MACHINES (SVM) WITH LINEAR KERNEL	`svmLinear`	kernlab	C
SVM WITH POLYNOMIAL KERNEL	`svmPoly`	kernlab	degree, scale, C
SVM WITH RADIAL BASIS FUNCTION KERNEL	`svmRadial`	kernlab	sigma, C
NEURAL NETWORK	`nnet`	nnet	size, decay
LOGISTIC MODEL TREES	`LMT`	RWeka	iter
RULE-BASED	`JRip`	RWeka	NumOpt
REGULARIZED DISCRIMINANT ANALYSIS	`rda`	klaR	gamma, lambda

6 Results

6.1 Overview

This chapter aim is to discuss and validate the results obtained throughout this work. Firstly, the results of the nasal breath measure (NLB) are presented and the results from the variability and error analysis of measures by two domain experts using both methods are compared. Next, the preliminary results concerning the influence of using low resolution models, acquired by the NextEngine 3D Scanner, on fully automatic measures are presented. These results analyse the reliability of using the new models while keeping measures accuracy within a reasonable value. The results presented regard measures of eight skulls used by Neves, 2014. Then, the results of the morphologic traits successfully detected, run in fifty-one skulls, are presented (the nasal aperture width, the anterior nasal spine and the postbregmatic depression) and finally, the results from the gender classification.

6.2 Nasal Breath Measure

As explained in section 4, determining the nasal aperture width made possible the nasal breath measure (NLB) automation.

Table 8 presents the nasal breadth measure (NLB) taken by two anthropologists (CC and MT) using traditional methods (Traditional) and using the application, manually (App Manual) and Automatically (App Auto), on eight different specimens.

Table 8 - Nasal breadth measure taken by two Anthropologists using CraMs (automatic e manual method) and using traditional methods (in mm).

ID	App Auto	Anthropologist #1		Anthropologist #2	
		Traditional CC	App manual CC	Traditional MT	App manual MT
21	28	28	26	27	30
25	29	28	28	27	29
38	25	24	24	24	27
39	26	27	26	25	28
57	26	27	25	24	27
65	33	34	32	30	32
66	29	30	29	27	30
67	26	26	26	25	27

The results suggest that the measures obtained with the application, manually and automatically, are similar and in some cases are identical. Between measures obtained with traditional methods and CraMs, the disparity obtained can be considered in most cases better or similar to the disparity between anthropologists using the traditional methods. To further investigate the results obtained, a deeper analysis was performed, which is shown in the next section.

Inter- and Intra-Observer variability

To corroborate the improvements observed using CraMs extra studies were performed. The variability of the measurement, between the same and different methods, was calculated as well as the standard deviation. Anthropologists already do the calculation of the variability to evaluate the measurements taken with the traditional methods. Therefore, its use will allow the evaluation of the measurements using the application in a more coherent and comparable way.

Inter-observer variability represents the variation that results on the same measurements taken by different experts. Intra-observer variability represents the variation when the same expert takes the measurements at different times. The problem is that since the measure to be analysed is automatic, the inter- and intra-observer variation will always be zero. So, we consider the Intra-

observer variability represents the variation when the same expert takes the measurements at different times, but always with a different method.

Figure 69 shows the intra-observer and Figure 70 the inter-observer variability in percentage by both anthropologists (CC and MT), using CraMs (APP and Manual) and Traditional methods (Traditional). Mean values are represented as rhombus, the maximum and minimum values are expressed as the limits of the vertical lines. These results were obtained from tests conducted in eight specimens by the two anthropologists and using both methods.

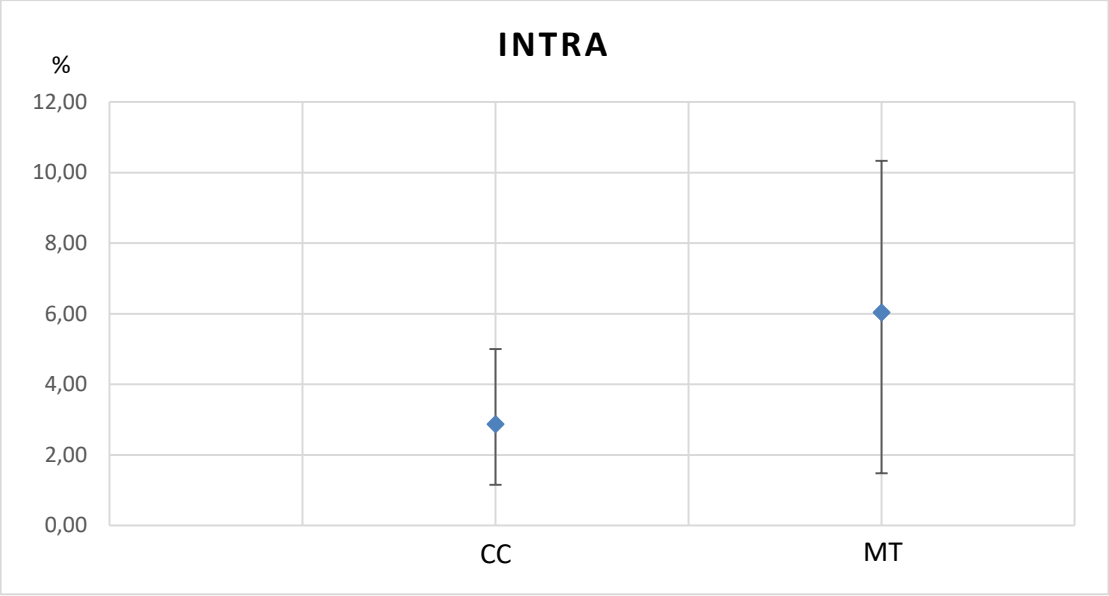

Figure 69 - Bar plots with the intra-observer variability in percentage for the measure of the nasal breath of each specialist (CC and MT) using CraMs (automatically and manually) and traditional methods.

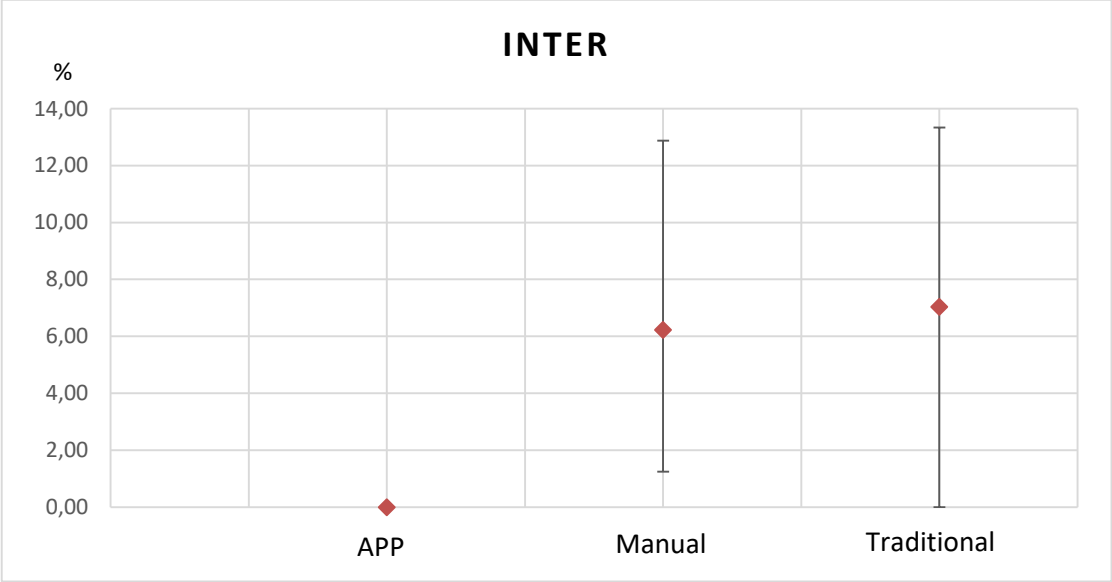

Figure 70 - Bar plots with the inter-observer variability in percentage for the measure of the nasal breath between specialists using CraMs, automatically and manually, or traditional methods.

In order to quantify the variation, using the new automatic method, a table was created. The idea is to compare the measurements obtained by experts with different methods (Table 9).

Table 9 – Comparison of differences between the measures obtained by the experts with different methods. Units in mm.

ID	CC			MT		
	Auto - Traditional	Traditional - Manual	Auto - Manual	Auto - Traditional	Traditional - Manual	Auto - Manual
21	0	2	2	1	3	2
25	1	0	1	2	2	0
38	1	0	1	1	3	2
39	1	1	0	1	3	2
57	1	2	1	2	3	1
65	1	2	1	3	2	1
66	1	1	0	2	3	1
67	0	0	0	1	2	1
mean	**0.75**	**1**	**0.75**	**1.63**	**2.63**	**1.25**

The measurements taken, using CraMs do not produce an inter-observer variation because its calculation is completely automatic, thus, creating always the same results. In Table 10 the results are synthetized for easier interpretation, by showing the average difference percentages for each method.

Table 10 - Average difference percentages of inter-observer variation obtained for the NLB.

App	Manual	Traditional
0.00	6.23	7.04

A typical way to indicate the error margin in craniometry is using the technical error of measurements (*TEM*) (Perini, Oliveira, Ornellas, & Fátima Palha de Oliveira, 2005). This value is the consequential variability from repeated measurements. This method was used by Santos (2013) and Neves (2014) to validate the measures and quantify the inter- and intra-observer errors, so it will also be used to validate the NLB. It's calculated by equation (8) followed by equation (9).

$$Absolute\ TEM = \sqrt{\frac{\sum d_i^2}{2n}} \tag{8}$$

$$Relative\ TEM = \frac{Absolute\ TEM}{VAV} * 100 \tag{9}$$

Where d = measures deviation, n = number of measures, i = index of the measure, *TEM* = Technical error of measurement (expressed in percentage), *VAV* = Variable average (average of the average between all the observations, for each measure).

TEM values between 0% and 10% usually indicates that the measure is valid. Values above are usually not seen as legitimate when assessing inter-observer measures. For intra-observer measures the values must be between 0% and 7.5%. In the calculation of TEM values for the intra-observer, the measurements taken by each expert with the traditional methods and with CraMs, were considered.

Considering the TEM Values in Table 11, we can easily see that the different experts have a higher variability between them, using traditional methods, than each one with the application CraMs.

Table 11 - Relative TEM values for inter-observer, different experts with the same method (orange) and intra-observer, the same expert using traditional methods and the application, automatically (App) and manually (Manual) (Blue). Values in percentage.

App	Manual	Traditional	CC	MT
0.00	5.38	5.92	2.38	4.56

6.3 Results with the NextEngine

As seen in section 2.4, there is a reduction in the accuracy and detail of the models resulting from the acquisition process with the new NextEngine 3D Laser Scanner. This resulted in some concern regarding the variability of the measures taken with this scanner when compared with the measures obtained with the high resolution models and with the traditional methods. A decrease of the measures accuracy could put in jeopardy the use of the application with experts that use this scanner. Thus, to assess the results obtained with the models produced by the new scanner, automatic measures were retaken with the new models. This process was previously performed on analysed skulls acquired with the Breuckmann, by Neves (2014).

Table 12 presents the three automatic measures (ZYB - bizygomatic width, BBH - Basion-Bregma height, XCB - maximum skull width) taken by CraMs (App) and by two anthropologists using traditional methods (Antr), on eight specimens acquired with the NextEngine scanner. Measures with the value β (highlighted in bold) were considered to be difficult to obtain manually by the experts for that specific specimen, so as no conclusions could be taken for these models, we didn´t take measures with the application. Table 12 shows the three CraMs automatic measures taken in models acquired with the Breuckmann scanner.

Table 12 - Measures taken by two experts using CraMs automatic (with models acquired with the NextEngine scanner and the Breuckmann scanner) and traditional methods. The measures with the value β were considered difficult to obtain by the experts for that specific specimen.

Measure	Specimen #21				Specimen #25			
	User #1	User #2	NextEngine	Breuckmann	User #1	User #2	NextEngine	Breuckmann
1 - ZYB	β	β	β	β	136	137	137	136,7
2 - BBH	β	β	β	β	142	143	142,7	142,7
3 - XCB	124	126	128,8	127,5	131	131	135	135

Measure	Specimen #57				Specimen #65			
	User #1	User #2	NextEngine	Breuckmann	User #1	User #2	NextEngine	Breuckmann
1 - ZYB	β	β	β	119,4	134	136	136,1	β
2 - BBH	β	β	β	132,9	139	139	140,1	133
3 - XCB	137	137	138,2	137,7	123	124	130,3	121,3

Measure	Specimen #38				Specimen #39			
	User #1	User #2	NextEngine	Breuckmann	User #1	User #2	NextEngine	Breuckmann
1 - ZYB	119	121	121,8	β	β	β	β	136,2
2 - BBH	133	133	130,2	β	132	133	134,4	138,8
3 - XCB	136	137	137,9	138,6	114	117	121,4	β

Measure	Specimen #66				Specimen #67			
	User #1	User #2	NextEngine	Breuckmann	User #1	User #2	NextEngine	Breuckmann
1 - ZYB	β	β	β	β	126	126	127,7	126,5
2 - BBH	130	130	136,6	129,8	131	130	132,4	131
3 - XCB	133	137	140,1	β	122	126	126,5	131,5

Inter- and Intra-Observer variability

As in section 6.2, the variability of the measurement and the standard deviation were calculated. Figure 71 shows the inter-observer variability in percentage using CraMs automatic (APP) and Traditional methods (Traditional) and Figure 72 shows the intra-observer variability for both anthropologists (CC and MT). Mean values are represented as rhombus, the maximum and minimum values are expressed as the limits of the vertical lines. The values used results from the tests conducted in eight specimens by the two anthropologists and using both methods.

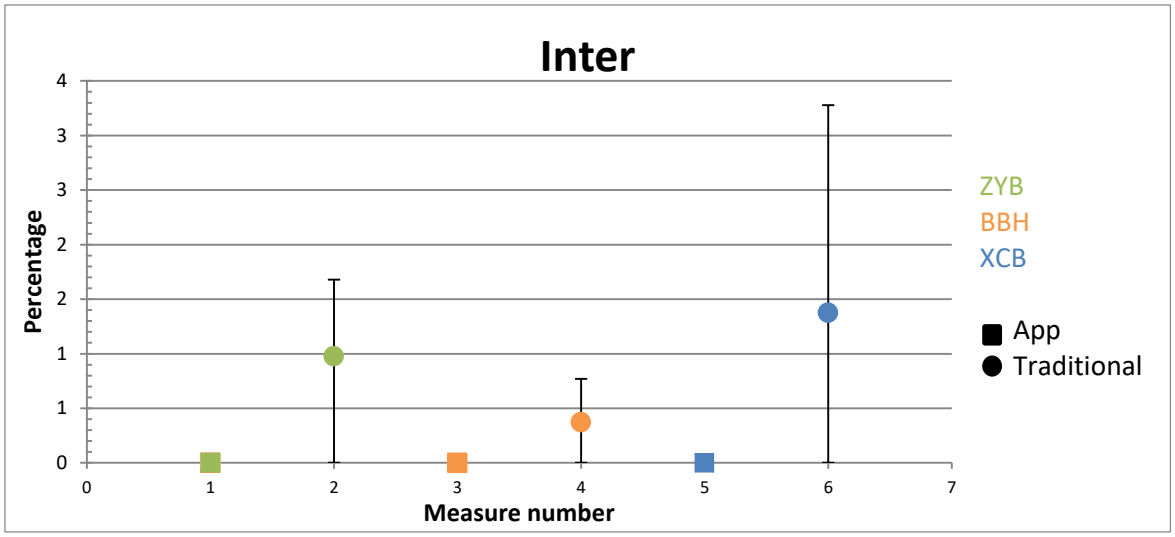

Figure 71 - Bar plots with the inter-observer variability, in percentage for the three automatic measures, between two specialists using CraMs (automatically) and traditional methods.

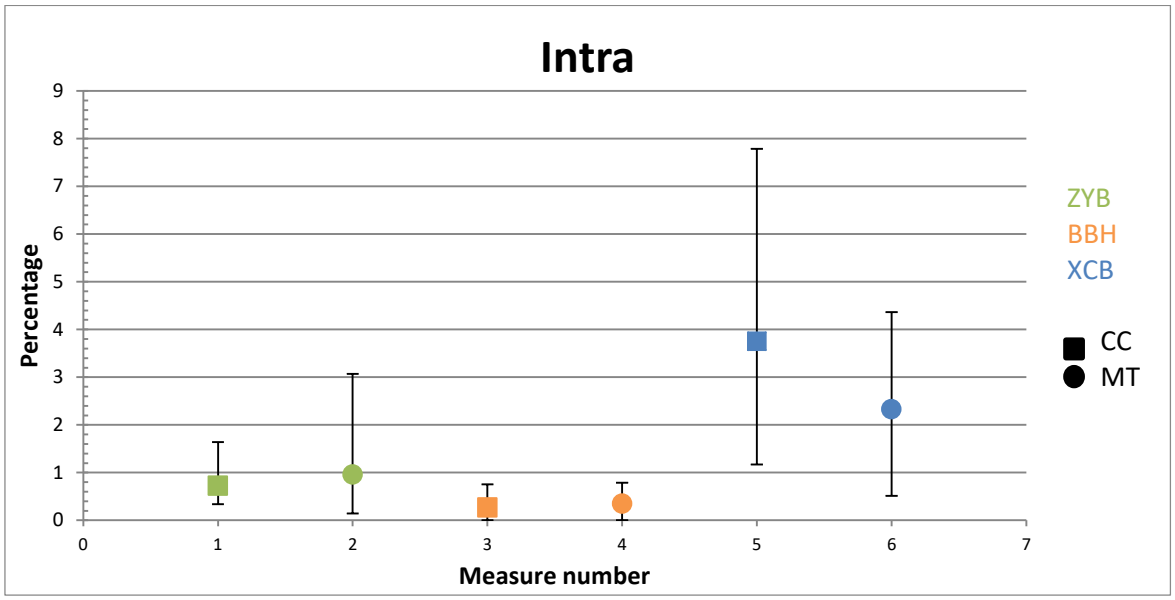

Figure 72 - Bar plots with the intra-observer variability, in percentage for the three automatic measures, between CraMs and traditional methods for two different experts (CC and MT).

As before, measures resulting from automatic landmarks, do not produce an inter-observer variation (Table 13).

Table 13 - Average difference percentages of inter-observer variation obtained for the three automatic measures.

App	Traditional
0.00	0.9

To calculate TEM values the intra-observer measurements taken by each expert with the traditional methods and with CraMs (Table 14) were considered. The difference between the results with both scanners in comparison with traditional methods can be easily explained by the fact that these measures result from automatic points, so alignment plays an important part in these measurements, as well as, any distortion and deformations.

Table 14 - Relative TEM values for inter-observer, different experts with the same method (orange) and intra-observer, the same expert using traditional methods and the application (with models from NextEngine or Breuckmann) (blue).

App (%)		Traditional (%)	CC (%)		MT (%)	
NextEngine	Breuckmann	0.88	NextEngine	Breuckmann	NextEngine	Breuckmann
0.00	0.00		1,91	1,89	1,42	1,31

Now, comparing the results obtained with the models scanned by Breuckmann scanner with the ones of the NextEngine, as expected, we get worse values of TEM, due to the decrease in the resolution. Yet, not so meaningful, as to put in doubt the use of the application. These results meet the interval in which the measures are admissible, less than 10%.

In comparison with the Breuckmann scanner, contrary to what one may think, the main causes of the worst results are the post-processing of the model after the acquisition. The software and user input responsible for refining the data and assembling it into a complete 3D mesh model cause the main problems. Firstly, the process of trying to combine the different captures and blend them together into a single fully healed model with no overlaps, is not completely accurate (Figure 73). Secondly, the user must refine the scan data, removing unnecessary parts, like remains of the structure that holds the model or noise that is added to the mesh. As can be observed, if not removed, these cause errors in the automatic detection process (landmark right eurion, Figure 74). This happens mainly because this procedure is not by a qualified technician in 3D acquisition.

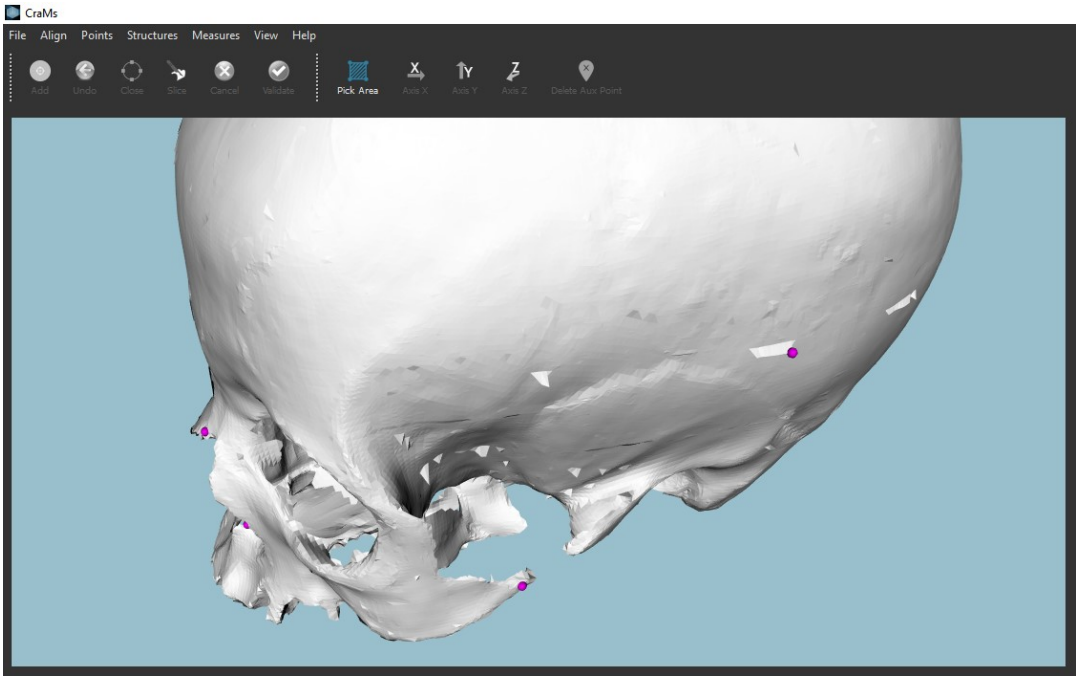

Figure 73 - Example of the process that tries to combine the different captures which is not completely accurate.

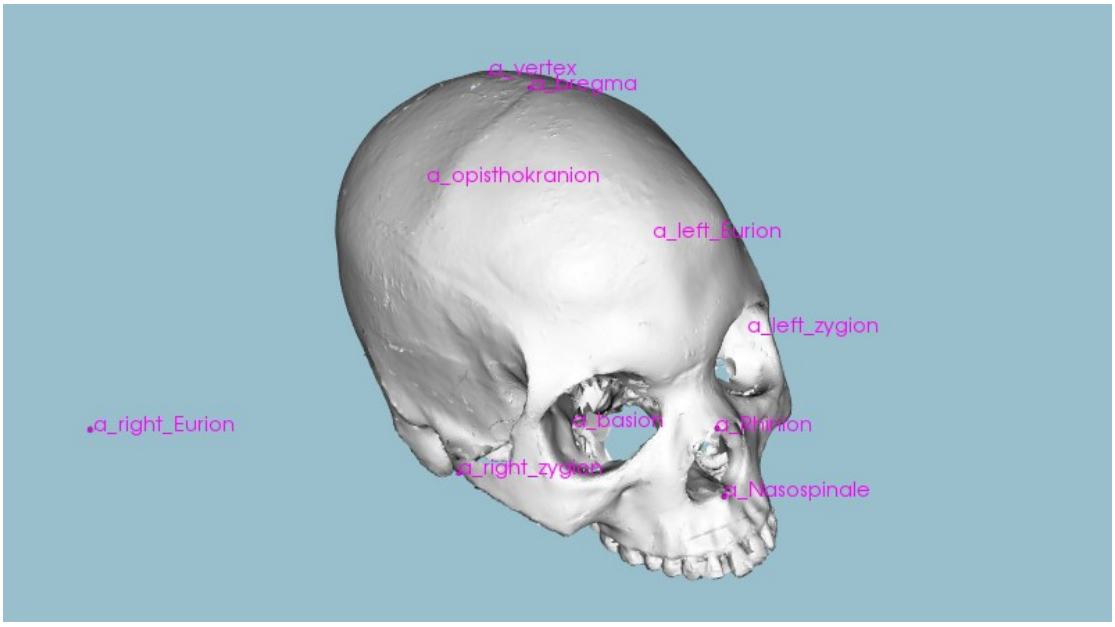

Figure 74 - Example of noise in the scan data that was not removed by the user, causing errors in the automatic detection process.

Some of the differences may result from a slight variance in alignment (Figure 75).

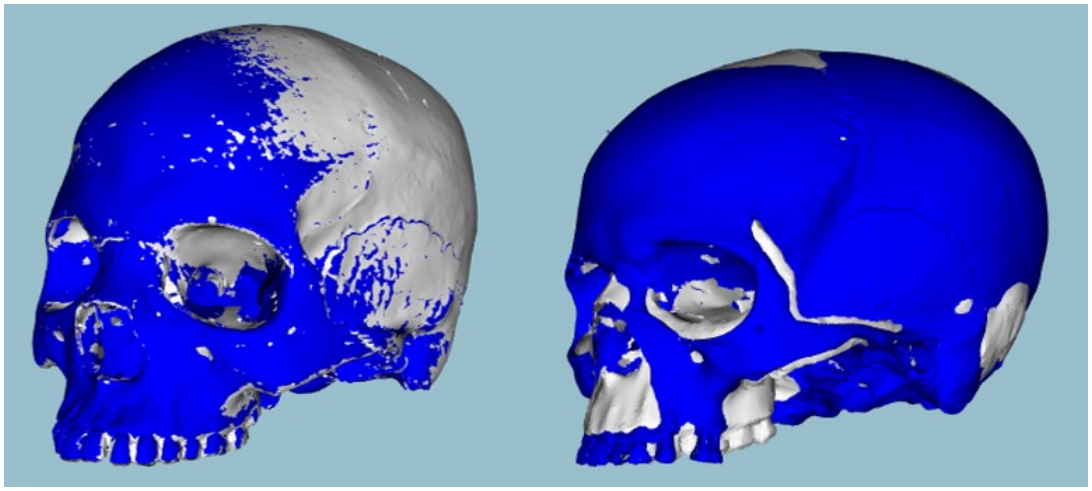

Figure 75 - Slight variance in alignment of the models acquired with different scanners.

These results show that the measures obtained using the application and the traditional measures, have a similar disparity, as does the disparity between anthropologists using the traditional methods. One advantage of the models with low resolution is the easier handling due to the fluidity and quick response of the application.

6.4 Nasal Aperture Width

Table 15 presents the results of the nasal aperture width classification using CraMs (NAW Automatic) in comparison with the classification made by two anthropologists (NAW Manual). The distance average of the pixels and the probability of the correct identification for each one of the three forms of nasal opening is also shown. Four of the fifty-one models were too damaged to be identified by the anthropologists, so no information could be obtained by performing the tests in these models. After having made tests in forty-seven specimens, we observed an 87% success rate in identifying the structure, of which 9% of rhi and 4% of ns points were marked manually. 95% success rate in identifying the structure type 3, 100% when identifying the structure type 2 an 71% structure type 1. The model CEIXXI_079 was the only one in which there was disagreement between the two anthropologists.

After several tests, the empirical results were evaluated and the values were chosen for the different parameters of the algorithm: search of slope variance was in 10, 20 and 30 neighbours before, the minimum distance was 1 mm and at last, the variance was 3 neighbours before and after.

Table 15 - Results of NAW classification - Nasal aperture width in Manual and Automatic. Euclidean distance average of the pixels, the probability of each classification using equation (6). The green, yellow and orange colours mean right, impossible and wrong classifications, respectively. Distance average is in pixels.

ID	NAW Manual	NAW Auto	Distance average			%		
			1	2	3	1	2	3
PAVd'09_020	3	3	34,59	20,59	7,67	1	5	94
PAVd'09_021	3	3	34,27	14,62	11,14	2	30	68
PAVd'09_025	3	3	45,16	29,29	12,16	2	6	92
PAVd'09_038	2	2	24,22	8,478	16,07	4	84	12
PAVd'09_039	3	3	33,73	13,70	4,02	0	3	97
PAVd'09_041	3	3	42,38	24,58	7,29	0	3	97
PAVd'09_057	3	3	30,79	13,09	6,48	1	11	88
PAVd'09_063	2	2	20,99	7,881	26,0	5	92	3
PAVd'09_065	3	3	57,15	36,31	17,4	3	10	87
PAVd'09_066	3	3	37,31	20,73	5,00	0	2	98
PAVd'09_067	3	3	40,12	21,39	4,91	0	1	99
PAVd'09_069	3	3	36,11	18,31	3,57	0	1	99
PAVd'09_075	3	3	32,41	16,36	9,17	2	15	83
PAVd'09_077	3	3	33,25	15,33	10,9	3	25	72
PAVd'09_078	3	3	24,64	17,75	12,3	9	22	69
PAVd'09_081	3	3	36,18	18,67	3,87	0	1	99
PAVd'09_082	3	3	39,27	20,63	1,17	0	0	100
PAVd'09_093	3	3	40,67	24,57	9,12	1	5	94
PAVd'09_095	3	3	35,15	24,04	8,14	1	4	95
PAVd'09_110	3	3	38,13	18,05	13,4	3	28	69
PAVd'09_133	3	3	29,31	10,04	5,11	0	12	88
PAVd'09_163	3	2	19,10	19,10	3,32	1	99	0
PAVd'09_169	3	3	33,57	33,57	14,86	0	5	95
CEIXXI_002	1	1	13,14	6,64	16,12	11	83	6
CEIXXI_003	1	1	9,96	14,43	31,64	72	26	2
CEIXXI_005	1	1	6,23	10,37	31,23	82	17	1
CEIXXI_006	1	2	11,52	8,55	21,44	30	66	4
CEIXXI_009	1	2	10,65	5,52	20,62	11	88	1
CEIXXI_011								
CEIXXI_013								
CEIXXI_014	2	2	14,16	11,41	19,25	29	60	11
CEIXXI_017	1	2	20,74	9,13	15,24	7	77	16
CEIXXI_018	1	1	7,36	21,34	40,86	96	3	1
CEIXXI_019	1	1	9,45	13,24	30,45	74	24	2
CEIXXI_023	1	1	11,73	12,73	29,84	55	42	3
CEIXXI_024								
CEIXXI_026	1	1	10,62	13,32	32,13	67	31	2
CEIXXI_027	1	1	9,24	14,42	33,54	78	20	2
CEIXXI_028	1	1	12,65	16,54	36,76	69	28	3
CEIXXI_036	2	2	16,52	9,71	18,43	14	77	9
CEIXXI_040								
CEIXXI_050	1	2	12,63	8,13	23,25	22	75	3
CEIXXI_069	1	2	10,75	6,32	19,52	17	80	3
CEIXXI_071	2	2	16,32	11,48	22,55	22	69	9
CEIXXI_072	1	1	7,54	10,75	2,86	73	25	2
CEIXXI_076	1	2	11,76	6,24	18,14	14	83	3
CEIXXI_079	1/2	2	16,84	9,85	21,43	14	80	6
CEIXXI_088	2	2	18,72	7,19	20,13	5	91	4
CEIXXI_092	2	2	20,25	9,62	11,65	6	61	33
CEIXXI_133	1	2	11,54	6,34	19,35	14	84	2
CEIXXI_135	2	2	17,22	7,52	19,34	6	89	5

Although the results have been fairly accurate in identifying the nasal aperture width, the degradation state of some skulls (fractured pieces of bone) caused a reduction in the performance, an incorrect identification of the two craniometric points and/or a wrong classification of the correct structure (Figure 76).

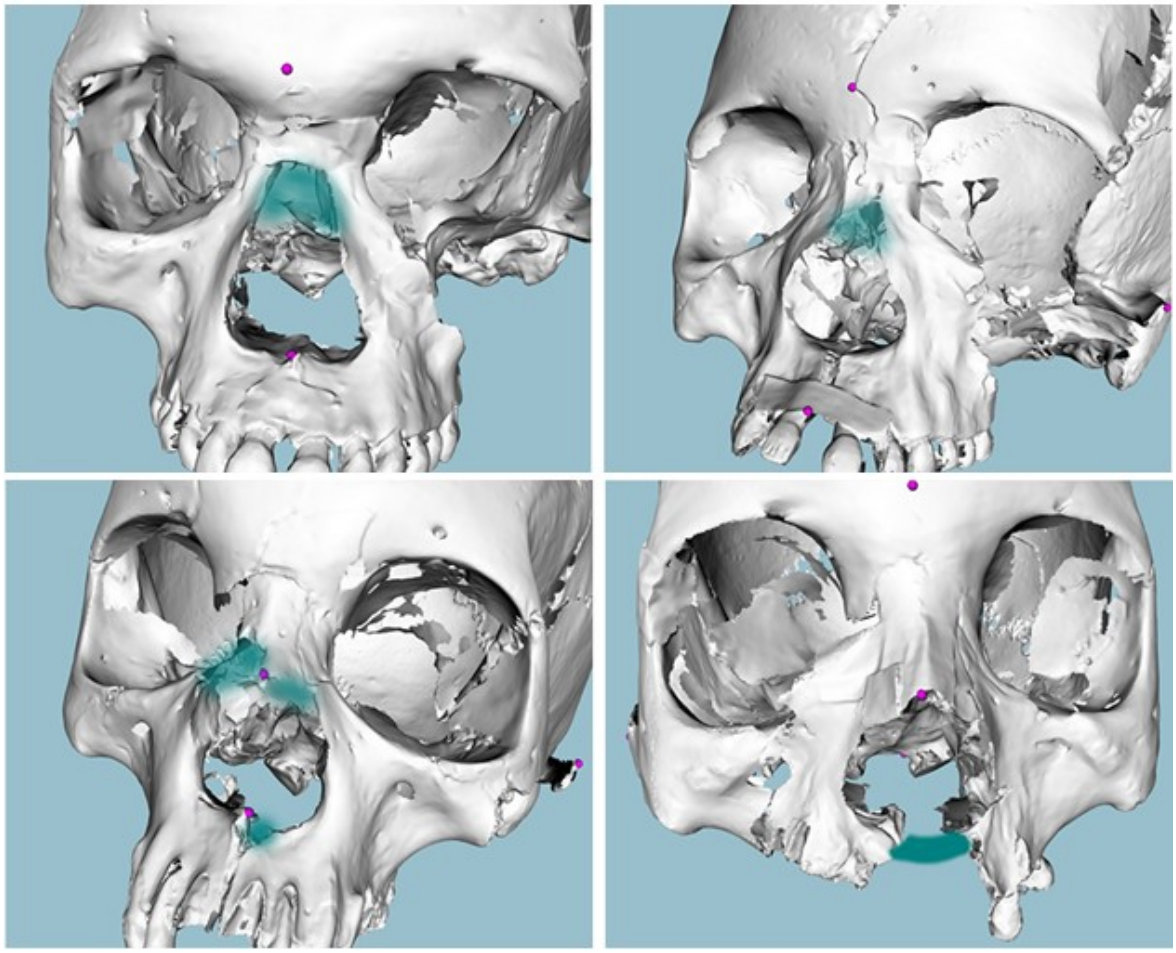

Figure 76 – Nasal aperture width detection (fractured areas represented in green). Wrong Classification and detection of rhinion (top left), Wrong detection of rhinion and nasospinale (top right), decrease of time performance of the algorithm (bottom left), Impossible classification and detection of nasospinale (bottom right).

6.5 Postbregmatic Depression

Table 16 presents the results of the postbregmatic depression classification by the anthropologists (PD Manual) and using CraMs (PD Automatic). The tests ran in forty-five specimens had a 100% success rate in identifying the structure. Six of the fifty-one models were too damaged to be identified by the anthropologists, so no results could be obtained by performing the tests in these models.

Table 16 - Results of PD classification - postbregmatic depression identified using manual and automatic methods. The green and yellow colours mean a right and impossible classifications, respectively.

ID	PD Manual	PD Auto
PAVd'09_020		
PAVd'09_021	0	0
PAVd'09_025	0	0
PAVd'09_038	0	0
PAVd'09_039	0	0
PAVd'09_041		
PAVd'09_057	0	0
PAVd'09_063		
PAVd'09_065	0	0
PAVd'09_066	0	0
PAVd'09_067	0	0
PAVd'09_069	1	1
PAVd'09_075		
PAVd'09_077	0	0
PAVd'09_078	1	1
PAVd'09_081	0	0
PAVd'09_082	0	0
PAVd'09_095	0	0
PAVd'09_110	0	0
PAVd'09_133		
PAVd'09_163	0	0
PAVd'09_169	0	0

ID	PD Manual	PD Auto
CEIXXI_002	0	0
CEIXXI_003	0	0
CEIXXI_005	0	0
CEIXXI_006	0	0
CEIXXI_009	0	0
CEIXXI_011	0	0
CEIXXI_013	0	0
CEIXXI_014	0	0
CEIXXI_017	0	0
CEIXXI_018	0	0
CEIXXI_019	0	0
CEIXXI_023	0	0
CEIXXI_024	0	0
CEIXXI_026	0	0
CEIXXI_027	0	0
CEIXXI_028	0	0
CEIXXI_029	0	0
CEIXXI_036	0	0
CEIXXI_040		
CEIXXI_050	0	0
CEIXXI_069	0	0
CEIXXI_071	0	0
CEIXXI_072	0	0
CEIXXI_076	0	0
CEIXXI_079	1	1
CEIXXI_088	0	0
CEIXXI_092	0	0
CEIXXI_133	0	0
CEIXXI_135	0	0

Although, we can considerer that the method developed to classify the postbregmatic depression presents promising results, more models with this trait should be added to the study in order to guarantee the efficiency of this method.

6.6 Anterior Nasal Spine

Table 17 presents the results of the anterior nasal spine classification using CraMs (ANS Automatic) in comparison with the classification made by anthropologists (ANS Manual). Tests were run with

forty-one specimens. We can observe a 93% success rate in identifying the structure. Ten of the fifty-one were impossible to identify by the anthropologists, because they were too damaged, so no information could be obtained by performing the tests in these models. All the wrong classifications were obtained for type 3 (which was classified as type 2).

Table 17 - Results of ANS classification - Anterior nasal spine identified using manual and automatic methods. The colour greed, yellow and orange means a right, impossible and wrong classifications, respectively.

ID	ANS Manual	ANS Auto
PAVd'09_020		
PAVd'09_021	1	1
PAVd'09_025	1	1
PAVd'09_038	2	2
PAVd'09_039	1	1
PAVd'09_041		
PAVd'09_057		
PAVd'09_063		
PAVd'09_065	1	1
PAVd'09_066	2	2
PAVd'09_067	1	1
PAVd'09_069	1	1
PAVd'09_075	1	1
PAVd'09_077	2	2
PAVd'09_078	1	1
PAVd'09_081	2	2
PAVd'09_082	2	2
PAVd'09_095		
PAVd'09_110	3	3
PAVd'09_133		
PAVd'09_163	1	1
PAVd'09_169	1	1

ID	ANS Manual	ANS Auto
CEIXXI_002	3	3
CEIXXI_003	2	2
CEIXXI_005	3	3
CEIXXI_006	2	2
CEIXXI_009	3	2
CEIXXI_011		
CEIXXI_013	2	2
CEIXXI_014	2	2
CEIXXI_017	2	2
CEIXXI_018	3	3
CEIXXI_019	2	2
CEIXXI_023		
CEIXXI_024		
CEIXXI_026	2	2
CEIXXI_027	3	2
CEIXXI_028	2	2
CEIXXI_029	3	3
CEIXXI_036	2	2
CEIXXI_040		
CEIXXI_050	3	3
CEIXXI_069	2	2
CEIXXI_071	2	2
CEIXXI_072	3	3
CEIXXI_076	3	2
CEIXXI_079	3	3
CEIXXI_088	2	2
CEIXXI_092	2	2
CEIXXI_133	2	2
CEIXXI_135	3	3

One explication for these results is that many of the models with ANS type 3, suffered peri- or post-mortem flaw, i.e. they were damaged (Figure 77). More models of this type are needed to ensure that the values chosen, for the parameters that select the area that will allow the process of

classification to differentiate between type 2 and type 3, are more effective. Additionally, if the nasospinale is slightly misplaced the results can be different.

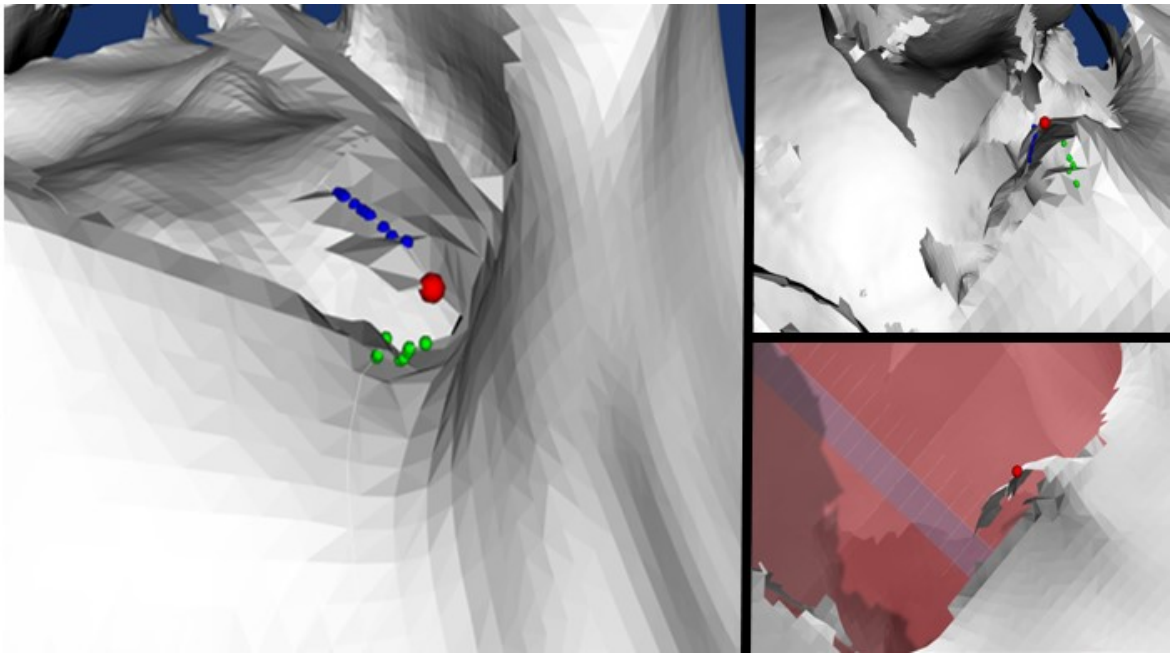

Figure 77 – One of the many models, with type 3 ANS classification, that suffered peri- or post-mortem flaw. Viewed from above (Left) and from front using normal view (right from above) or with the help from a plane to highlight the flaws.

6.7 Landmarks Mesh

From the mesh skulls database created, an expert use forty models (twenty skulls from women, twenty skulls from men) to train ten different machine learning algorithms. Each algorithm was used to classified ten skulls, obtaining overall accuracies ranging from 72% to 88% (Table 18).

Sensitivity (or recall) and predictive value (or precision) are also calculated using equation (10) and equation (11)(Olson & Delen, 2008).

$$sensitivity = \frac{TP}{TP+FP} \tag{10}$$

$$precision = \frac{TP}{TP+FN} \tag{11}$$

Where TP is True Positive, FP is False Positive and FN False Negative.

Table 18 - Sex estimation accuracy metrics of classification algorithms (with 5-fold Cross-Validation) on the CEIXXI sample.

		Sensitivity		Predictive Value	
Model	**Overall Accuracy**	Female	Male	Female	Male
C5.0Rules	0.83	0.79	0.87	0.8518	0.8181
C5.0Tree	0.84	0.84	0.83	0.8305	0.8524
knn	0.85	0.93	0.77	0.7941	0.9230
svmLinear	0.79	0.74	0.84	0.8113	0.7761
svmPoly	0.85	0.83	0.87	0.8571	0.8437
svmRadial	0.88	0.83	0.94	0.9230	0.8529
nnet	0.72	0.48	0.94	0.8750	0.6590
LMT	0.80	0.72	0.87	0.8400	0.7714
JRip	0.82	0.76	0.87	0.8461	0.7941
rda	0.85	0.93	0.77	0.7941	0.9230

Although the data base is relatively small, we already can see good results in the classification. So, conciliating a nearly-automated software, geometric morphometrics and machine learning we were able, computationally, to estimate sex without the technical expertise of physical anthropologists. These methods seem promising and further investigation must be made.

7 Conclusion and Future Work

7.1 Conclusion

CraMs is an application to help anthropologists perform more consistent craniometric analyses ensuring a better preservation of the specimen by avoiding physical manipulation and transportation. The new version, developed in this work, is more usable, more reliable and includes more measures.

Measures taken with CraMs can be classified in three major categories: Automatic, Semi-Automatic and Manual. With the new four points (in the nasal area), two more measures became automatic, so from the twenty-four measurements that anthropologists typically use, CraMs can be used to take all of them, six fully Automatic, fourteen Semi-Automatic and four Manual.

CraMs is the first application that tries to classify automatically the ancestry based on non-metric traits. The methods developed show good results, although, there are still many traits that were not addressed. The fact that these methods overcame the difficult of obtaining and classifying the traits with traditional methods is a significant improvement.

In terms of gender, the new method that analysis the mesh of points in a way that was impossible to the anthropologists can bring great advantages. The results obtained so far were very positive,

the fact that the preliminary tests already allow a classification with a high percentage of accuracy is encouraging.

The user interface modifications and improvements were another important step to improve usability, making CraMs an application that can be used in day to day operations and extremely useful for the anthropologists in their future studies.

Although, the study made regarding the impact on the measures when using the NextEngine scanner was preliminary it provided useful information. The fact that the domain experts can use models with less resolution and have little or no error induced from it, is really interesting. By reducing the complexity of the model without affecting the measures, the flow of interaction with the application will improve significantly. Also, it shows that there is no need of an expensive scanner to obtain good results with CraMs.

All the results obtained so far, are very positive and begin to show the potential of CraMs towards the definition of a new more objective methodology in the field of Anthropology.

7.2 Future Work

CraMs still has a lot of room to improve and expand. There is still a vast number of technologies and methods that have not been explored. Future work in this project might involve:

Alignment

- Improving the ICP alignment method by using a database of template models, already aligned, and choosing the most anatomically similar one to obtain the best alignment results;
- Develop a method to automatically align the models. Even though the ICP method works well it might still need user interaction in some cases;

New methods and improvements

- Developing methods to increase the number of points detected automatically (using for example texture information available from the acquisition process);

- Other feature analysis and classification methods can be tested to improve accuracy, robustness or speed (given the need for user interaction) using for example segmentation, shape analysis, volume analysis, etc.;

- Improving the sharp edge structure detection methods, developed by Neves (2014), in order to make them automatic and more accurate;

- Develop methods to detect and classify automatically the non-metric traits that weren't addressed in this work;

- Since some of the models are fragmented, a method to help align fragments and reconstruct the mesh in the missing areas would be of great use;

- Another idea worth investigating once a significant database of point coordinates is available is to make an Atlas of models. The database of models could be used to, firstly, find the model that best fits the skull in analysis and, secondly, map the points correctly found on the stored model to the model to be analysed and further used methods like neighbouring to find the correct anatomical positions. This way, the user could be freed of the task of picking some points and, would only need to make the validation of each point. If any of the automatically found points was not correct the user could use the picking procedure to correctly indicate the point. After the processing, the skull model could be stored as a template model to be further used in the atlas database;

Interface and Optimization

- The application handles some CPU intensive tasks; Optimization could also be addressed as further work;

- Better support for user interaction, through the full integration of the phantom (force feedback device) to ease point selection;

- Also the integration of the Oculus 3D, would allow to have a fully immersive experience in the 3D world when performing the tasks.

References

Adams, A. D., Collyer, M., Sherratt, E., & Adams, M. D. (2016). Geometric Morphometric Analyses of 2D/3D Landmark Data - Package “geomorph.”

Agathos, A. G. (2009). *Part based 3D representation for the retrieval of 3D graphical models. PhD Dissertation*. University of the Aegean. Retrieved from http://users.iit.demokritos.gr/~agalex/

An, Y., Li, Z., & Shao, C. (2013). Feature Extraction from 3D Point Cloud Data Based on Discrete Curves. *Mathematical Problems in Engineering*, *2013*, 1–19.

Balzeau, A., Crevecoeur, I., Rougier, H., Froment, A., Gilissen, E., Grimaud-Hervé, D., … Semal, P. (2010). Applications of imaging methodologies to paleoanthropology: Beneficial results relating to the preservation, management and development of collections. *Comptes Rendus Palevol*, *9*(6–7), 265–275. http://doi.org/10.1016/j.crpv.2010.07.006

Bass, W. M. (2005). *Human Osteology: A Laboratory and Field Manual* (5th ed.). Missouri Archaeological Society.

Benhabiles, H. (2013). *3D-mesh segmentation: automatic evaluation and a new learning-based method. Theses*. Universit´ e des Sciences et Tech- nologie de Lille, France.

Besl, P. J., & McKay, H. D. (1992). A method for registration of 3-D shapes. *IEEE Transactions on Pattern Analysis and Machine Intelligence*, *14*(2), 239–256. http://doi.org/10.1109/34.121791

Blakey, M. L. (2001). Bioarchaeology of the African diaspora in the Americas: its origins and scope. *Annual Review of Anthropology Anthropology*, *30*(2001), 387–422. http://doi.org/10.2307/3069222

Blanchette, J., Summerfield, M., Gorman, M., & Mcfarlane, N. (2004). *C ++ GUI*

Programming with Qt 3. *Education* (Vol. 75). Hall, Publisher Prentice. http://doi.org/10.1016/S0883-153X(07)00034-3

Brues, A. (1990). The once and future diagnosis of race. In *Gill, G. W.; Rhine, S. Skeletal attribution of race: methods for forensic anthropology* (pp. 1–7). Maxwell Museum of Anthropology, University of New Mexico.

Buck, T. J., & Vidarsdottir, U. S. (2004). A proposed method for the identification of race in sub-adult skeletons: a geometric morphometric analysis of mandibular morphology. *Journal of Forensic Sciences*, *49*(6), 1159–1164. http://doi.org/10.1520/JFS2004074

Byers, S. N. (2011). *Introduction to Forensic Anthropology* (4th ed.). Pearson.

Chin, J. P., Diehl, V. A., & Norman, K. L. (1988). Development of an instrument measuring user satisfaction of the human-computer interface. *Proceedings of the SIGCHI Conference on Human Factors in Computing Systems*, (April 2016), 213–218. http://doi.org/10.1145/57167.57203

Coelho, C. R. S. (2012). *Uma identidade perdida no mar e reencontrada nos ossos : Avaliação das afinidades populacionais de uma amostra de escravos dos séculos XV-XVI*. University of Coimbra.

Colombo, A., Cusano, C., & Schettini, R. (2006). 3D face detection using curvature analysis. *Pattern Recognition*, *39*(3), 444–455. http://doi.org/10.1016/j.patcog.2005.09.009

Dodge, Y., Cox, D., & Commenges, D. (2003). *The Oxford Dictionary of Statistical Terms*. *Technometrics* (Vol. 20). http://doi.org/10.1198/tech.2004.s820

Eck, M., DeRose, T., Duchamp, T., Hoppe, H., Lounsbery, M., & Stuetzle, W. (1995). Multiresolution analysis of arbitrary meshes. *Proceedings of the 22nd Annual Conference on Computer Graphics and Interactive Techniques - SIGGRAPH '95*, *6*, 173–182. http://doi.org/10.1145/218380.218440

Ferguson, E., Kerr, N., & Rynn, C. (2011). Race and Ancestry. In *Black, S.; Ferguson, E. Forensic Anthropology 2000 to 2010* (1st ed., pp. 119–153). CRC Press.

Ferraro, R. F. (1995). *Learn 3D Graphics Programming on the PC*. Addison Wesley Publishing Company.

Ferreira, M. T., Vicente, R., Navega, D., Gonçalves, D., Curate, F., & Cunha, E. (2014). A new forensic collection housed at the University of Coimbra, Portugal: The 21st century identified skeletal collection. *Forensic Science International*, *245*, 202.e1-202.e5. http://doi.org/10.1016/j.forsciint.2014.09.021

Gill, G. W. (1998). Craniofacial Criteria in the Skeletal Attribution of Race. In *Reichs, K.J. Forensic osteology: advances in the identification of human remains* (2nd ed., pp. 293–315). Illinois: Charles C. Thomas Publisher.

Gonzalez, P. N., Bernal, V., & Perez, S. I. (2011). Analysis of sexual dimorphism of craniofacial traits using geometric morphometric techniques. *International Journal of Osteoarchaeology*, *21*(1), 82–91. http://doi.org/10.1002/oa.1109

Gumhold, S., Wang, X., & MacLeod, R. (2001). Feature extraction from point clouds, (April 2016), 293–305.

Hefner, J. T. (2009). Cranial Nonmetric Variation and Estimating Ancestry, *54*(5), 985–995. http://doi.org/10.1111/j.1556-4029.2009.01118.x

Howells, W. W. (1973). Cranial Variation in Man -A study by multivariate analysis of patterns of difference among recent human populations. *Papers of the Peabody Museum of Archaeology and Ethnology*, *67*, 1–259.

Kannan, S. (2008). *Quantitative Analysis of Masticatory Performance in Vertebrates*. Retrieved from http://books.google.fr/books?id=H7CS4A4bObYC

Kaufhold, J., & Hoogs, A. (2004). Learning to segment images using region-based perceptual features. *Proceedings of the 2004 IEEE Computer Society Conference on Computer Vision and Pattern Recognition*, *2*(April 2016), 954–961. http://doi.org/10.1109/CVPR.2004.1315268

Klepinger, L. L. (2006). *Fundamentals of Forensic Anthropology*. (Wiley-Liss, Ed.) (1st ed.). http://doi.org/10.1016/j.trac.2008.11.003

Kuhn, M. (2008). Building Predictive Models in R Using the caret Package. *Journal Of Statistical Software*, *28*(5), 1–26. http://doi.org/10.1053/j.sodo.2009.03.002

Lavoué, G., Dupont, F., & Baskurt, A. (2005). A new CAD mesh segmentation method, based on curvature tensor analysis. *CAD Computer Aided Design*, *37*(10), 975–987. http://doi.org/10.1016/j.cad.2004.09.001

Morita, Y., Ogihara, N., Kanai, T., & Suzuki, H. (2013). Technical Note : Quantification of Neurocranial Shape Variation Using the Shortest Paths Connecting Pairs of Anatomical Landmarks. *American Journal of Physical Anthropology*, *151*(4), 658–666. http://doi.org/10.1002/ajpa.22315

Neves, L. (2014). *Measures and detection of morphology for craniometry using 3D models. Master Dissertation*. Universidade de Aveiro.

Neves, M. J., Almeida, M., & Ferreira, M. T. (2010). Separados na vida e na morte - Retrato do tratamento mortuário dado aos escravos africanos na cidade moderna de Lagos. *XELB - In Actas of 7º Encontro de Arqueologia Do Algar*, *10*(1), 547–560.

Neves, M. J., Almeida, M., & Ferreira, M. T. (2011). História de um arrabalde durante os séculos xv e xvi: o "poço dos negros" em Lagos (Algarve, Portugal) e o seu contributo para e estudo dos escravos africanos em Portugal. *Câmara Municipal de Lagos*, 29–46.

Olson, D., & Delen, D. (2008). *Advanced Data Mining Techniques*. *Springer-Verlag*. http://doi.org/10.1017/CBO9781107415324.004

Pauly, M., Keiser, R., & Gross, M. (2003). Multi-scale Feature Extraction on Point-Sampled Surfaces. *Eurographics 2003*, *22*(3), 281–289.

Pavlidis, T., & Liow, Y. T. (1990). Integrating Region Growing and Edge Detection. *IEEE Transactions on Pattern Analysis and Machine Intelligence*, *12*(3), 225–233. http://doi.org/10.1109/34.49050

Pereira, C., & Mello e Alvim, M. (1979). *Manual Para Estudos Craniométricos E Cranioscópicos*. (Univ. Federal de Santa Maria, Ed.).

Perini, T. A., Oliveira, G. L. de, Ornellas, J. S., & Fátima Palha de Oliveira. (2005). Technical error of measurement in anthropometry. *Revista Brasileira de Medicina Do Esporte*, *11*, 81–85. http://doi.org/http://dx.doi.org/10.1590/S1517-86922005000100009

Razdan, A., & Bae, M. (2003). A hybrid approach to feature segmentation of triangle meshes. *Computer-Aided Design*, *35*(9), 783–789. http://doi.org/10.1016/S0010-4485(02)00101-X

Ross, A. H., Slice, D. E., & Williams, S. E. (2010). *Geometric Morphometric Tools for the Classification of Human Skulls. Research Report*. Retrieved from https://www.ncjrs.gov/App/Publications/abstract.aspx?ID=253252

Santos, D. A. (2013). *3D skull models: a new craniometric approach. Master Dissertation*. Universidade de Aveiro.

Schroeder, W., Martin, K., & Lorensen, B. (2006). *Visualization Toolkit: An Object-Oriented Approach to 3D Graphics, 4th Edition* (4th ed.). Kitware Inc.

Shamir, A. (2006). Segmentation and shape extraction of 3D boundary meshes. In *Eurographics 2006* (pp. 137–149). The Eurographics Association.

Shneiderman, B. (1998). *Designing the User Interface: Strategies for Effective Human-Computer Interaction*. *Book*. Addison-Wesley. Retrieved from http://www.aw-bc.com/DTUI/

Sholts, S. B., Miller, K. W. P., Wärmländer, S. K. T. S., & Walker, P. L. (2007). The application of three-dimensional midfacial profiling in the identification of human skeletal remains. In *18th International Symposium on Human Identification*. Los Angeles, California.

Sholts, S. B., Walker, P. L., Kuzminsky, S. C., Miller, K. W. P., & Wärmländer, S. K. T. S. (2011). Identification of group affinity from cross-sectional contours of the human midfacial skeleton using digital morphometrics and 3D laser scanning technology. *Journal of Forensic Sciences*, *56*(2), 333. http://doi.org/10.1111/j.1556-4029.2011.01701.x

Spradley, M. K., & Jantz, R. (2011). Sex Estimation in Forensic Anthropology: Skull Versus Postcranial Elements. *Journal of Forensic Sciences*, *56*, 289–296. http://doi.org/10.1111/j.1556-4029.2010.01635.x

Stephens, C. (2000). A Measure of Truth ? An Examination of the History , Methodology , Theory and Practice of Craniometric Analysis : With Special Focus on its Application in Forensic Identification. *Totem: The University of Western Ontario Journal of Anthropology*, *8*(1), 84–108.

Team, R. D. C. (2015). *R: A language and environment for statistical computing*. Vienna, Austria: R Foundation for Statistical Computing. Retrieved from http://www.r-project.org

Vieira, M., & Shimada, K. (2005). Surface mesh segmentation and smooth surface extraction through region growing. *Computer Aided Geometric Design*, *22*(8), 771–792. http://doi.org/10.1016/j.cagd.2005.03.006

Vioarsdóttir, U. S., O'Higgins, P., & Stringer, C. B. (2002). A geometric morphometric study

of regional differences in the ontogeny of the modern human facial skeleton. *Journal of Anatomy*, *201*, 211–229. http://doi.org/10.1046/j.1469-7580.2002.00092.x

Wachowiak, M. J., & Karas, B. V. (2009). 3D Scanning and Replication for Museum and Cultural Heritage Applications. *Techniques de Balayage et de Reproduction En Trois Dimensions Pour Applications Muséales et Culturelles.*, *48*(2), 141–158. http://doi.org/10.2307/27784660

Weber, G. W. (2013). Another link between archaeology and anthropology: Virtual anthropology. *Digital Applications in Archaeology and Cultural Heritage*, *1*(1), 3–11. http://doi.org/10.1016/j.daach.2013.04.001

Zuckerberge, E., Ayellet, T., & Shlafman, S. (2002). Polyhedral Surface Decomposition with Applications. *Computers & Graphics*, *26*(5), 733–743.

Appendix A – CraMs User Manual

Tool Bar

This toolbar gives the user quick access to important features (Figure 1).

Figure 1 - Toolbar

Buttons (from left to right):

- Pick Points- Activate to pick points or deactivate to move the model
- Undo – Undo the last action or actions
- Close structure – Use to close structure when marking orbit
- Slice – Activate a cut to help mark some points (Lambda)
- Cancel – Cancel action
- Validate – Validate last action made (point or structure marked)

File Menu

In this menu it is possible to open a model with the extension ".ply" as shown in Figure 2.

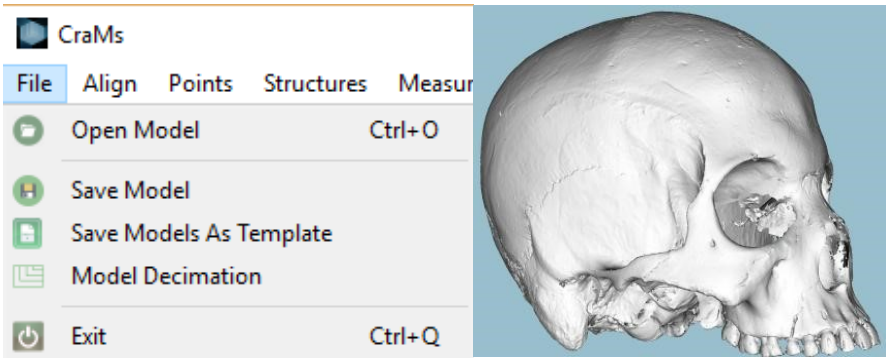

Figure 2 - Open Model menu (left) and the result (right).

It is also possible to save the model (normally or as a template), decimate the model and exit the application.

Align Menu

It is possible to align the model manually by picking seven reference points. During the manual alignment it is possible to restart the process. Press the Align button when all points are marked.

It is recommended the usage of the Semi-Automatic alignment method. Before loading the template, the user can check or uncheck the option to align centroids as explained at the end of section 3.2.2. Then load the template model (".ply" file). Figure 3 shows the manual and Semi-Automatic align menu

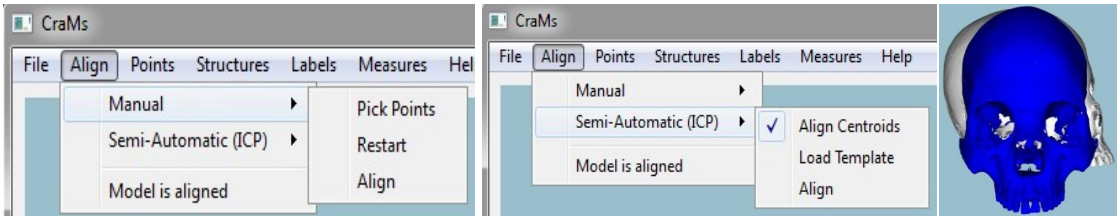

Figure 3 - Manual align menu (left), Semi-Automatic menu (middle) and the result of loading a Template model (right).

After loading a template, it is possible to pre-align the two models manually with the x, y and z key (using the shift key to change the direction). When the orientation of the models is similar click the Align button to start the process. Figure 4 illustrates the process. The user can save the alignment to file.

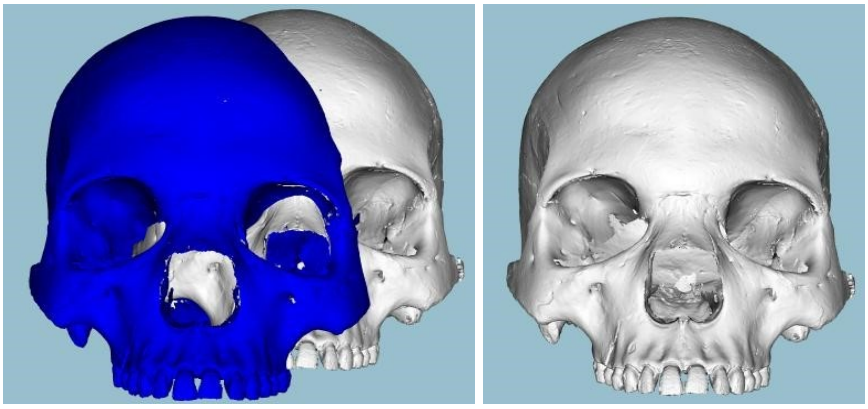

Figure 4 - Optimal orientation (left) and the result of the alignment (right).

If the user has the alignment file, he/she can select the option “from file” in the menu “Align” and then choose the file.

It is possible to skip the alignment process by clicking the "Model is aligned" button in the Align menu, if the model is already aligned.

Points Menu

After the skull is aligned it is possible to mark points. Some of them can be marked automatically by using the *Try Automatic* button. These points can be deleted and marked manually through the *Correct Automatic Points* sub-menu as shown in Figure 5.

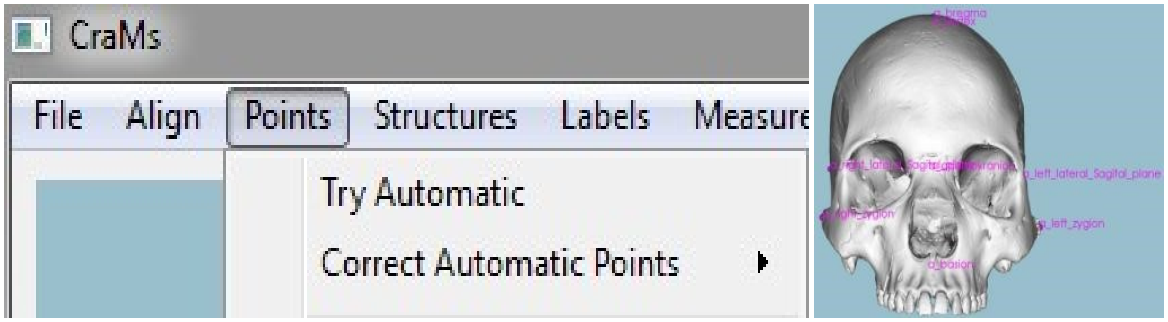

Figure 5 - Automatic points sub-menu (left) and the result of the "Try Automatic" button (right).

From this menu it is also possible to mark the rest of the points. Some keys may be useful for this process (see Additional keys section for more information). Some of the points are defined using a neighbourhood while others are fully manual, as shown in Figure 6. All points can be deleted.

Figure 6 - Example of points defined using neighbourhood (left) and fully manual (right).

A fully marked skull should look something like what is shown in Figure 7.

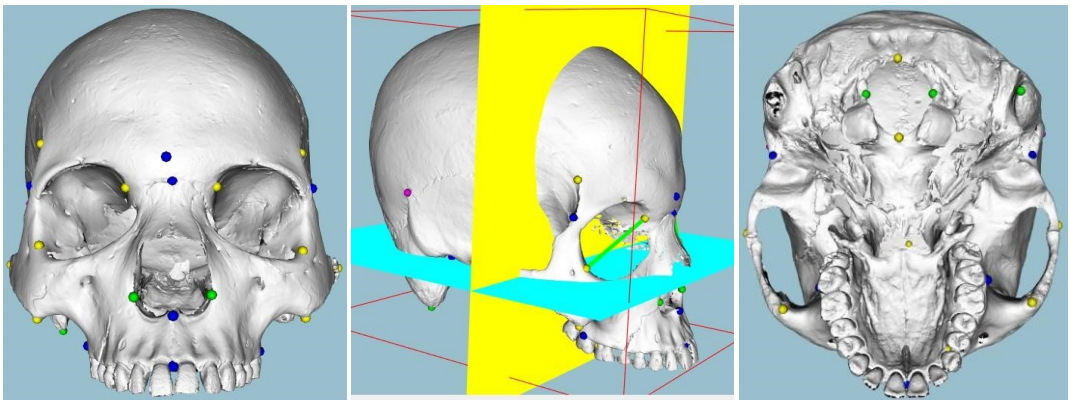

Figure 7 - Fully marked skull front (left), side with planes (middle) and bottom (right) view.

From this menu, it is also possible to delete all marked points.

Structures Menu

From here it is possible to detect structures such as the orbits, sutures and non-metric structures. For the orbits it is possible to mark two structures (right and left) as shown in Figure 8. Use the Sharp Edges method and follow the instructions given to detect the orbits. You can also delete or hide the detected structures.

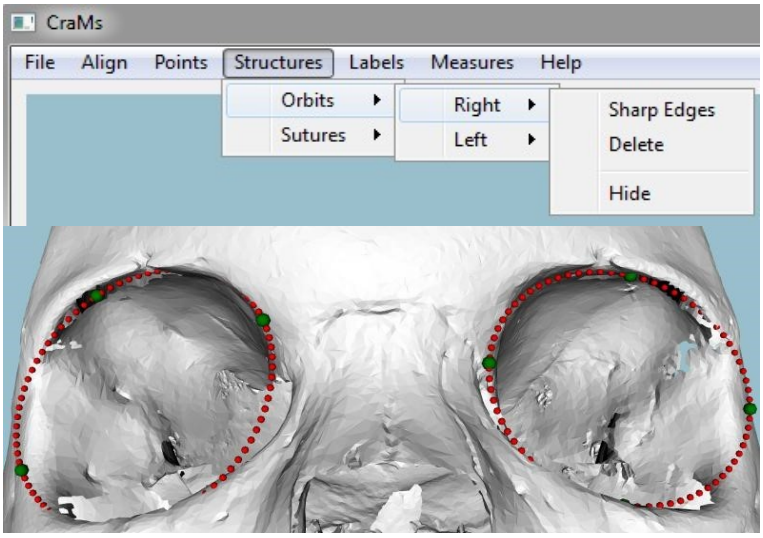

Figure 8 - Orbits structure sub-menus (Top) and results of having both orbits detected (Bottom).

The suture detection method is similar to the orbit detection method but uses only two reference points. The two points should be marked at the extremities of the suture. Figure 9 shows the results obtained from using this method.

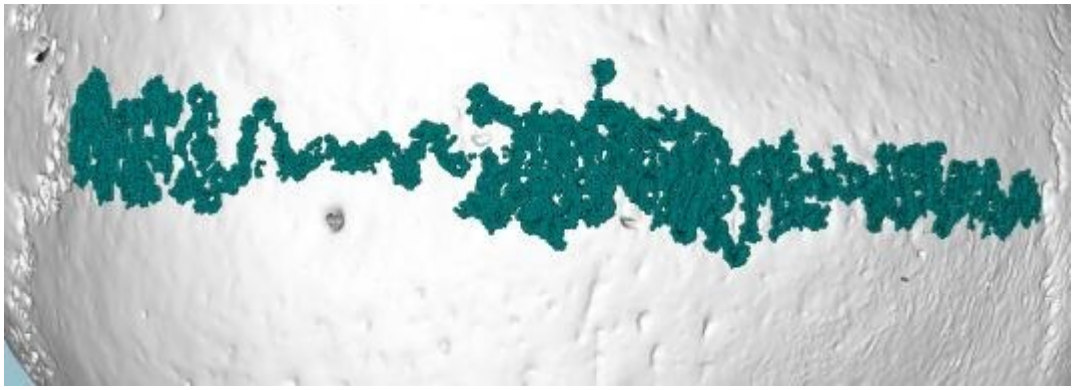

Figure 9 - Results of the suture detection method.

For the non-metric structures, you have two menus, the “Ancestry Estimation” (Figure 10) that allows the user to input manually the classifications of the morphological characteristics in order to obtain the probability of the model bellowing to each one of the population affinities (African, European, American Indian, Asian). The PBD and the INA can be calculated pressing the button auto.

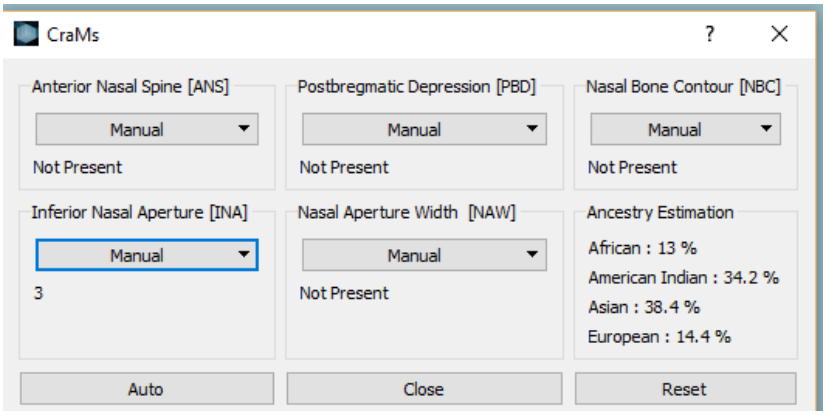

Figure 10 - Data entry window, designed for the collection of skull non-metric traits studded in this work (manually or using the methods developed), that gives the ancestry probability classification.

The NAW can be classified in the menu “Nasal” (Figure 11). The search of structure can be automatic or manual. You can also see the results, delete or hide the detected structures.

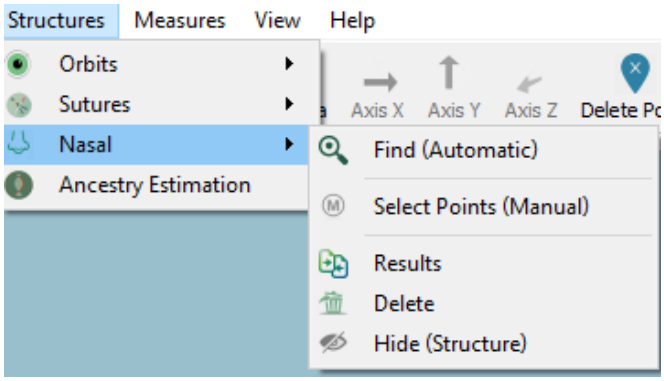

Figure 11 - The “Nasal” menu that gives access to the NAW detection and classification method.

View Menu

From this menu it is possible to change the styles, show or hide the labels for each category of points marked and show or hide list of points. Figure 12 shows the Labels menu, which can be used to identify which are the marked points.

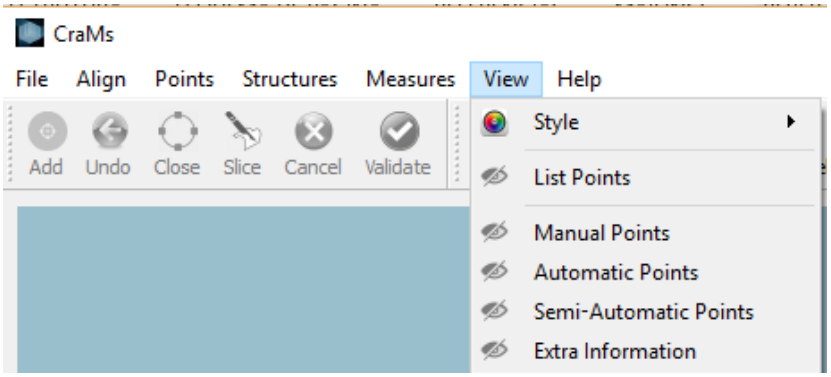

Figure 12 - View menu.

The figure 13 shows the list of points menu. These can be used to identify which are the marked points, to mark points more easily without access to the top menus and also is showed the category to witch the points belong (automatic, semi-automatic, manual).

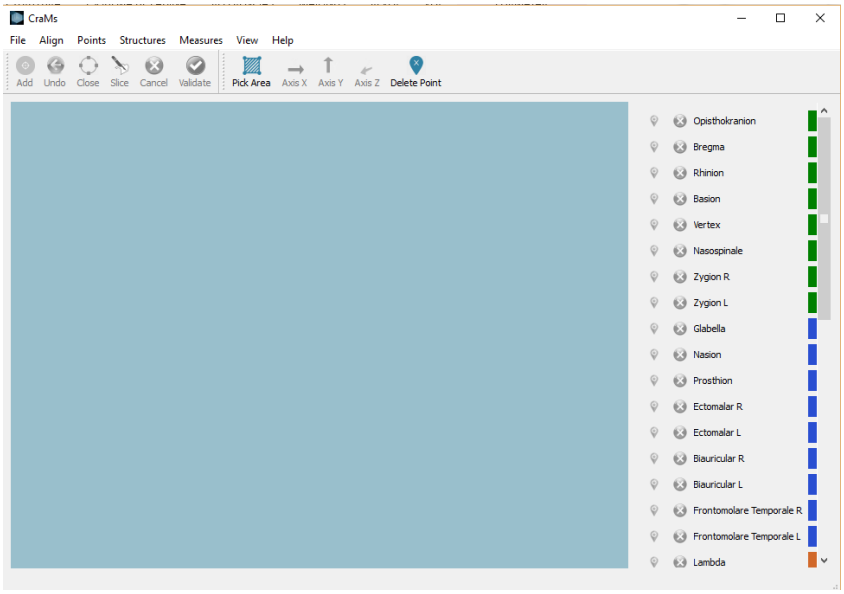

Figure 13 – List of points menu.

Measures Menu

When all the desired points are marked it is possible to calculate the measures through the *Measures* menu. From this menu it is also possible to read the points marked from a saved file and to see the list of measures. If any point is missing a warning will be presented. Figure 14 shows the Measures menu and an example of the warning.

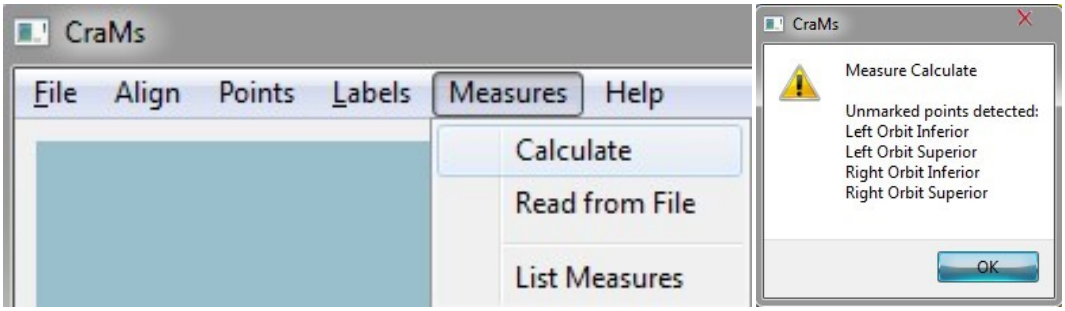

Figure 14 - Measures menu (left) and unmarked points warning (right).

When the warning is presented the user must choose to go back and mark the missing points or to ignore them and proceed with the calculation, as shown in Figure 15.

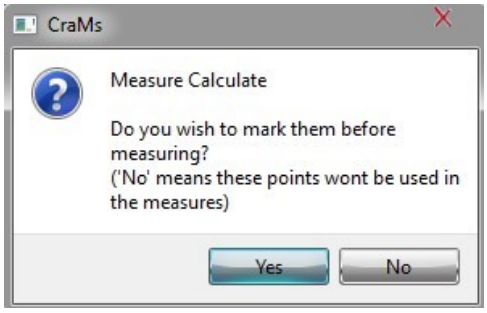

Figure 15 - Confirmation menu.

After the calculations all the measures are presented and the user can go back (by clicking the OK button) or save them, as shown in Figure 16.

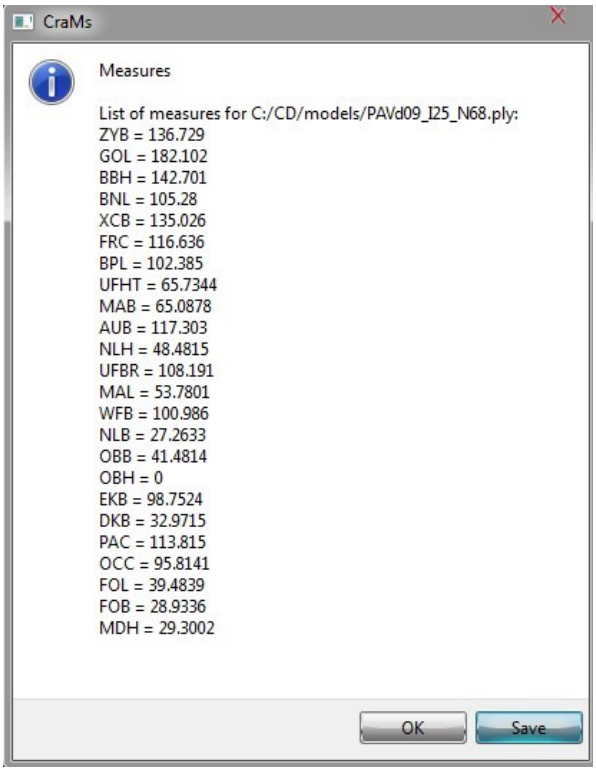

Figure 16 - List of measures.

Finally, the user can type his/her name (shown in Figure 17) and choose the destination of the measures file.

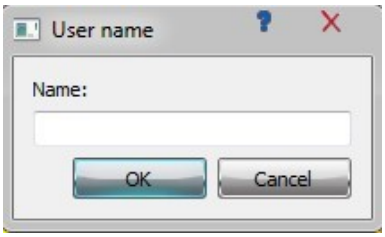

Figure 17 - Name input menu.

Additional keys

There are a couple of useful keys that might help and improve the usage of the application.

Key shortcuts:

- p ->Pick Points- activate to pick points or deactivate to move the model;
- ctrl + z -> Undo the last action or actions;
- enter -> Validate the last action made (point or structure marked).

These two can be used to mark points more accurately:

- The "F" key can be used to focus on the point the mouse pointer is;
- The "R" key resets the view (removing focus).

These keys can be used to manipulate the model and the view:

- "Control" key can be used to rotate the model;
- "Shift" key can be used to drag the model;
- Holding the left mouse button and moving the cursor will rotate the model;
- Scrolling up or down on the middle mouse button will zoom in or out.

By right clicking on the display area it is possible to access a menu that has a couple of functionalities. These include changing the background colour and toggling the visibility of many different objects. This menu is shown in Figure 18.

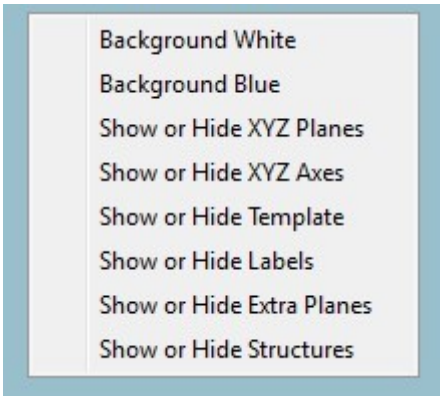

Figure 18 - Right click menu.

Farthest point of X, Y, Z axis search tool

Use the tool to mark the auxiliary point

1 – To use the tool is necessary that the model is aligned;

2 – Press this icon to turn on the tool; 

3 - Rotate the model into the best position to locate the area where the point will be inserted;

4 - Press “r”;

5 – Select the area where the point is included;

- If you want to rotate the skull:
  - 5.1 – Press “r”;
  - 5.2 – Rotate the skull;
  - 5.3 – Return to step 4.

6 – Select the axes that you want to use (Figure 19).

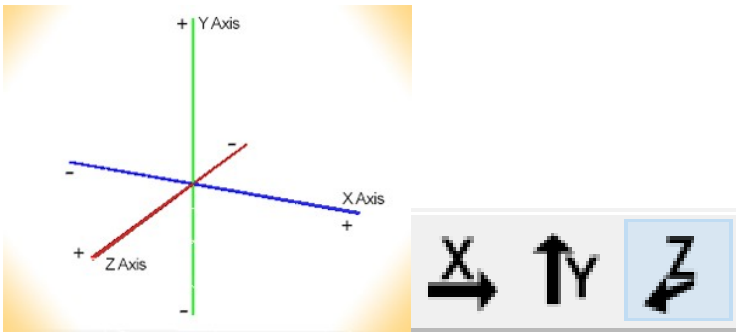

Figure 19 – Axes representation (left) and menu to select the axis to use (right).

- The marked point will appear with the colour green (Figure 20).
- If you selected the wrong axis, just select the intended axis again.

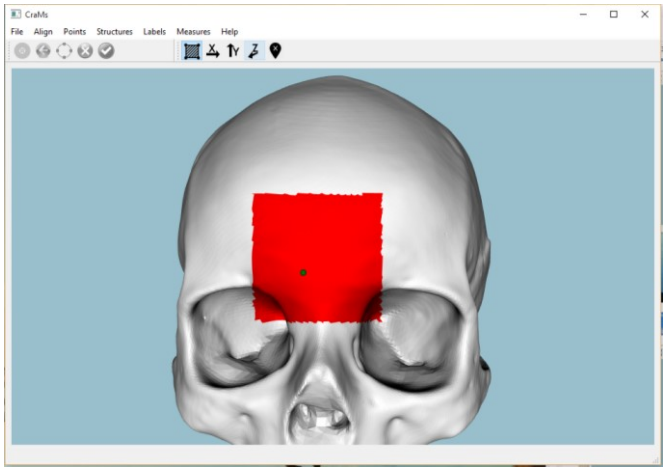

Figure 20 – Representation of the model after select search area and the axis.

7 – Press this icon again to turn of the selection mode:  (Figure 21);

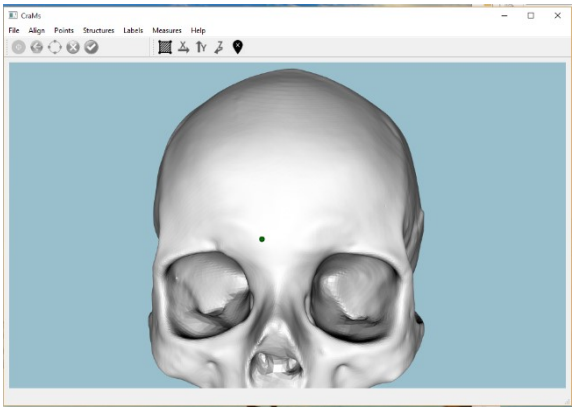

Figure 21 – Representation of the model after using the Farthest point of X, Y, Z axis search tool.

8 – To delete the auxiliary point press the icon  , at any time;

Use the tool to mark the manual point

1 - To use the tool it is necessary to have an aligned model;

2 – Select the point that you want to mark, on the menu (for ex: “Zygion”)

3 - Press this icon to turn on the tool; 

4 - Rotate the model into the best position to locate the area where the point will be inserted;

5- Press “r”;

6 – Select the area where the point is included;

- If you want to rotate the model:
    - 5.1 – Press “r”;
    - 5.2 – Rotate the model;
    - 5.3 – Return to step 4.

7 – Select the axis that you want to use.

- The marked point will appear with the respective colour (in this case purple).
- If you selected the wrong axis, press the “Undo” icon,  . Then, just select the intended axis again.

8 – Press this icon again to turn of the selection mode:  ;

9 – Press this icon to validate the point:  .

Appendix B – Usability Test

TASKS

(Use the manual if needed)

1 – Load a Model

2 – Align the model using the semi-automatic method and save the alignment

3 – Click the option that search the automatic points

4 – Correct the position of the bregma, an automatic point

5 – Mark the point Lambda, using the auxiliary tool "Slice"

6 – Calculate the measures and save to a File

7 – Search for the highest point in the parietal bone

8 – Identifying the probability of being African ancestry, knowing that the PBD is "Absent"

QUESTIONS

What tasks were impossible to complete and why?

What were the two tasks more difficult to complete and why?

Is the side panel (list of points) easy to use or did you prefer to use the menu? Why?

What could be changed or added to improve the user experience?

Classification:

Overall reaction to the program

1 2 3 4 5 6 7 8 9 10

Terrible ○ ○ ○ ○ ○ ○ ○ ○ ○ ○ Wonderful

Screen layout

1 2 3 4 5 6 7 8 9 10

Confusing ○ ○ ○ ○ ○ ○ ○ ○ ○ ○ Clear

Use of terminology throughout the program

1 2 3 4 5 6 7 8 9 10

Inconsistent ○ ○ ○ ○ ○ ○ ○ ○ ○ ○ Consistent

Information displayed on the screen

1 2 3 4 5 6 7 8 9 10

Inadequate ○ ○ ○ ○ ○ ○ ○ ○ ○ ○ Adequate

Arrangement of information on the screen

1 2 3 4 5 6 7 8 9 10

Illogical ○ ○ ○ ○ ○ ○ ○ ○ ○ ○ logical

Tasks can be performed in a straight-forward manner

1 2 3 4 5 6 7 8 9 10

Never ○ ○ ○ ○ ○ ○ ○ ○ ○ ○ Always

Organization of the information on the program

1 2 3 4 5 6 7 8 9 10

Confusing ○ ○ ○ ○ ○ ○ ○ ○ ○ ○ Clear

Forward navigation

1 2 3 4 5 6 7 8 9 10

Impossible ○ ○ ○ ○ ○ ○ ○ ○ ○ ○ Easy

Overall experience of finding information

1 2 3 4 5 6 7 8 9 10

Difficult ○ ○ ○ ○ ○ ○ ○ ○ ○ ○ Easy

Speed of the program

1 2 3 4 5 6 7 8 9 10

Slow ○ ○ ○ ○ ○ ○ ○ ○ ○ ○ Quick

Appendix C – CraMs Installation and Configuration

This appendix serves as a manual to the installation and configuration of the CraMs project using Visual Studio 2010.

Libraries used (make sure to include them in the Path Environment Variable):

- VTK 5.10.1
- QT 4.8.5
- Wild Magic 5.11
- Boost 1.55.0
- OpenCV 2.4.11

C/C++ -> General -> Additional Include Directories:

- boost\boost_1_55_0;
- GeometricTools\WildMagic5\SDK\Include;
- VTK/include/vtk 5.10;
- Qt/4.8.5/include;
- Qt/4.8.5/include/QtGui;
- Qt/4.8.5/include/QtCore;
- opencv\build\include\opencv2
- opencv\build\include;
- opencv\build\include\opencv2
- «Code folder».

C/C++ -> Preprocessor -> Preprocessor Definitions:

- QT_DLL;
- QT_GUI_LIB;
- QT_CORE_LIB;
- QT_NO_DEBUG;
- WM5_CORE_DLL_IMPORT;
- WM5_MATHEMATICS_DLL_IMPORT;
- WM5_CORE_IMPORT_DLL;
- WM5_MATHEMATICS_IMPORT_DLL;
- CMAKE_INTDIR="Release".

Linker -> Input -> Additional Dependencies:

- VTK lib files:

  QVTK.lib; vtkRendering.lib; vtkGraphics.lib; vtkIO.lib; vtkCommon.lib; vtkViews.lib; vtkInfovis.lib vtkWidgets.lib vtkHybrid.lib vtkexoIIc.lib vtkVolumeRendering.lib vtkverdict.lib; vtkImaging.lib; vtk-5.10\vtkftgl.lib; vtk-5.10\vtkfreetype.lib; vtkFiltering.lib; vtkDICOMParser.lib; vtkNetCDF_cxx.lib; vtkNetCDF.lib; vtkhdf5_hl.lib; vtkhdf5.lib; LSDyna.lib; vtkmetaio.lib; vtksqlite.lib; vtkpng.lib; vtktiff.lib; vtkjpeg.lib; vtkexpat.lib; vtksys.lib; vtklibxml2.lib; vtkzlib.lib; vtkalglib.lib.

- QT lib files:

  QtGui4.lib; QtCore4.lib; QtWebKit4.lib; QtXmlPatterns4.lib; QtNetwork4.lib; QtSql4.lib.

- Wm5 lib files:

  Wm5Core.lib; Wm5Mathematics.lib

- Wm5 lib files:
  opencv_calib3d2411.lib; opencv_contrib2411.lib; opencv_core2411.lib; opencv_features2d2411.lib; opencv_flann2411.lib; opencv_gpu2411.lib; opencv_highgui2411.lib; opencv_imgproc2411.lib; opencv_legacy2411.lib; opencv_ml2411.lib; opencv_nonfree2411.lib; opencv_objdetect2411.lib; opencv_photo2411.lib; opencv_stitching2411.lib; opencv_ts2411.lib; opencv_video2411.lib; opencv_videostab2411.lib;

Linker -> General -> Additional Include Directories:

opencv\build\x86\vc10\lib; opencv\build\x86\vc10\bin

Annex 1 – Measures

These were the 24 measures used by the iDryas team to classify the skulls. The figures shown were taken from the master thesis of Catarina Coelho (Coelho, 2012), one of the team's specialists.

1. ZYB (bizygomatic width): the distance between both *Zygion* points;

2. BBH (*Basion-Bregma* height): distance between *Basion* and *Bregma;*

3. XCB (maximum skull width): maximum width perpendicular to the sagittal plane;

4. GOL (maximum skull length): distance (straight line) between *Glabella* and *Opisthokranion*;

5. BNL (*Nasion-Basion* length): distance between *Basion* and *Nasion;*

6. FRC (frontal line): distance, in the sagittal plane, between the *Nasion* and *Bregma*;

7. BPL (*Basion-Prosthion* length): the distance (strait line) between *Basion* and *Prosthion*;

8. UFHT (superior facial height): distance between *Nasion* and *Prosthion*;

9. MAB (*maxillo-alveolar* width): is the maximum width of the alveolar arch on the outer surface (the distance between both *Ektomalare* points);

10. AUB (Biauricular width): the minimum exterior width measured in the root of the zygomatic processes;

11. NLH (nasal height): distance between the *Nasion* and Nasospinale;

12. UFBR (superior facial width): distance between both *Frontomolare-Temporale* points;

13. PAC (parietal line): distance, in the sagittal plane, between *Bregma* and *Lambda*;

14. FOL (length of the *Foramen Magnum*): distance between *Basion* and *Opisthion*;

15. WFB (minimum facial width): distance between both *Frontotemporale* points;

16. NLB (nasal width): maximum width of the nasal aperture;

17. OBB (orbital width): distance between *Dakyon* and Ekto*konchion*;

18. OBH (orbital height): distance between the border of the inferior and superior orbit.

19. EKB (bi-orbital width): distance between both *Ektokonchion points;*

20. DKB (inter-orbital width): distance between both *Dakyon points;*

21. OCC (occipital line): distance, in the sagittal plane, between *Lambda* and *Opisthion*;

22. FOB (width of the *Foramen Magnum*): distance between the lateral margins of the *Foramen Magnum*, in the lateral point with biggest curvature;

23. MAL (*maxillo-alveolar* length): distance between the *Prosthion* and *Alveolon*;

24. MDH (height of the *Mastoid process*): distance, in projection, between the *Frankfurt plane* and the nadir point of the *Mastoid process*;

Annex 2 – Points of Interest

All figures shown in this appendix were taken from (Pereira & Mello e Alvim, 1979). The following points were defined as being feature points to use in the classification of the skulls:

1. Alveolon (alv): intersection point of the mid line of the palate with the perpendicular tangent to the posterior border of the alveolar arch;

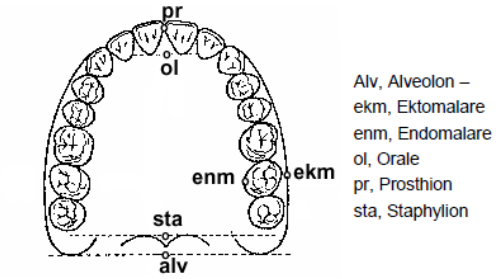

Figure 1 - Palatal arch

2. Basion (ba): the point is situated on middle border of the anterior margin of the foramen magnum. This feature point is defined as the point with minimum Y coordinate in the Z axis (considering a threshold of ±0.01 mm in X and ±10 mm in Z coordinates);
3. Bregma (b): intersection point between the sagittal suture and the coronal suture. The algorithm selects a starting point as the coordinate with greater Y value on the region of points of X and Z within a ±0.01 mm threshold. Then, it analyses neighbour points in order to find a discontinuity in the Y values, i.e., sudden smaller followed by higher Y values with

the aim of finding the coronal suture. Once the suture region is found, the Bregma is selected as point in the region with smaller Y coordinate;

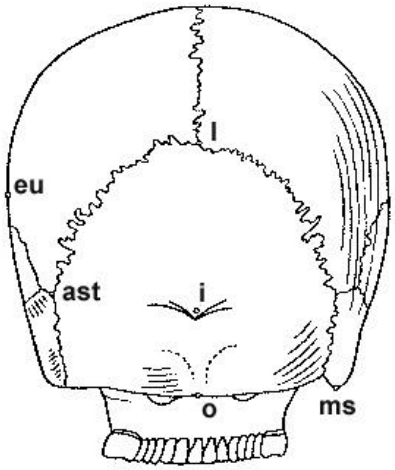

Ast, Asterion – eu, Eurion – i, Inion – 1, Lambda – mas, Mastoidale – o, Opisthion.

Figure 2 - Skull back view

4. Dakyon (d): point located at the apex of the angle formed by the frontolacrimal suture and lacrimomaxilar suture;
5. Ektokonchion (ek): Point located on the outer edge of the orbit and the furthest possible of the *maxillofrontale* point;
6. Ektomalare (ekm): Point situated in the palatal surface of the alveolar arch, in the middle portion of the second molar;
7. Eurion (eu): Most lateral point of the *neurocranium*. Has no fixed location and varies from one individual to another and from one population to another;
8. Frontotemporale (ft): most anterior point of the temporal line, located approximately at the root of the zygomatic apophysis of the frontal bone;
9. Frontomolare-Temporale (fmt): point most posterior and lateral of the frontomalar suture, in the temporal region;

10. Glabella (g): Point located just above the frontonasal suture, between the superciliary arches. Commonly is the most salient point of the front, in the sagittal plane. It may, however, constitute or form a depression, with the superciliary arch (a single continuous elevation);

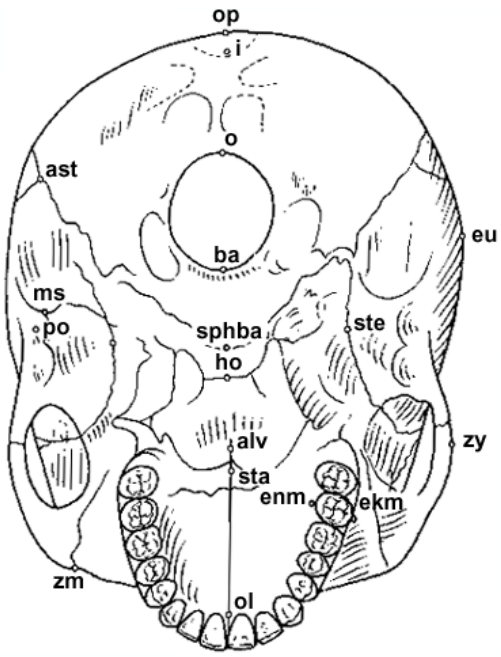

alv, Alveolon - ast, Asterion - ba, Basion - ekm, Ektomalare - enm, Endonmlare - eu, Eurion - ho, Hormion - i, Inion - ms, Mastoideale - o, Opisthion - op, Opisthokranion - ol, Orale - po, Porion - sphba, Sphenobasion - sta, Staphylion - ste, Stenion - zy, Zygion - zm, Zygomaxillare.

Figure 3 - Skull bottom view

11. Lambda (l): Intersection point between the sagittal and lambdoid sutures;
12. Mastoidale (ms): Lowest point of the mastoid process of the temporal;
13. Nasion (n): Intersection point of the frontonasal suture and suture internasal. Corresponds to the root of the nose;
14. Nasospinale (ns): Lowest point in the inferior edge of the piriform aperture at the base of the nasal spine, designed in the Sagittal Plane. This point is called by some authors Subnasale or Nasale;
15. Opisthion (o): Mid point of the posterior edge of the occipital hole;
16. Opisthokranion (op): Point that is the furthest from the *glabella* in sagittal plane of the occipital. Sometimes coincides with the *inion*. There are cases where this occipital region is more or less flat;

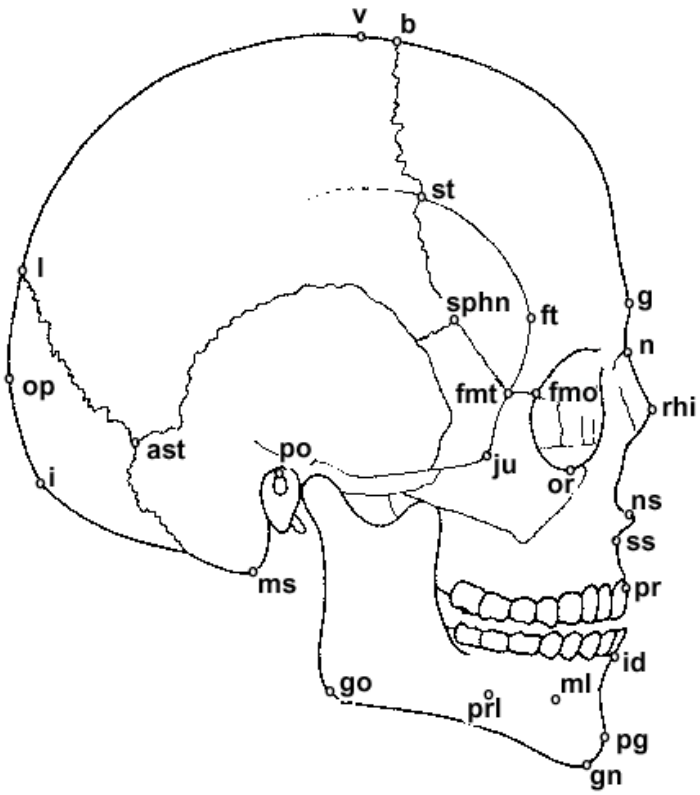

ast, Asterion – b, Bregma – fmo, Frontomalare orbitale – fmt, Frontomale temporale – ft, Frontotemporale – g, Glabella – gn, Gnathion – go, Gonion – i, Inion – id, Infradentale – ju, Jugale – l, Lambda – ms, Mastoidale – ml, Mentale – n, Nasion – ns, Nasospinale – op, Opisthokarion – or, Orbitale – pg, Pogonion – po, Porion – prl, Prominentia laterale – pr, Prosthion – rhi, Rhinion – sphn, Sphenion – st, Stephanion – ss, Subspinale – v, Vertex

Figure 4 - Skull side view

17. Porion (po): Point on the upper and outer border of the external auditory canal;
18. Prosthion (pr): Most anterior point of the alveolar ridge between the central incisors. Corresponds to the lower end and anterior interalveolar septum in the sagittal plane;
19. Vertex (v): Highest point of the skull located in the sagittal suture and in the frankfurt plane;
20. Zygion (zy): Most lateral point of the zygomatic arch, on each side. Given the aligned skull both Zygion are defined as the points with maximum and minimum X coordinates, respectively to the right and left points. Since the zygomatic arch might not be the largest zone of the skull, we only consider the portion of the skull with negative Y values;
21. Zygomaxillare (zm): Lowest point of the maxilomalar suture.

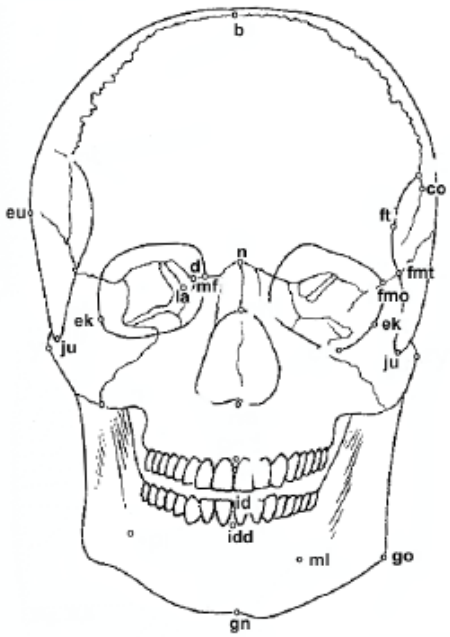

b, Bregma – co, Coronale – d, Dakyon – ek, Ektokonchion – eu, Eurion – fmo, Frontomalare orbitate- fmt, Frontomolare temporale – ft, Frontotemporale – gn, Gnathion – go, Gonion – id, Infradentale – idd, Infradentale dentale – ju, Jugale – la,Lacrimale – mf, Maxillofrontale – ml, Mentale – n, Nasion – ns, Nasospinale – or, Orbitale – prl, Prominentia laterale – pr, Prosthion – prd, Prosthion dentale – rhi, Rhionion – st, Stephanion – zy, Zygion – zm, Zygomaxillare

Figure 5 - Skull front view

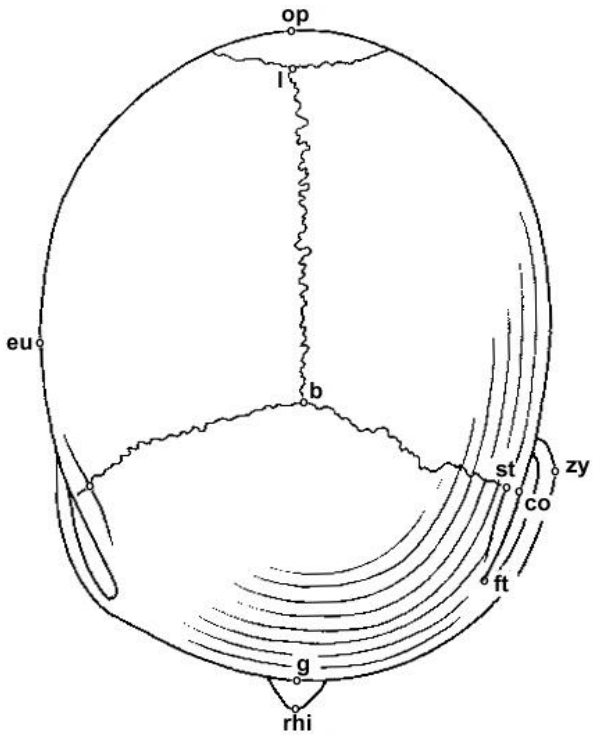

b, Bregma – co, Coronale – eu, Eurion – ft, Frontotemporale – g, Glabella – l, Lambda – op, Opisthokranion – rhi, Rhinhion – st, Stephanion – zy, Zygion

Figure 6 - Skull top view

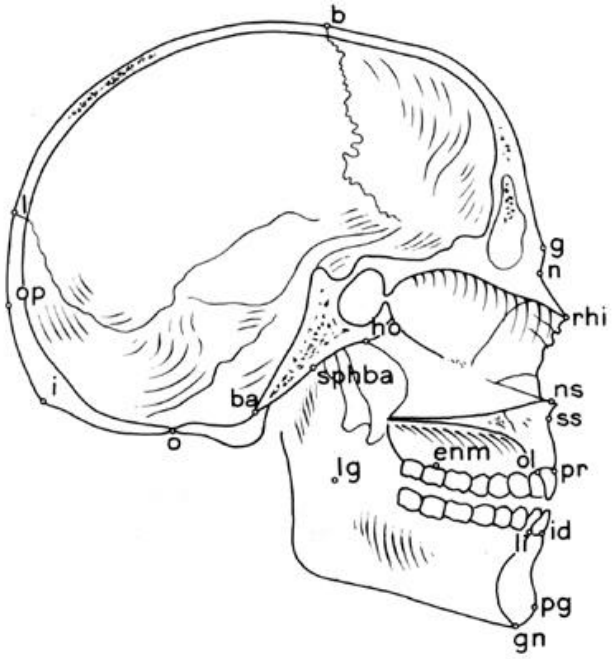

Ba, Basion – b, Bregma – enm, Endomalare – g, Glabella – gn, Gnathion – ho, Hormion – i, Inion – id, Infradentale – l, Lambda – li, Linguale – lg, Lingulare – n, Nasion – ns, Nasospinale – o, Opisthion – ol, Orale – op, Opisthokranion – pg, Pogonion – pr, Prosthion – rhi, Rhinion – spha, Sphenobasion – ss, Subspinale.

Figure 7 - Skull inside side view

Annex 3 – Morphological traits

These were the eleven traits used by Hefner (2009) to estimating the individuals Ancestry. The description of the morphologic traits and the figures shown were taken from the paper of Hefner (2009):

ANS—One commonly encountered problem when assessing an ANS is the extreme fragility of this area, which is often damaged either peri- or postmortem. Those crania exhibiting trauma, pathology (including alveolar resorption), or postmortem damage to the overall inferior nasal margin were excluded from the analysis. The ANS is scored progressively as slight, intermediate, and marked: (i) Slight: minimal-to-no projection of the ANS beyond the INA, (ii) intermediate: a moderate projection of the ANS beyond the INA, and (iii) marked: a pronounced projection of the ANS beyond the INA (Figure 1).

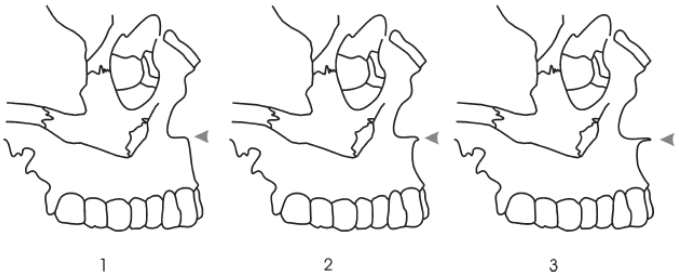

Figure 1 - Character states for the anterior nasal spine morphology

INA—Inferior nasal morphology is defined as the most inferior portion of the nasal aperture, which, when combined with the lateral alae, constitutes the transition from nasal floor to the vertical portion of the maxillae, superior to the anterior dentition. INA is an assessment of the shape of the inferior border of the nasal aperture. Bilateral asymmetry was noted. In those instances where bilateral asymmetry did occur, the left side was used. INA is scored as follows: (i) an inferior sloping of the nasal floor which begins within the nasal cavity and terminates on the vertical surface of the maxilla, producing a smooth transition. The morphology is distinct from INA 2 regarding the more posterior origin and the greater slope of INA 1; (ii) sloping of the nasal aperture beginning more anteriorly than in INA 1, and with more angulation at the exit of the nasal opening; (iii) the transition from nasal floor to the vertical maxilla is not sloping, nor is there an intervening projection, or sill. Generally, this morphology is a right angle, although a more blunted form may be observed; (iv) any superior incline of the anterior nasal floor, creating a weak (but present) vertical ridge of bone that traverses the inferior nasal border (partial nasal sill); and (v) a pronounced ridge (nasal sill) obstructing the nasal floor-to-maxilla transition (Figure 2).

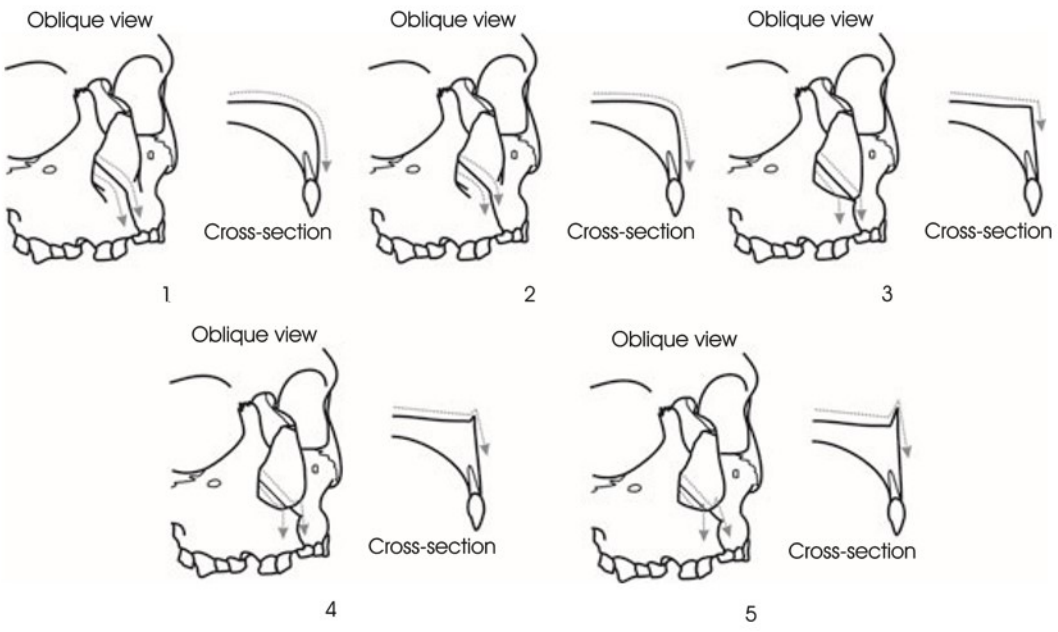

Figure 2 - Character states for the inferior nasal aperture morphology.

IOB—Interorbital breadth (IOB) is a morphoscopic trait that could be measured with calipers using the defined measurement dacryon to dacryon, rather than scored nonmetrically. For this study, IOB is assessed as: (i) narrow, (ii) intermediate, and (iii) broad. This assessment is made relative to the facial skeleton (Figure 3).

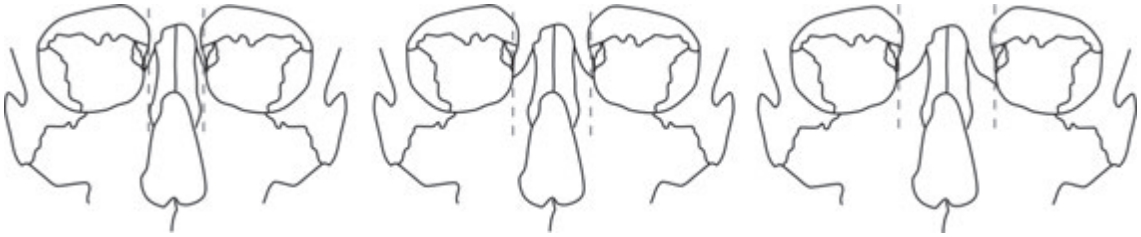

Figure 3 - Character states for the interorbital breadth.

MT—The malar tubercle (MT) is a caudally protruding tubercle located on the inferior margin of the maxilla and zygomatic bone in the region of the ZS. MT is scored following Hauser and De Stefano, who recommend placing a transparent ruler at the intersection of the ZS and the inferior margin of the malar to the deepest point on the curvature of the maxilla. An assessment is then made on the extent of protrusion beyond the ruler's edge. In instances where the suture is directly on the tubercle, the ruler is placed from the deepest curvature of the maxilla to the deepest anterior curvature on the zygomatic. It should be noted that a MT may be present on the maxilla, the zygomatic, or along the ZS. Observers should not consider the tubercles on the lateral zygomatic arch. A completely absent MT is rare. MT is scored as follows: 0—no projection of bone; 1—a trace tubercle below the ruler's edge (roughly 2 mm or less); 2—a medium protrusion below the ruler's edge (roughly 2–4 mm); 3—a pronounced tubercle below the ruler's edge (roughly 4 mm or more) (Figure 4).

Figure 4 - Character states for the malar tubercle.

NAW—The width of the nasal aperture width (NAW) is assessed relative to the facial skeleton. It is scored as 1—narrow; 2—medium; or 3—broad (Figure 5).

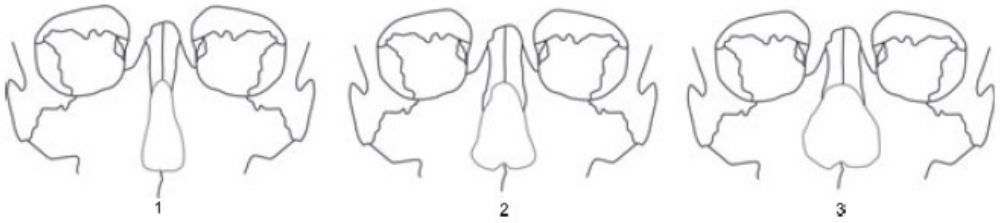

Figure 5 - Character states for the nasal aperture width.

NBC—Nasal bone contour (NBC) is defined as the contour of the midfacial region (particularly the contour of the nasal bones and the frontal process of the maxilla) c. 1 cm below nasion. Visual interpretation of nasal contour is not the most effective manner of analysis due to high inter- and intra-observer error. The use of a contour gage permits a more reliable and consistent assessment of nasal contour. To assess NBC, the cranium is placed in a position that allows the observer to gently, but with consistent and balanced pressure, place the contour gage (Figure 7) directly on the nasal bones c. 1 cm inferior to nasion, while maintaining the gage roughly perpendicular to the palate and parallel to the orbits. NBC is scored as follows: 0—low and rounded NBC; 1—an oval contour, with elongated, high, and rounded lateral walls; NBC 1 presents a circular shape and lacks steep walls. Brues (2) suggests the term Quonset-hut to describe this shape, although the term is somewhat dated; 2—steep lateral walls and a broad (roughly 7 mm or more), flat superior surface ‘‘plateau,’’ noted on the contour gage as a flat cluster of needles in the midline; 3—steep-sided lateral walls and a narrow superior surface ‘‘plateau’’; 4—triangular cross-section, lacking a superior surface ‘‘plateau’’ (Figure 6).

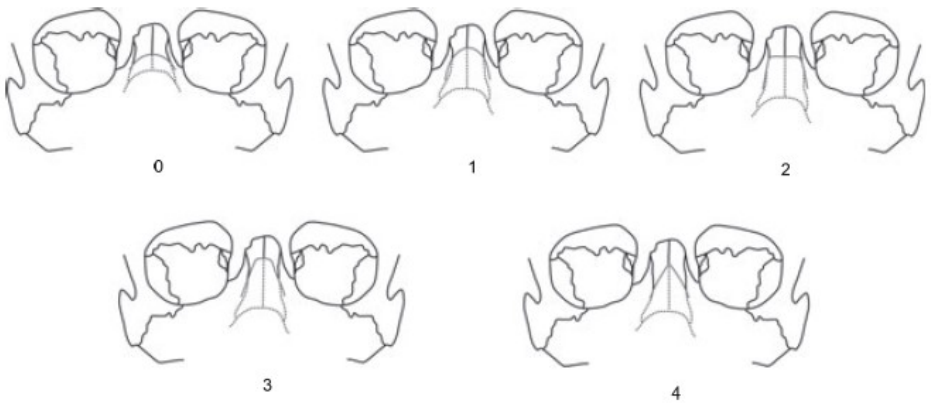

Figure 6 - Character states for the nasal bone contour.

Figure 7 - A typical contour gage.

NO—Nasal overgrowth (NO) is defined as an inferior projection of the lateral border of the nasal bones beyond the maxillae at nasale inferious. Assessment of NO does not include anterior bulging of the nasal bones. Observations should be made on the left side. If the left side is damaged, the right side may be substituted. If both nasal bones are missing or fractured (anti-, peri-, or postmortem), the trait is not scored. It is often useful to run a finger along the borders of the maxilla and nasal bones near nasale inferious to determine whether a projection is present. NO is scored dichotomously as 0—absent or 1—present (Figure 8).

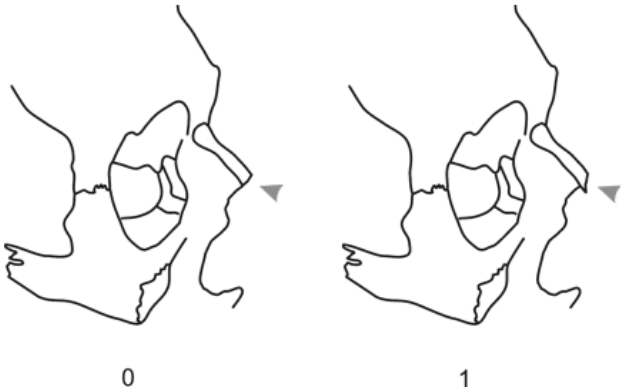

Figure 8 - Character states for the nasal overgrowth.

PBD—Postbregmatic depression is a slight to broad depression along the sagittal suture, posterior to bregma that is not the result of pathology (e.g., premature synostosis). Observed in lateral profile, the trait is scored as either 0—absent (no depression) or 1—present (Figure 9).

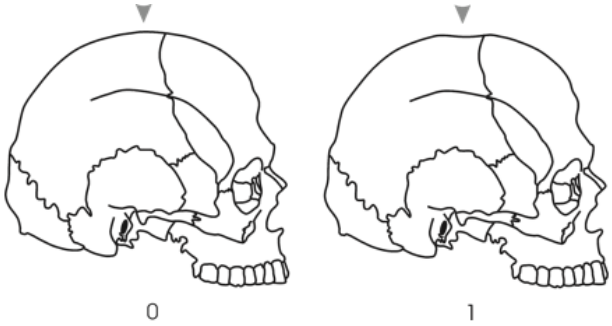

Figure 9 - Character states for the postbregmatic depression.

SPS—In adult crania, a secondary complex suture may persist, which is generally referred to as the supranasal suture (SPS), or sutura supranasalis. This suture does not represent the nasal portion of a persistent metopic suture, which is usually a single, non-oscillating line. The SPS is the fusion of the nasal portion of a frontal suture that appears as a complex of interlocking bony spicules at glabella. SPS is scored as follows: 0—completely obliterated; 1—open (unfused); 2—closed, but visible (Figure 10).

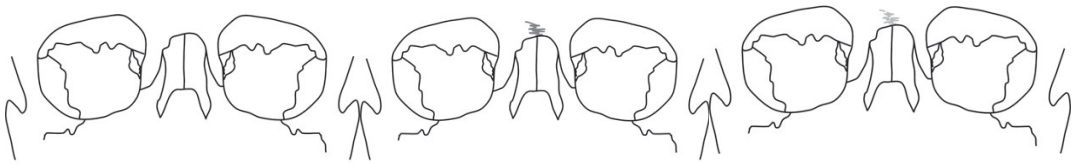

Figure 10 - Character states for the supranasal suture.

TPS Shape—The course of the TPS is highly variable, although certain themes persist. TPS is not scored unilaterally, although asymmetrical sutures are not uncommon. The entire suture is observed, but the medial one-half in the region of the palatine suture is most closely scrutinized. When an asymmetrical suture is present (the two branches of the suture do not come into contact at midline) the general theme is recorded (e.g., straight or jagged). Slight undulations of the suture should not be considered when making a determination. If the suture is obliterated, it is not scored. TPS is scored as follows: (i) the suture crosses the palate perpendicular to the median palatine suture, with no significant anterior or posterior deviations. If the right and left halves of the suture do not contact each other at midline, but the suture is otherwise straight, score the suture as a 1; (ii) the suture crosses the palate perpendicular to the median palatine suture, but near this juncture a significant anterior deviation, or bulging, is present. If the right and left halves of the suture do not contact each other, but the suture is otherwise bulging anteriorly, a score of 2 is used; (iii) the suture crosses the palate, but deviates anteriorly and posteriorly (e.g., M-shaped) in the region of the median palatine suture. If the right and left halves of the suture do not contact each other, but the suture is otherwise jagged, a score of 3 is used; and (iv) the suture crosses the palate

perpendicular to the median palatine suture, but near this juncture a posterior deviation, or bulging, is present (Figure 11).

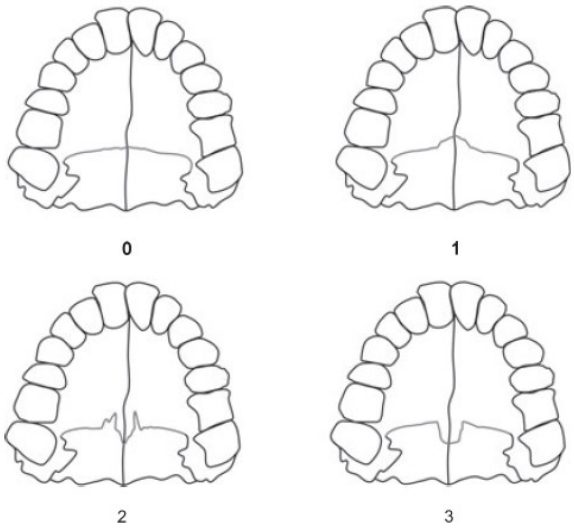

Figure 11 - Character states for the transverse palatine suture.

ZS Shape—The ZS is the suture between the maxilla and the zygomatic. The course of the suture is best observed in the anterior view. In instances of asymmetrical manifestations, the left side is preferred. The infraorbital suture should be ignored when making a determination. Assessment of ZS is based primarily on the approximate location of greatest lateral projection of the suture, and also on the number of major angles present. ZS is scored as follows: 0—A suture with no angles and greatest lateral projection at the inferior margin of the malar. Sutures having greatest lateral projection at the inferior margin, but a slight angle near the midpoint of the suture should be scored as 0; 1—a suture with one angle and greatest lateral projection near the midline; 2—a suture with two or more angles (presenting a jagged and/or S-shaped appearance) and a variable position for greatest lateral projection. The figure shows both S-shaped and jagged courses of the suture (Figure 2).

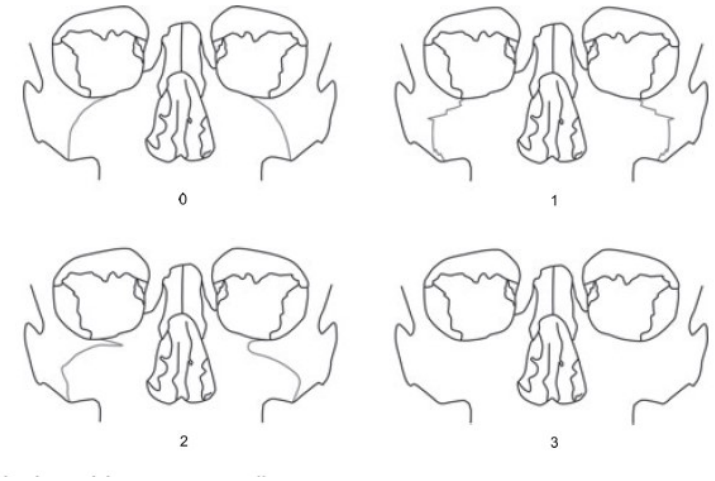

Figure 12 - Character states for the shape of the zygomaticomaxillary suture.